Assen Zlatarov University
Burgas, Bulgaria

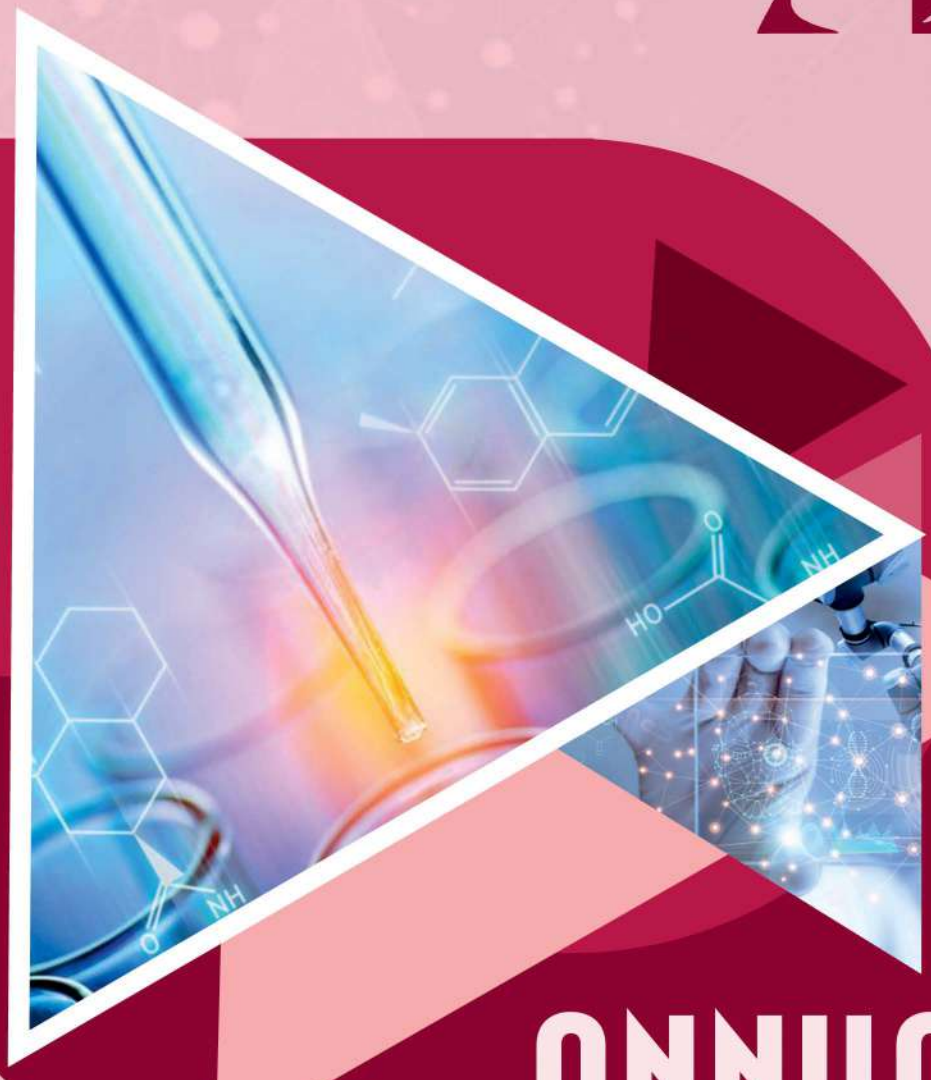

ANNUAL

1

VOLUME LI, BOOK 1, 2022

TECHNICAL AND NATURAL SCIENCES

ASSEN ZLATAROV UNIVERSITY
BURGAS, BULGARIA

ANNUAL

Vol. LI, BOOK 1, 2022

TECHNICAL AND NATURAL SCIENCES

Assen Zlatarov University

Assen Zlatarov University
Annual, Vol. LI, Book 1, 2022
Burgas 8010, Bulgaria
ISSN 2603-3968

ASSEN ZLATAROV UNIVERSITY
BURGAS, BULGARIA

ANNUAL

Vol. LI, BOOK 1, 2022

TECHNICAL AND NATURAL SCIENCES

BURGAS ● 2022

VOLUME LI (1). CONTENTS

Galina Grigorova, Galina Yordanova, Ruska Nenkova	Influence of food, stress and sleep on students' health	7
Antonia Ilieva, Dimitrina Kiryakova	Tensile properties of silane-treated wood flour polypropylene composites before and after thermal ageing	10
Vasil Ivanov	Research of a parallel oscillating scheme in Simulink	17
Dimitrina Kiryakova, Ganka Kolchakova	Structural and surface characteristics of chemically modified waste egg shells	21
Dimitrina Krasteva, Katya Gabrovska, Yavor Ivanov	Determination of the antimicrobial effectiveness of the antibiotic Ciprofloxacin	26
Mehmed Hasan	Operational reliability in a smart grid	32
Ruska Nenkova, Galina Yordanova, Galina Grigorova	Synergistic action of preservatives on different types of microorganisms	36
Stanislav Popov, Todor Petkov, Veselina Bureva	Probability modeling using logistic regression and MapReduce	40
Yordanka Tasheva, Aleksander Dimitrov, Milena Dimitrova	Some features of gasoil oxidation	44

Articles presented at the Challenges for Medical Science and Practice in the 21st Century Congress of Medicine, Burgas, 1-3 September 2022

Mihai Petrov	Entropical thermodynamic description of humans and health as a unique functional element in the concept of health ecology and the biosphere	48
Mihai Petrov	Investigation of the influence of aerosol and gas pollutants on ecosystems, the respiratory system and human health	54
Nikolay Kostadinov	Physical activity in type 2 diabetes – a key role in treatment	61
Zlatka Cholakova, Nikolay Mirinchev	Geodes unusual manifestation of urolithiasis. Two cases of bladder and kidney presence of geodes	65
Petia Tzvetkova	Reproductive view of the city of Burgas in the context of the psycho-social factors of the demographic crisis	71
Petia Tzvetkova	Spermatological indicators on Torsio testis	75
Ganka Bekyarova, Yoana Kisselova-Kaneva, Nicolai Bekyarov, Stefka Stoeva	Association between ADMA, oxidative stress and endothelial dysfunction in metabolic syndrome	79

S. Chavdarov, St. Shishkov, Sv. Todorov, E. Laleva, K. Minkova, M. Mihaylova	Metastatic brain tumours	84
Sv. Todorov, St. Shishkov, S. Chavdarov, K. Minkova, M. Mihaylova, E. Laleva	Vertebroplasty	87

ANNUAL OF ASSEN ZLATAROV UNIVERSITY, BURGAS
BULGARIA, 2022, v. LI(1)

INFLUENCE OF FOOD, STRESS AND SLEEP ON STUDENTS' HEALTH

Galina Grigorova, Galina Yordanova, Ruska Nenkova
E-mail: galinakirova@abv.bg

ABSTRACT

The effect of food, stress and sleep on adolescents' health has been studied. The study covers 130 students aged from 12 to 14 in the Burgas region. The students have been interviewed in the period of April - May 2022. From the data obtained, it could be concluded that 52% of the surveyed students eat according to the principle of rational nutrition. 45% of the respondents do not get enough sleep for the day and usually go to bed after 11.00 pm.

Key words: *health, nutrition, stress, sleep, students*

INTRODUCTION

According to the WHO, "health is a state of complete physical, mental and social well-being and not merely the absence of a disease or infirmity". Food, optimal physical activity, sleep, stress, and noise are key factors for human health. The rational, balanced diet is optimal when it meets the energy needs of the body [1]. A healthy lifestyle creates good conditions for normal physiological and mental processes, reduces the probability of various diseases and prolongs human life. Some causes of disorders in the metabolism, nervous system, hypertension, reduced pulmonary ventilation, impaired functions of endocrine glands, reduced strength and elasticity of muscles, speed of reaction and coordination abilities are the unbalanced nutrition, stress and insufficient amount of sleep. Though sleep consumes a considerable portion of our lives, its biological functions and biochemical implications are still poorly understood. Efficient and effective sleep is more than just a luxury; it is critical for the proper functioning of many organs, particularly the brain. The sleep–wake cycle is the most obvious example of a circadian process, as it occurs with a consistent 24-h rhythm and can be shifted according to environmental cues. The body's circadian clock system maintains these 24-h rhythms in physiological functions, including the sleep–wake cycle, and synchronizes them to the light–dark cycle. Disturbances of both sleep and the underlying circadian rhythms have long been associated with many neurological and psychiatric diseases, including Alzheimer Disease (AD). AD, a devastating age-related neurodegenerative disease characterized by aggregation and accumulation of amyloid-β (Aβ) and tau proteins, is the most common cause of dementia in older people worldwide. AD patients often exhibit disrupted day–night activity patterns and fragmented or mistimed sleep, which can cause great morbidity and is a major cause of institutionalization [2].

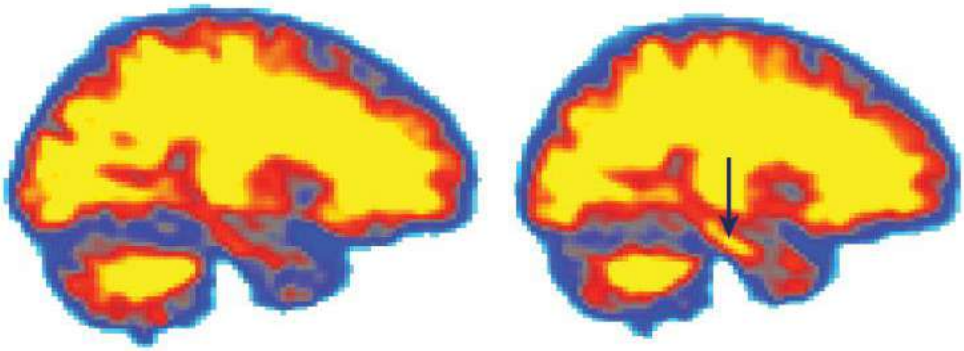

Fig. 1. Accumulation of amyloid-beta (in yellow) in the brain of well-rested people (left) and people who have gone without sleep for 31 hours (right). An increased amount of amyloid-beta in the hippocampus is indicated by an arrow. Credit: E. Shokri- kojori/nih [3]

In an experiment, a comparison between the brains of people during rest and people after 31 hours of sleeplessness has been made. The results present that during a long period of insomnia, the content of beta-amyloid increases by 5% in two areas of the brain, the thalamus and hypothalamus [3].

The examination of sleep and its disorders have been investigated by means of polysomnography - simultaneous registration of electroencephalography (EEG), electrooculography (EOG) of eye movements and electromyography (EMG) of skeletal muscle activity. The aim of the present study is to analyse the physical and mental health status of students [4].

EXPIREMENT

The survey studies the influence of basic factors such as food, sleep and stress among students aged 12 to 14 from Burgas region. 130 students have been examined in the period of April-May 2022. Statistical analysis, interview and survey methods have been used for the purposes of this study.

RESULTS AND DISCUSSION

The alternation of wakefulness and sleep is one of the many circadian rhythms in living organisms. Circadian rhythms are coordinated by the alternation of day and night. The absence of coordination results in transformation the wake-sleep cycle of 24 hours into 33 hours. The data from the survey indicate that 52% of the participants in this study eat according to the rules of rational nutrition. The consumed food is corresponding to the energy needs of the body to maintain metabolism and physical activity. They consume home-cooked food that provides the body with the optimal satisfaction of biologically active substances in a certain quantitative and qualitative ratio of proteins, fats and carbohydrates. 48% of the surveyed students skip breakfast and eat fast food or packaged food rich in quick carbohydrates. Healthy eating is defined as “eating practices and behaviours that are consistent with improving, maintaining and/or enhancing health.” Among collective factors, familial factors and the nature of foods available in the physical environment, including at home, schools and in fast-food establishments, stand out as significant influences on healthy eating in children and youth. The media, particularly television, also have an enormous potential influence and can overshadow familial influences. Individual factors identified include knowledge, attitudes and food preferences; only the latter have been identified as a strong determinant of healthy eating in both children and youth [5]. 48% of the students pointed out that the stress at school is related to examinations and presentations in front of classmates and the teacher. The cumulative daily events experienced by children have a deleterious effect on future health [6, 7] and mediate the impact of acute events on psychological health [8]. Recurrent or prolonged stress may lead to problems such as headaches [9, 10], abdominal pain [10, 11], school absenteeism [12], overeating [13] and tobacco use [14]. Children need a repertoire of coping strategies to effectively manage stressful encounters [15] and develop resilience [16]. 45% of the respondents do not get enough sleep during the twenty-four hours and usually go to bed after 11:00 p.m. Insufficient sleep poses an important and complicated set of health risks in the adolescent population. Not only is deficient sleep (defined as both sleep duration inadequate to meet sleep needs and sleep timing misaligned with the body's circadian rhythms) at epidemic levels in this population, but the contributing factors are both complex and numerous and there are a myriad of negative physical and mental health, safety and performance consequences. Causes of inadequate sleep identified in this population include internal biological processes such as the normal shift (delay) in circadian rhythm that occurs in association with puberty and a developmentally-based slowing of the "sleep drive", and external factors including extracurricular activities, excessive homework load, evening use of electronic media, caffeine intake and early school start times. Consequences range from inattentiveness, reduction in executive functioning and poor academic performance to increased risk of obesity and cardio-metabolic dysfunction, mood disturbances which include increased suicidal ideation, a higher risk of engaging in health risk behaviours such as alcohol and substance use, and increased rates of car crashes, occupational injuries and sports-related injuries. In response to these concerns, a number of promising measures have been proposed to reduce the burden of adolescent sleep loss, including healthy sleep education for students and families, and later school start times to allow adolescents to obtain sufficient and appropriately-timed sleep [17].

CONCLUSION

Balanced food, efficient and effective sleep are reducing stress levels and are an essential element in a healthy lifestyle. Calm communication between students, as well as between teachers and students, is a major factor in building self-aware individuals. Studying in a quiet, harmonious, peaceful environment are important factors in maintaining excellent health and self-confidence. Unhealthy food, listening to loud music, as well as assembly in rooms with high noise level, are all risk factors for personal and public health.

REFERENCES

1. Garchev, R. Practical Seminars in Physiology, ARSO Medical Literature Publishers, Sofia, 2015.
2. Erik, S. Musiek, David D. Xiong, David M Holtzman. Sleep, circadian rhythms, and the pathogenesis of Alzheimer Disease, Experimental & Molecular Medicine volume 47, page 148, 2015.
3. Shokri, Kojori/Nih E. Can sleep protect or cure us from Alzheimer's disease, Bulgarian Science News, July 19, 2018.
4. Garchev, R., L. Vitanov. Human physiology, Medical Publishing, APCO, Sofia, ARSO Medical Literature Publishers, Sofia 2020.
5. Jennifer, P. Taylor, Susan Evers, Mary McKenna. Determinants of Healthy Eating in Children and Youth, Canadian Journal of Public Health volume 96, pages S22–S29, 2005.
6. Carter, J. S., Garber J., Ciesla J. A., & Cole D. A. Modeling relations between hassles and internalizing and externalizing symptoms in adolescents: A four-year prospective study. Journal of Abnormal Psychology, 115, 428-442 2006.
7. Compas, B., Malcarne V., & Fondacaro D. Coping with stressful events in older children and young adolescents. Journal of Consulting and Clinical Psychology, 56(3), 405-411, 1988.
8. Wagner, B., Compas, B., & Howell, D. Daily and major life events: A test of an integrative model of psychosocial stress. American Journal of Community Psychology, 16(2), 189-205, 1988.
9. Strine, T., Okor C., McGuire L., & Balluz L. The associations among childhood headaches, emotional and behavioral difficulties, and health care use. Pediatrics, 117(5), 1728, 2006.
10. White, K., & Farrell A. Anxiety and psychosocial stress as predictors of headache and abdominal pain in urban early adolescents. Journal of Pediatric Psychology, 31(6), 582-596, 2005.
11. Thomsen, A. Parent reports of coping and stress responses in children with recurrent abdominal pain. Journal of Pediatric Psychology, 27(3), 215-226, 2002.
12. Strine, T., Okor C., McGuire L., & Balluz L. The associations among childhood headaches, emotional and behavioral difficulties, and health care use. Pediatrics, 117(5), 1728, 2006.
13. Jenkins, S., Rew L., & Sternglanz R. Eating behaviors among school-age children associated with perceptions of stress. Issues in Comprehensive Pediatric Nursing, 28, 175-192, 2005.
14. Orlando, M., Ellickson P. L., & Rand K. J. The temporal relationship between emotional distress and cigarette smoking during adolescence and young adulthood. Journal of Consulting and Clinical Psychology, 69, 959-970, 2001.
15. Grant, K. E., Compas B. E., Thurm A. E., McMahon S. D., Gipson P. Y., Westerholm R. Stressors and child and adolescent psychopathology: Evidence of moderating and mediating effects. Clinical Psychology Review, 26, 257-283, 2006.
16. Rutter, M. Implications of resilience concepts for scientific understanding. Annals of the New York Academy of Sciences, 1094, 1-12, 2006.
17. Owens, J. A., Weiss M. R. Insufficient sleep in adolescents: causes and consequences. Minerva Pediatrica, 69(4):326-33617, Feb 2017.

ANNUAL OF ASSEN ZLATAROV UNIVERSITY, BURGAS
BULGARIA, 2022, v. LI(1)

TENSILE PROPERTIES OF SILANE-TREATED WOOD FLOUR POLYPROPYLENE COMPOSITES BEFORE AND AFTER THERMAL AGEING

Antonia Ilieva, Dimitrina Kiryakova
E-mail: dskiryakova@abv.bg

ABSTRACT

Polypropylene composites with untreated and silane-treated wood flour were obtained and their tensile properties were determined before and after ageing for 1 and 2 months. It was found out that the ageing leads to an increase of the tensile strength of the initial polypropylene to 23 – 27 MPa. Up to 40 mass% content of untreated and treated wood flour in the compositions, the values of the tensile strength remained the same and above this quantity they decreased. The use of more than 30 mass% of the fillers in the polymer matrix leads to decrease of the elongation at break of the materials to 2 – 4% and it did not depend on the surface treatment, the amount of the filler and the thermal ageing period. The increased values of the elasticity modulus (1200 – 1500 MPa) of the wood flour-polypropylene composites allow to achieve high hardness of the materials obtained.

Key words: *polypropylene, wood flour, surface treatment, tensile properties, ageing*

INTRODUCTION

Nowadays, one of the most perspective fields of research is the creation of new materials. In the context of sustainable development, special interest is paid to composites and materials which can, to a certain extent, replace valuable and hardly renewable natural resources.

In recent decades, numerous researchers focused their attention on the development and study of composite materials based on thermoplastics containing various by type and quantity wood fillers obtained from waste timber. As a result of their efforts, various kinds of composites were obtained: some with wood fibers or flakes as structural component and polymers as binding substance; others which are based on a polymer matrix filled with fine wood particles, wood flour.

Among the main advantages of the plant-based fillers are: abundance, low density with comparatively high volume; low abrasiveness which is friendly to the industrial equipment, hence lower production costs; annual reproducibility and, last but not least, biodegradability [1, 2]. This makes them a real alternative to the inorganic fillers. Depending on the nature, physical and chemical composition, as well as on compounding conditions, composites based on the same filler may have quite different properties. The introduction of filler might make the composites cheaper with preserved or slightly worsened physico-mechanical properties or might contribute to their reinforcement (regardless of the price).

A disadvantage of the wood fillers in their use for preparation of polyolefin composites is the weak interphase interaction between the hydrophilic filler and the hydrophobic polymer matrix [3]. For this reason, special attention is paid to the modification or the treatments of the filler by physical or chemical methods aimed at improvement of the filler-matrix interaction and obtaining acceptable properties. Various methods are used to improve the interphase adhesion, including treatment of the wood flour with silanes, stearic acid, maleic anhydride, sodium hydroxide, etc. [4–6].

The present paper reports the studies on the possibility to obtain wood-polymer composites on the basis of polypropylene and the effects of the addition of silane coupling agent on the tensile characteristics of the composites obtained by thermal ageing.

EXPERIMENTAL

Materials

Wood flour (WF) was supplied by Kronospan Bulgaria Ltd; polypropylene (PP) grade 6531, commercial product of Lukoil Neftochim Burgas with melt index 3.5 g 10 min^{-1} (230°C/2.160 kg) and vinyltrimethoxysilane (VTMS) with chemical formula $C_5H_{12}O_3Si$, boiling point 123°C, mo-

lecular weight 148.23 g mol^{-1}, density 0.968 g mL^{-1} and purity 98%, product of Sigma-Aldrich.

Preparation of the filler

The wood flour was dried in a laboratory dryer at temperature 60°C for 24 h. The fraction composition of filler was determined on laboratory analytic vibro sieves. The set of sieves used contained sieves with opening diameters 0.8; 0.63; 0.315; 0.25; 0.16; 0.1 and less than 0.1 mm. The selected fraction with a particle size between 0.25 – 0.16 mm was stored in containers for further characterization and chemical modification.

Wood flour surface treatments

The treatment of the initial wood flour was carried out in 0.003% solution of VTMS in distilled water. The solution obtained was stirred with magnetic stirrer for 5 min. Further, the wood flour was soaked in silane solution at ratio 1:5 for 15 min and dryed in a dryer at 100°C to hydrolyze the coupling agent [7].

After treatment, the resulting filler was stored at room temperature in glass containers. Untreated and treated wood flour samples with VTMS were designated as WF and sWF, respectively.

Preparation of silane-treated wood flour polypropylene composites

The mixing of the polymer with treated and untreated wood flour was carried out in a laboratory roll mill at temperature 170°C and mixing duration of 5 min. The compositions prepared were pressed on a laboratory press PHI (England) between aluminium foils under the following conditions: samples thickness about 1 mm, temperature 180°C, melting period 10 min at 180°C, pressing pressure 9 MPa for 5 min, followed by cooling to 40°C at cooling rate 20ºC min^{-1}. The series of polypropylene composites obtained had filler contents as follows: 1; 3; 5; 10; 20; 30; 40 and 50 mass%, respectively.

Thermal ageing

The thermal ageing of the samples of polypropylene and its composites with wood-flour (WF) and silane treated wood flour (sWF) was carried out in ECOCELL 111 laboratory dryer with natural convection, at temperature of 60°C for periods of one and two months.

Light microscopy

The optical properties of the modified and unmodified wood flour were observed with inverted phase fluorescent microscope ZEISS Axio Vert A1, at total magnifications of: 50×, 100× and 200×.

Fourier Transform Infrared Spectroscopy (FT-IR)

The effect of the different treatments on the chemical structures of the wood flour was studied by FT-IR analysis. The infrared spectra of the fillers before and after the chemical treatment were registered in the wave number region from 4000 to 400 cm^{-1} on a Nicolet iS 50 FT-IR Thermo Scientific spectrophotometer equipped with DTGS KBr detector (4 cm^{-1}) at scan number of 32.

Tensile Properties

The tensile strength (σ, MPa), elongation at break (ε, %) and the Young modulus (E, MPa) for the initial polypropylene and its composites with untreated and silane-treated wood flour before and after thermal ageing were measured according to EN ISO 50527-1 on an INSTRON 4203 dynamometer (England) at speed of 50 mm min^{-1} and room temperature.

RESULTS AND DISCUSSION

It was established that the use of the coupling agent for treatment of the initial wood flour led to a decrease of the filler loose density from 0.1989 g cm^{-3} for WF to 0.1794 g cm^{-3} for sWF, respectively.

The fractionation analysis of the initial powdery wood flour carried out indicated that the predominant fraction had laboratory sieve opening diameter of 0.16 mm (Fig. 1). It was nearly 53% of the total mass analyzed and for this reason it was selected for further treatment and preparation of the polymer compositions.

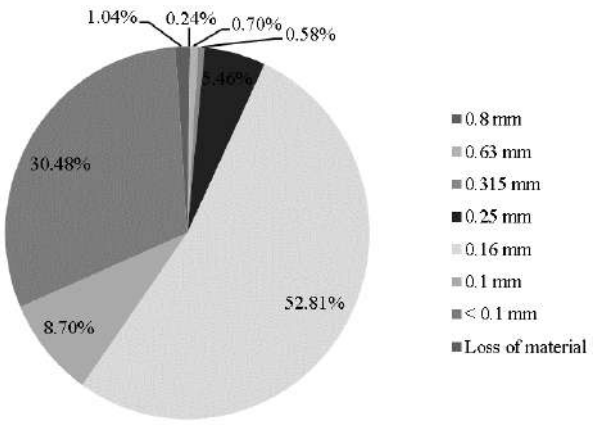

Fig. 1. Fractional composition of wood flour

The state and the morphology of the surface are important factors determining the wetting of the WF by the PP matrix and they have strong

influence on the degree of dispersion and the properties of the composite materials obtained. It was observed by the microscopic studies that the wood flour surface significantly changed after the treatment with silane (Fig. 2b). The changes in the morphology were probably due to the formation of silane coating on the surface of the WF [8].

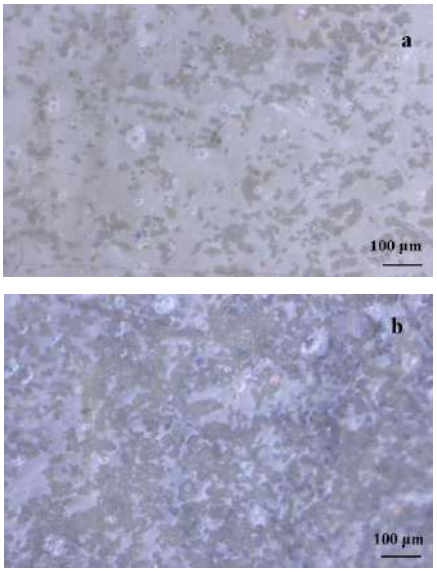

Fig. 2. Microphotographs of untreated (a) and VTMS-treated wood flour (b)

The modifying effect of the VTMS additive on the surface of the WF filler was confirmed by FT-IR spectroscopy. The changes in the absorption bands of WF before and after its treatment are presented in Table 1, as well as the spectrum of the vinyltrimethoxysilane introduced (Fig. 3).

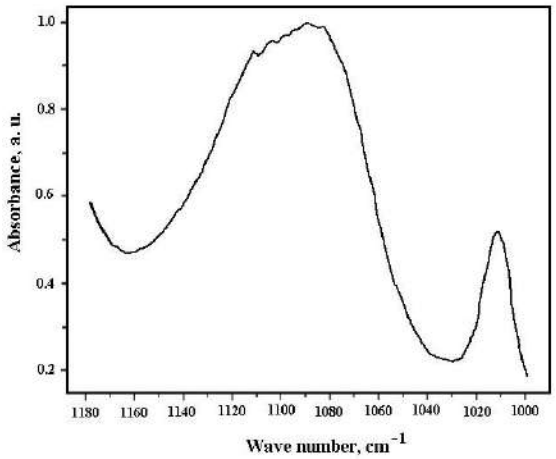

Fig. 3. FT-IR spectrum of vinyltrimethoxysilane [9]

As can be seen in Table 1, the infrared spectrum of the untreated wood flour contains intense bands at 604, 1056, 2898 and 3383 cm^{-1}. Beside them, peaks were registered also at wave number values of 1106, 1153, 1270, 1373, 1420, 1510, 1592, 1640 and 1730 cm^{-1}. The absorption bands at 604, 1640 and 3383 cm^{-1} are characteristic for off-plane vibrations, bending vibrations and stretching vibrations of the O–H fragments present in the structure of the wood flour [10]. The clear peaks at 1056 and 1270 cm^{-1} indicate C–O stretching vibrations in the structures of cellulose and lignin. On the other hand, the shoulder shaped bands localized at 1106 and 1153 cm^{-1} indicate for bending vibrations of C-O-C in lignin composition [11]. The bands in the range from 1300 to 1500 cm^{-1} characterize off-plane vibrations, bending vibrations of the C–H bonds in the structure of methyl (–CH_3) and methylene (–CH_2) fragments. Beside the off-plane and bending vibrations, the presence of C–H stretching vibrations in cellulose were also registered in the infrared spectrum of unmodified wood flour as an intense peak at wave number value of 2898 cm^{-1}. The absorption band located at 1730 cm^{-1} is due to C=O stretching vibrations of carbonyl groups taking part in lignin composition. The bands at 1510 and 1592 cm^{-1} indicate in-plane vibrations of C=C in the structure of aromatic rings present in the cellulose and lignin compositions [12].

It was found out that the profile of the infrared spectrum of the wood flour underwent certain changes after the treatment with silane coupling agent (VTMS) expressed as slight increase of the intensities of the absorption bands at 604, 1106, 1153, 1640, 2898 and 3383 cm^{-1}. To find an explanation of the effects observed, the nature of the chemical interactions (C–H, O–C and Si–O) in silane structure was taken into account (Fig. 3). The presence of the latter is the reason why the infrared spectrum of VTMS contained bands at 1098 (O–C bending vibration) 1192 (O–C stretching vibration) and 2842 cm^{-1} (C–H stretching vibration) [13]. Thus, the higher intensities of the bands at 1106, 1153 and 2898 cm^{-1} observed in the wood flour spectrum after the treatment might be due to superposition of additional C–O and C–H vibrations in the structure of CH_2=Si(OCH_3)$_3$.

Unlike the bands mentioned above (1106, 1153 and 2898 cm^{-1}), the change of the intensities of the bands at 604, 1640 and 3383 cm^{-1} (all of them connected with the O–H vibrations in the wood flour) was unexpected since the structure of the silane coupling agent does not contain hydroxyl groups.

Table 1. Characteristic peaks observed in the FT–IR spectra of untreated and silane-treated WF

Wave length, cm^{-1}	Characteristic peaks
604, 1640, 3383	off-plane vibrations, bending vibrations and stretching vibrations of the O–H fragments present in the structure of the wood flour
1056, 1270	C–O stretching vibrations in the structures of cellulose and lignin
1106, 1153	bending vibrations of C-O-C in lignin composition
1373, 1420	off-plane vibrations, bending vibrations of the C–H bonds in the structure of methyl ($–CH_3$) and methylene ($–CH_2$) fragments
1510, 1592	in-plane vibrations of C=C in the structure of aromatic rings present in the cellulose and lignin compositions
1730	C=O stretching vibrations of carbonyl groups taking part in lignin composition
2898	C–H stretching vibrations taking part in cellulose composition

In other words, the change of the intensities of the bands at 604, 1640 and 3383 cm^{-1} after the WF treatment with $CH_2=Si(OCH_3)_3$ should not be related to superposition of vibrations of chemical bonds (O–H) of the VTMS. This is the reason to look for another cause which could explain the differences registered, namely the existence of surface interaction between wood flour and silane. Since the bands at 604, 1640 and 3383 cm^{-1} characterize O–H groups, the surface effects are probably related to the formation of intermolecular hydrogen bonds (Si–O···C–O(H) and C–O···H–C) by the interaction of oxygen atoms from the structure of WF/VTMS with hydrogen atoms from the structure of VTMS/WF. It should be noted that the absorption bands at 604, 1640 and 3383 cm^{-1} underwent only a slight increase of their intensities but did not change their position and width. The preservation of the band position means that the nature of the surface intermolecular hydrogen bonds is strictly electrostatic. The lack of widening of the infrared bands after the wood flour treatment might be related to the small number of newly formed intermolecular interactions, probably due to the low content of silane coupling agent (< 1 wt.%).

Table 2. Tensile strength of PP composites with different contents of untreated and silane-treated wood flour before and after ageing

Sample	Tensile strength σ, MPa					
	Before ageing		After ageing for 1 month		After ageing for 2 months	
	WF	sWF	WF	sWF	WF	sWF
Initial PP	15.04		19.12		17.49	
PP + 1 mass%	24.08	23.73	27.26	22.84	27.43	26.23
PP + 3 mass%	23.35	22.44	25.25	25.81	27.17	26.38
PP + 5 mass%	23.92	22.87	25.08	23.28	25.81	26.28
PP + 10 mass%	22.78	22.35	22.91	25.32	24.89	25.86
PP + 20 mass%	21.02	22.37	22.69	22.05	23.63	23.82
PP + 30 mass%	18.53	20.66	18.24	19.50	22.54	23.24
PP + 40 mass%	17.00	16.54	15.15	18.73	20.50	19.94
PP + 50 mass%	14.67	9.78	13.81	12.12	17.45	12.86

The influence of the additive of WF and sWF and their amount on the tensile strength (σ, MPa) of the PP composites was studied before and after ageing and the results obtained are presented in Table 2. As can be seen from the table, even at WF and sWF content as low as 1 mass%, the tensile strength of the samples with WF and sWF (24.08 and 23.73 MPa, respectively) was higher than that of pure polypropylene (15.04 MPa). With the further increase of the filler content up to 30 mass% (WF and sWF), the tensile strength remained in the range from 18.53 to 20.66 MPa and it was still higher than that of the initial PP [14]. The improvement of the tensile strength and the preservation of its value up to 30 mass% content of sWF in the composites are

probably due to adhesion at the phase boundary between the wood flour and PP matrix as a result of the treatment of the filler with modifying agent (VTMS). By this method, the adhesion between the two components of the composite materials can be substantially improved so the strain in the PP matrix is uniformly distributed to the wood fibers.

At 40 mass% content of untreated and silane-treated WF, the tensile strength of the compositions studied had values close to these of the initial PP – about 17 MPa. At higher contents σ started decreasing to reach 14.67 and 9.78 MPa, respectively. The decrease of the tensile strength of the PP-WF composites observed is in accordance with previous studies [15].

The effect of 30-day and 60-day ageing on the tensile properties of PP filled with WF or sWF was of a similar trend. The increase of the tensile strength from 19.12 and 17.49 MPa for the initial PP subjected to ageing to 23 – 27 MPa might be due to cross-linking processes taking place between polymer chains which could also lead to higher values of σ.

Table 3. Elongation at break of PP composites with different contents of untreated and silane-treated wood flour before and after ageing

Sample	Elongation at break ε, %					
	Before ageing		After ageing for 1 month		After ageing for 2 months	
	WF	sWF	WF	sWF	WF	sWF
Initial PP	42.8		20.7		39.9	
PP + 1 mass%	19.3	10.4	19.3	10.4	12.6	15.6
PP + 3 mass%	9.7	10.0	9.7	10.0	10.9	8.6
PP + 5 mass%	6.9	6.4	6.5	6.4	9.6	7.1
PP + 10 mass%	6.8	5.6	6.8	5.6	9.8	6.8
PP + 20 mass%	5.3	4.2	5.3	4.2	5.7	5.4
PP + 30 mass%	3.6	3.0	3.6	3.1	4.3	3.9
PP + 40 mass%	2.9	2.6	2.9	2.6	2.8	2.7
PP + 50 mass%	2.2	1.8	2.2	1.8	2.3	1.8

The elongation at break (ε, %) of the compositions containing untreated and silane-treated WF in PP matrix, as well as the materials based on them was determined after ageing. For the samples of initial polypropylene, the elongation at break was 42.8% while for these subjected to ageing for 30 and 60 days it was 20.7 and 39.9 %, respectively (Table 3). The lower value of the elongation at break of PP after 1month ageing was probably due to its oxidation. This is because the macrochain of polypropylene contains tertiary carbon atoms which are sensitive points of attack during ageing [16].

After the introduction of 1 mass% wood flour, as well as silane-treated wood flour in PP matrix, the elongation at break decreased from 42.8% to 19.3 and 10.4 %, respectively. The introduction of higher amounts of filler results in further decrease of the elongation. At contents in the range 30 – 50 mass% WF in the compositions ε was almost independent on the surface treatment of the filler and its amount [14]. For all these compositions (containing more than 30 mass% WF and sWF), the elongation at break before and after treatment remained in the interval from 2% to 4%. Such behavior after introduction of natural fillers in PP has been observed by a number of authors [15, 17]. The decrease of the elongation at break of the composites probably due to the decreased mobility of the macromolecules because of the creation of physical bonds between the filler and the polymer.

It can be seen from Table 4 that all the compositions with untreated and silane-treated WF, before and after the ageing period, possessed a comparatively higher elasticity modulus (E, MPa) compared to the initial PP and PP after 1 month (695 MPa) and 2 months (526 MPa), respectively. Other researchers [17–19] found out that the value of the elasticity modulus of the filler is one of the main factors which affected the modulus of the composite obtained with it, i.e. the high elasticity modulus of wood flour, compared to that of pure PP, may be responsible for the increase of the property studied after the addition of WF in the PP matrix.

Table 4. Modulus of elasticity of PP composites with different contents of untreated and silane-treated wood flour before and after ageing

Sample	Modulus of elasticity *E,* MPa					
	Before ageing		After ageing for 1 month		After ageing for 2 months	
	WF	sWF	WF	sWF	WF	sWF
Initial PP	756		695		526	
PP + 1 mass%	855	948	855	948	738	779
PP + 3 mass%	931	950	931	880	739	895
PP + 5 mass%	984	951	984	852	851	987
PP + 10 mass%	999	963	999	963	954	1038
PP + 20 mass%	1081	1149	1081	1149	973	1149
PP + 30 mass%	1131	1215	1131	1315	1201	1162
PP + 40 mass%	1141	1251	1141	1251	1378	1588
PP + 50 mass%	1197	1251	1197	1173	1251	1034

A significantly higher increase of the elasticity modulus was observed after the addition of sWF, especially for the materials containing 30 and 40 mass% filler. For instance, the elasticity modulus of the PP materials containing 40 mass% sWF reached values of 1250 MPa [14]. The modulus of the same composition subjected to ageing for 30 days remained the same. The higher value of the elasticity modulus in this case was probably due to the improved adhesion between polypropylene and the VTMS treated WF [17]. This additional increase of the modulus was observed also with still higher sWF content up to 50 mass% in the composites. Pure PP subjected to 2 months ageing showed significant decrease of the elasticity modulus values. The same tendency was found also for the composites containing up to 20 mass% WF filler which was attributed to the predominating phase in the composite – poly-propylene. At filler content from 30 to 50 mass% WF, the elasticity modulus increased probably due to the higher modulus of the wood flour.

CONCLUSIONS

Composite materials were obtained on the basis of PP with filler of 1 to 50 mass% untreated and silane-treated wood flour. The surface of the filler was treated with silane coupling agent – vinyltrimethoxysilane. From the microscopic studies and the changes observed in the FT-IR spectrum of the treated wood flour, a slight increase of the intensities of the absorption bands at 604, 1640 and 3383 cm^{-1} was confirmed. It was connected with the newly formed intermolecular interactions. The tensile characteristics of the wood flour filled composites obtained were determined after ageing and compared to those of pure polypropylene samples.

REFERENCES

1. Ezzahrae, M.F., A. Nacer, E. Latifa, Z. Abdellah, I. Mohamed and J. Mustapha. *Mater. Today Proc.*, https://doi.org/10.1016/j.matpr.2022.08.394, (2022), in press.
2. Karimah, A., M.R. Ridho, S.S. Munawar, D.S. Adi, Ismadi, R. Damayanti, B. Subiyanto, W. Fatriasari and A. Fudholi. *J. Mater. Res. Technol.*, **13**, (2021), p. 2442.
3. Syuhada, D. N. and A. R. Azura. *Polymers*, **13**, (2021), p. 3600.
4. Zhou, Y. *Interface Optimisation and Bonding Mechanism of Rubber-Wood-Plastic Composites, Brunel University, London, 2018*, PhD thesis.
5. Zelča, Z., S. Kukle and J. Kajaks. *Mater. Sci. (Textile and Clothing Technology)*, **11**, (2016), p. 6.
6. Souissi, S., F. Lachtar, A. Elloumi and A. Bergeret. *Iran. Polym. J*., (2022), https://doi.org/ 10.1007/s13726-022-01089-x.
7. Zahari, W.Z.W., R.N.R.L. Badri, H. Ardyananta, D. Kurniawan and F.M. Nor. *Procedia Manuf.*, **2**, (2015), p. 573.
8. Thakur, M., R. Gupta and V. Thakur. *Carbohydr. Polym.*, **111**, (2014), p. 849.
9. Li, Z., G. Hu, J. Corriou, S. Hoppe, C. Fonteix, R. Laine, J. Habimana and D. Deheunynck. *Polym. Eng. Sci.*, **53**, (2013), p. 1571.

10. Niu, Z., Y. Chen and J. Feng. *J. Appl. Polym. Sci*., **133**, (2016), p. 43108.
11. Zhao, X., K. Ouyang, S. Gan, W. Zeng, L. Song, S. Zhao, J. Li, M.S. Doblin, A. Bacic, X.-Y. Chen, A. Marchant, X. Deng and A.-M. Wu. *Front. Plant Sci.*, **5**, (2014), p. 602.
12. Emmanuel, V., B. Odile and R. Céline. *Spectrochim. Acta A Mol. Biomol. Spectrosc*., **136 C**, (2015), p. 125.
13. Ma, L., S. Dong, Z. He, Y. Yang, H. Jia, Y. Di, Y. Tanga and Y. Wang. *RSC Adv*., **6**, (2016), p. 98761.
14. Ilieva, A. and D. Kiryakova. Determination of Physico-Mechanical and Rheological Properties of silane-treated wood flour Polypropylene Composites, *J. Chem. Technol. Metall.*, (2022), in press
15. Bouza, R., M.J. Abad, L. Barral and M. Ladra, *Polym. Eng. Sci*., **49**, (2009), p. 324.
16. García-Montelongo, X.L., A. Martínez-De La Cruz, S. Vázquez-Rodríguez and L.M. Torres-Martínez. *Mater. Res. Bull*., **51**, (2014), p. 56.
17. Demir, H., U. Atikler, D. Balköse and F. Tıhmınlıoğlu. *Compos. Part A Appl. Sci. Manuf*., **37**, (2006), p. 447.
18. Ansari, M. and H. Ismail. *J. Reinf. Plast. Compos*., **28**, (2009), p. 3049.
19. Gironès, J., J. Méndez, S. Boufi, F. Vilaseca and P. Mutjé. *J. Appl. Polym. Sci*., **103**, (2007), p. 3706.

ANNUAL OF ASSEN ZLATAROV UNIVERSITY, BURGAS
BULGARIA, 2022, v. LI(1)

RESEARCH OF A PARALLEL OSCILLATING SCHEME IN SIMULINK

Vasil Ivanov
E-mail: vasil_bi@mail.bg

ABSTRACT

The processes in a parallel oscillating circuit consisting of resistor R, coil L and capacitor C in Simulink software environment with predominant resistive (R) character are modelled, with predominantly resistive inductive (RL) character and with predominant resistive capacitive (RC) character. The processes in the circuit for regulating the inductance L and the capacitance C in an established mode are investigated. The results of the simulations for the three variants are analyzed. After comparing the magnitudes of the active powers, the effect of the received active energy is determined.

Key words: *parallel oscillating circuit, filter, inductance L, capacitance C, resistance R, Simulink*

INTRODUCTION

There are two main types of resonance phenomena differentiated:

- voltage resonance or resonance of series-connected RLC elements in unbranched electrical circuit (EC);

- resonance at currents or resonance of parallel connected models of RLC passive elements.

- When modelling a resonant mode in parallel EC, its equivalent total conductivity Y_e consists only of the active ingredient G_e. Then the reciprocal value of the conductivity Y_e, the impedance Z_e, takes a maximum value. Therefore, the current is minimal and coincides in phase with the generated sinusoidal voltage.

Aims:

Simulation of the three mode states by setting the parameters of the parallel oscillating circuit RLC.

• Reporting data on the voltage and current data of a parallel oscillating circuit RLC after starting the simulation and recording reactive and active power.

• Analysis of the energy characteristics and diagrams in the three work modes.

THEORETICAL PRESENTATION

Resonance of currents:

Computational part used in the modelling of the resonant modes:

• The relationship between the angular frequency ω and the linear frequency f is determined by the dependence:

$$\omega = 2.\pi.f \quad (1)$$

• The frequency condition for resonance is:

When the own resonant frequency ω_0 of the oscillating circuit coincides in value with the angular frequency ω of the input sinusoidal signal, the phase difference φ_e between current and voltage is zero and resonance occurs. The difference between the two reactive conductivities of (2) determines the total conductivity of $\mathbf{B_e}$.

• The equivalent (full) conductivity of a parallel RLC oscillating circuit is:

$$\dot{Y}_e = G + j.B_e = \mathrm{G} + \mathrm{j}.(\omega_0.\mathrm{C} - \frac{1}{\omega_0.L}) \quad (2)$$

When the magnitudes of the inductive B_l and capacitive conductivity B_c are equalized, the resonance condition is fulfilled and $B_e = 0$. The equivalent conductivity Y_e becomes only active:

$$\dot{Y}_e = \mathrm{G} + j.(B_L - B_C) = G \quad (3)$$

• Resonant frequency

The own resonant frequency ω_0 of the parallel oscillating circuit is calculated when the values of inductance **L** and capacitance **C** are amended according to the formula:

$$\omega_0.\mathrm{L} = \frac{1}{\omega_0.C} \text{ or } \omega_0^2.\mathrm{L}.C = 1 \quad (4)$$

or

$$\omega_0 = \frac{1}{\sqrt{L.C}} \quad (5)$$

• The wave resistance (loss) in Ω is:

$$\rho = \sqrt{\frac{L}{C}} = \omega_0.\mathrm{L} = \frac{1}{\omega_0.C} \quad (6)$$

• The wave conductivity of the resonance is:

$$\gamma = \sqrt{\frac{C}{L}}, \quad (7)$$

• Quality factor (Q - factor) on the RLC circlet in resonance mode is:

$$Q = \frac{\sqrt{\frac{C}{L}}}{G} = \frac{\gamma}{G} \qquad (8)$$

Conclusions:

• The quality factor shows how many times the rms of the current in any of the elements is greater than the rms of the total resonance current. Therefore, at Q>1 in the circuit conditions are created for current amplification.

• Parallel resonance is popular in modern radio equipment at Q = 10 ÷ 500.

• In the ideal parallel RLC circuit, current resonance is received when the amplitudes of the reactive currents are equalized, $I_L = I_C$.

• The variable components of the inductive and capacitive elements have inversed phase, i.e. at the maximum value of the energy in the capacitor the energy in the coil is of the same magnitude but with the opposite sign.

• In the theory of alternating current circuits, it is proved that the current through an ideal coil lags behind the voltage by 90º, and the current through the ideal capacitor precedes the voltage by 90º.

• Capacitor C and coil L continuously exchange energy throughout resonance. The phase difference between current and voltage in resonant mode is φe = 0. Therefore, the reactive power emitted by the source is zero and no energy exchange between the source and the oscillating circuit takes place.

• The initial accumulation of energy takes place when the circuit is connected to the source. It only covers the active losses in the resistor R. It is associated with heat loss or the Joule effect.

EXPERIMENTAL

Resonance of currents:

Modelling in a Simulink software environment of parallel resonance [1, 2, 3, 4, 5];

Model of the experimental setup:

The experiment in parallel resonance mode involved three ideal elements according to the diagram in Fig.1.

The diagram in Fig.1 shows the pictograms (coloured differently) of the source with parameters: sinusoidal voltage U_{in} with the amplitude of U_{max} =50V, a current I_{RLC} and linear frequency as networked f=50Hz The pictograms of the passive elements are also shown: capacitor C, coil L and its active resistance R_L.

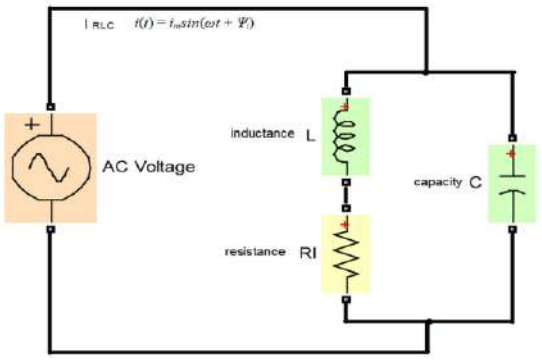

Fig. 1. Scheme constructed with an ideal sinusoidal source and a parallel oscillating circuit R, L and C in the Simulink programming environment.

1. Model of the first version of a parallel oscillating circle with setting for **predominant resistive - inductive nature.**

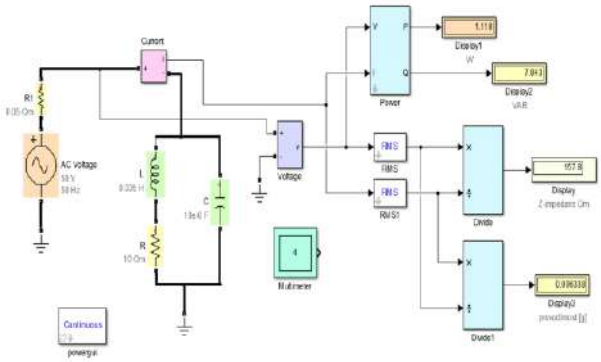

Fig. 2. Scheme in Simulink environment of parallel oscillating scheme with setting for predominant RL character.

The model in Fig. 2 was started and the rms values of active power (W), reactive power (VAR), impedance (Ω) and conductance (Siemens) were measured. The readings from the simulation are visualized on Display1, Display2, Display3 and Display4.

Specific values are set in the capacitor and coil model dialogs for this mode of operation of the oscillating circuit: for the capacitor $C=10.10^{-6}$ F, for the coil L=0.335 H and for the resistor R=10 Ω. After substitution with values in (5) for the resonant frequency of the oscillating circuit, the following is obtained:

$$\omega_0 = \frac{1}{\sqrt{L.C}} = \frac{10^3}{\sqrt{0.335.10}} = 546.358, s^{-1} \qquad (9)$$

The calculated circuit frequency is higher than the generator frequency as the measured imped-

ance of the circle Z is of magnitude **157.8 Ω** (Display in Fig.2). The reactive power Q has a positive sign and a magnitude of **7.843 VAR.** and shows a predominantly inductive nature of the circuit.

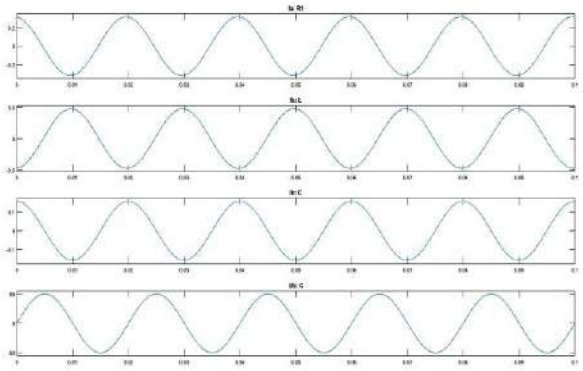

Fig. 3. The result of the simulation obtained from the Multimeter block in Fig. 2.

The charts in Fig. 3 are simulated by a Multimeter block set to measure four quantities. They report instantaneous values of currents in the models of L and C, as well as the input voltage of the parallel EV. I_L and I_C charts report $I_L > I_C$.

2. Model of the second version oscillating circuit of parallel RLC elements with setting to create resonance. The model in Fig. 4 has capacitor setting C=30.10-6 F and coil L=0.335 H. After substitution in equation (5), we obtain the own resonant frequency of the scheme, matching the source frequency [6]:

$$\omega_0 = \frac{1}{\sqrt{L.C}} = \frac{10^3}{\sqrt{0{,}335.30}} = \mathbf{314,44}s^{-1} \qquad (10)$$

The models of the measuring instruments shown in Fig. 4 read the maximum value of the impedance of the circuit **Z = 1119 Ω** and reactive power **Q = 0 VAR**.

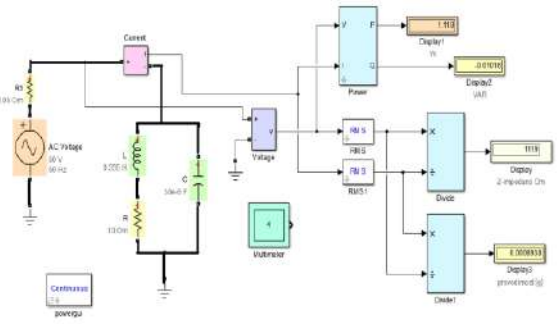

Fig. 4. Result diagrams and tabular data from the frequency synthesis of the output current with a control algorithm 35%/50%.

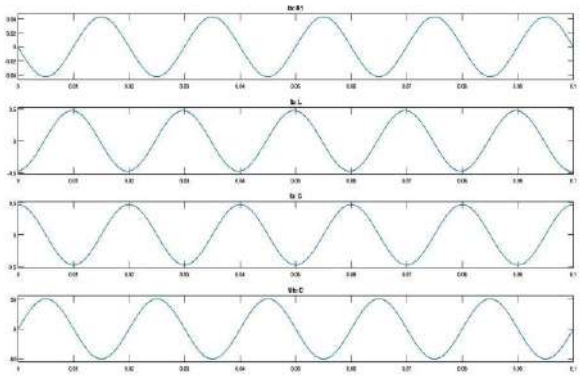

Fig. 5. Diagrams from the simulation obtained with the Multimeter block at resonance.

The diagrams in Fig. 5 show maxima of the same magnitude and opposite sign currents in the coil and capacitor $I_L = I_C$. This leads to their mutual compensation and zeroing of the reactive power.

The conclusion is that the reported impedance of the oscillating circuit Z is a maximum and purely active R.

3. Model of the third version of a parallel oscillating circuit. The elements are mainly set with resistive capacitive character.

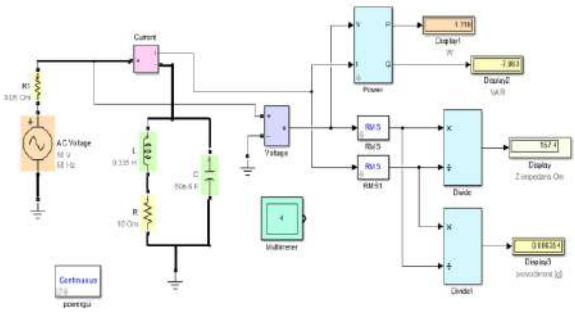

Fig. 6. Diagram of a parallel RLC scheme with a predominant RC character in a Simulink programming environment.

The simulation of Fig. 6 is started and the measuring instruments visualize the rms values of active power (W), reactive power (VAR), impedance (Ω) and conductivity (Siemens). Negative reactive power is predominant, which is defined as capacitive. The values are set for a capacitor C=50.10-6 F for coil L= 0.335 H and determine the resonant frequency of the oscillating circuit by (5):

$$\omega_0 = \frac{1}{\sqrt{L.C}} = \frac{10^3}{\sqrt{0.335.50}} = 47.376s^{-1} \qquad (11)$$

The measured circuit frequency is lower than the one generated by the source and determines a

higher capacitive conductivity B_C from that at resonance. For this reason, reactive power predominates Q with a negative sign shown by Display2. The measured impedance of the circuit is Z=157.4 Ω.

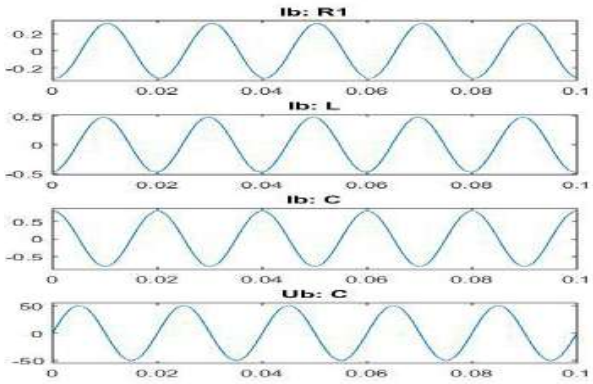

Fig. 7. Diagrams with predominantly resistive capacitive character.

The amplitudes of the sinusoidal functions of the two currents through the capacitor and the coil differ, both in phase and in amplitude. The higher maximum value of IC compared to IL (Fig.7).

4. Tabular data from the results of the simulation measurements and the calculations

Table 1. Kinetics characteristics of a parallel oscillation

Type modelling	Q_{RLC} VAR	Z Ω	G S	ω_{RLC} s^{-1}	ω_0 s^{-1}
R_L	7.84	157.8	0.006	546.4	314
R	0	1119	0.0009	314.4	314
R_C	-7.86	157.4	0.007	47.4	314

CONCLUSIONS

By simulating a parallel RLC oscillating circuit, the effect of equalizing the natural resonance frequency with that of the source is established [4]. The models prove the practical application of the formulas from the theoretical part and fulfil the set values exactly.

- At resonance, the impedance Z of the oscillating circuit is 1000 times higher in comparison with the two versions in Table 1 and is purely active.
- It finds application in the design of resonant amplifiers and receivers.
- The resonance is used in designing bandpass filters and in communication technologies.
- Selective properties are used to adjust the input steps and antennas of receiving and transmitting devices.
- Resonance is a condition for providing maximum power under active load and improving the power factor in electrical power stations [4,5].

REFERENCES

1. Ivanov V. *Simulation, modelling and analysis of a series oscillating circuit*. IOP Conf. Series: Materials Science and Engineering; International Scientific Conference on Communications, Information, Electronic and Energy Systems – CIEES 2021, AIP Conf. Proc. 2570, 030010-1–0300108, (Published Online: 18 August 2022): https://doi.org/10.1063/5.0100042;
2. Ivanov V. *Modeling of three-phase inverter power supply system in Simulink*. IOP Conf. Series: Materials Science and Engineering, 1032 (2020) 012054, doi:10.1088/1757-899X/1032/1/012054;
3. Ivanov V. *Analysis of computer simulation in software environment of one phase bridge voltage inverter for a photovoltaic system*. Annual of Assen Zlatarov University, Vol. XLVI, Burgas 8010, Bulgaria, , Book 1, 2017, ISSN 1312-1359;
4. Ivanov V. *Modeling of three-phase inverter power supply system in Simulink*. IOP Conf. Series: Materials Science and Engineering, 1032 (2020) 012054, doi:10.1088/1757 899X/1032/1/012054;
5. Ivanov V. *Modeling of single phase inverter system in Simulink software*. Assen Zlatarov University, Annual, Vol. XLIX, Book 1, 2020, Burgas 8010, Bulgaria, ISSN 2603-3968;
6. Ivanov V. *A simulation method for improving the efficiency of power lines from electric networks.* Proceedings of the Union of Scientists - Ruse, Book 1, Technical Sciences, Volume 16, ISSN 1311-106X, pp. 50- 56, 2022.

ANNUAL OF ASSEN ZLATAROV UNIVERSITY, BURGAS
BULGARIA, 2022, v. LI(1)

STRUCTURAL AND SURFACE CHARACTERISTICS OF CHEMICALLY MODIFIED WASTE EGG SHELLS

Dimitrina Kiryakova, Ganka Kolchakova
E-mail: gkolchakova@gmail.com

ABSTRACT

Most of the reagents used for the treatment of waste egg shells reported are expensive, dangerous and require the application of relatively complex modification methods. Therefore, the aim of the present paper is to consider the possibility of using a simple method for efficient surface treatment of waste egg shells with suitable modifying reagents. Egg shell powders were subjected to a chemical surface modification by the direct method. The effect of chemical treatment on the surface characteristics of waste egg shells was studied. Standard Brunauer-Emmett-Teller (BET) method was employed to study porous characteristics of unmodified and modified egg shells, including total pore volume, average pore radius, specific surface area and cumulative pore volume. The chemical structure of waste egg shells before and after treatment was characterized by SEM, XRD and FT-IR analyses and compared to that of commercial calcium carbonate $CaCO_3$.

Key words: *waste egg shells, modification, pore volume, specific surface area, structure*

INTRODUCTION

Egg shells consist of two parts: the egg shell itself, which contains mainly calcium carbonate, and the egg shell membrane, which has a protein structure. The chemical composition of egg shells has been widely reported in the literature [1, 2]. The main component of the shells is calcium carbonate in the form of calcite of 94–97% [3–5], 3–4.5% organic matter [6, 7] and insignificant amount of MgO (0.83%), SO_3 (0.66%), P_2O_5 (0.43%), Al_2O_3 (0.15%), K_2O (0.08%), SiO_2 (0.07%), Cl_2O_3 (0.06%) and SrO (0.04%) [5, 8]. The membrane of the egg shell is purely organic. It consists of various proteins whose composition has been discussed in the literature [2, 9–11]. The quantified density of egg shell is: 2.50 g/cm^3 [12], 2.53 g/cm^3 [3], 2.59 g/cm^3 [13] and 2.62 g/cm^3 [4] and it is slightly lower than that of mineral limestone, probably due to the porous nature of the egg shells.

Despite the potential of egg shells as an alternative to calcium carbonate, after proper treatment and treatment of their waste, the scope of their application can be further expanded. Reusing egg shells as a source of raw materials for other industries would help protect the environment and reduce production costs.

Most of the reagents used for the treatment of waste egg shells reported are expensive, dangerous and require the application of relatively complex modification methods. Therefore, the present paper considers the possibility of using a simple economical method for efficient surface treatment of waste egg shells with suitable environmentally friendly modifying reagents.

To achieve this goal, the direct method of modification was chosen, and H_2O_2 and $KMnO_4$ were used as modifying agents for the waste egg shells. The effect of direct chemical modification on the surface characteristics of waste egg shells before and after chemical treatment was observed and compared with that of commercial calcium carbonate.

EXPERIMENTAL

Materials

Hydrogen peroxide (H_2O_2), 30% aqueous solution purchased from Showa chemical Co. was used without further purification and potassium permanganate ($KMnO_4$) with molecular weight 158.03 g/mol and purity 99%, product of Sigma-Aldrich, were used as reagents for surface treatment of waste egg shells. Commercial calcium carbonate with chemical formula ($CaCO_3$) with molecular weight 100.09 g/mol and purity 99%, product of Sigma-Aldrich, was used to compare the surface characteristics of waste egg shells before and after chemical treatment.

Preparation of waste egg shells

The collected waste egg shells were washed with hot tap water without removing the membrane from them and left in air for 24 hours. Then they were dried in air oven at 90°C to constant weight. The dried egg shells were crushed mechanically and sieved. The selected fraction with a particle size smaller than 0.315 μm was stored in containers for further characterization and chemical modification.

Egg shells chemical surface modification

The egg shells powder was chemically modified by the direct method after immersion in the modifying solutions as follows: 50 g of egg shells powder were soaked in 5% solution of $KMnO_4$ and 30% solution of H_2O_2 under stirring at 25° for 1 hour at 420 rpm. After the treatment with the above reagents, the resulting modified egg shells were filtered, dried and stored in glass containers at room temperature until their characterization. Egg shell samples treated with $KMnO_4$ and H_2O_2 were designated as $KMnO_4$-ES and H_2O_2-ES, respectively.

Scanning electron microscopy

SEM analyses were performed on a JSM 6390 electron microscope (Japan) in conjunction with energy dispersive X-ray spectroscopy (EDS, Oxford INCA Energy 350) equipped with ultrahigh resolution scanning system (ASID-3D) in regimes of secondary electron image and back scattered electron image. Before attempting SEM characterization, the sample must be clean and completely dry. Surface oils or dirt must be removed with solvents such as methanol or acetone. The sample is mounted on a double coated conductive carbon tape that holds the sample firmly to the stage surface and can be used as a ground strap from the sample surface to sample holder. The samples were gold coated for ~ 40 s. Gold at that thickness will have little or no effect on elemental analysis. The accelerating voltage was 20 kV, I ~ 75 mA. The pressure was of the order of 10^{-4} Pa.

X-ray Diffraction analysis

The X-ray diffraction patterns were taken by using a PANalytical Empyrean apparatus at atmospheric pressure, room temperature, Ni-filtered Cu target K_α radiation in the interval $2\theta = 5 – 80°$.

Fourier Transform Infrared Spectroscopy (FT–IR)

FT-IR analysis was used to estimate the effect of modifying agents on the chemical structures of waste egg shells. Waste egg shells before and after chemical treatment were prepared in the form of KBr tablets and were analyzed using spectrophotometer Nicolet iS 50 FT-IR Thermo Scientific in the interval 4000 – 400 cm^{-1}. The results obtained were compared to these from commercial calcium carbonate $CaCO_3$.

Brunauer-Emmett-Teller (BET) method

Standard Brunauer-Emmett-Teller (BET) method was employed to study the porous characteristics of the initial and the modified samples of waste egg shells. The textural properties of the egg shell samples were obtained through BET analysis on an apparatus Surfer sorption analyzer (Thermo Scientific) using N_2 adsorption-desorption isotherms at –196°C. The BET surface area (m^2/g), total pore volume (cm^3/g), Barrett-Joyner-Halenda average pore radius (nm) and cumulative pore volume (cm^3/g) were thus obtained by the N_2 adsorption data.

RESULTS AND DISCUSSION

To identify the changes caused by the different treatments of egg shells powder surface, SEM analysis was carried out. SEM images of untreated and treated egg shell powders taken at 10 000× magnification are shown in Fig. 1. Before the treatment, the initial egg shells consisted of irregularly shaped particles of different sizes and many small pores (holes) of the same size can be observed on the particles surface. The SEM images of the ES samples after treatment with $KMnO_4$ and H_2O_2 showed identical morphology of the particles. Both samples consisted of irregularly shaped particles with different sizes. After the treatment, depositions of particles were observed on the surface of the egg shells ($KMnO_4$-ES) and the surface roughness was changed (H_2O_2-ES).

The subsequent Fig. 2 shows XRD diffraction patterns of the commercial $CaCO_3$, as well as the initial ES, H_2O_2-ES and $KMnO_4$-ES. The diffraction pattern of the commercial $CaCO_3$ contains intense peaks at diffraction angles (2θ) 29.42°, 35.99°, 39.42°, 43.17°, 47.53°, 48.5°, 57.39° and 61.40° [14]. The analysis of the registered peaks indicated that the diffraction angles are characteristic for the crystalline phase of calcite. They correspond to diffraction of X-rays from the following planes of the crystal lattice: 104, 110, 113, 202, 018, 116, 122 and 113.

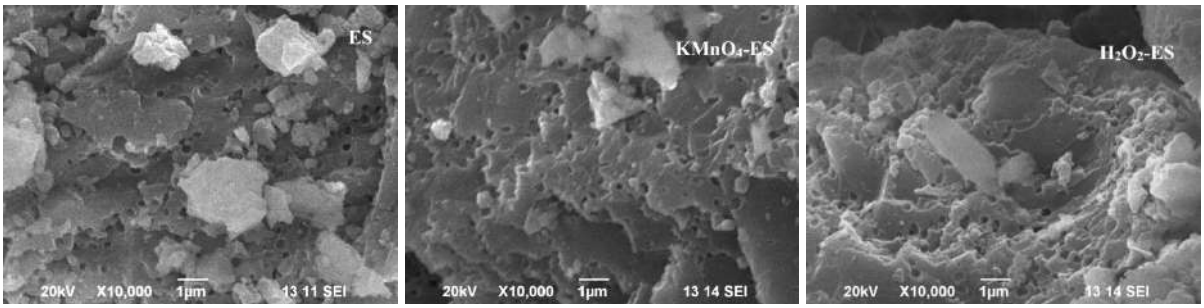

Fig. 1. SEM images of waste egg shells before and after chemical treatment

The number of diffraction peaks did not change significantly before and after treatment, which indicates that no new phases were formed after the modification. Only an insignificant change of the main crystal structure was observed, which resulted from the modification of the surface. It can be seen in the same Fig. 2 that, due to the treatment carried out, the intensities of diffraction peaks of H_2O_2-ES were smaller than those registered from raw egg shells, which might be attributed to the decrease of crystal size because of the modification. The relative crystallinity of the samples was higher than that of ES and H_2O_2-ES, since the treatment with $KMnO_4$ probably leads to removal of the impurities on the surface and changes surface roughness as it was confirmed by SEM (Fig. 1).

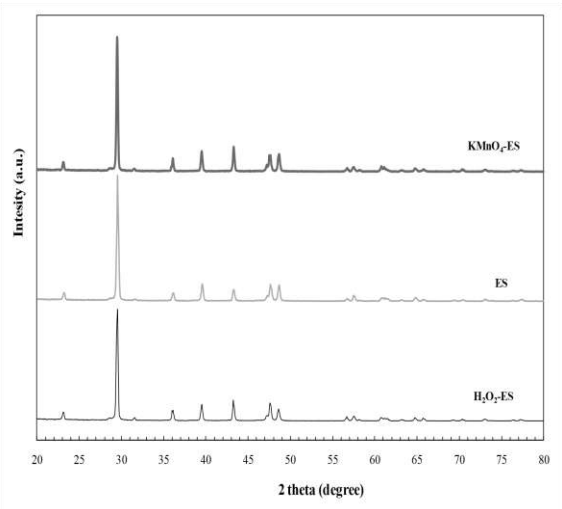

Fig. 2. XRD diffraction patterns of waste egg shells before and after chemical treatment

FT-IR analysis was used to evaluate the effect of the modifying agents on the chemical structures on the surface of waste egg shells. Fig. 3 shows the changes observed in the spectra registered from ES before and after the treatment, as well as the spectrum of the commercial calcium carbonate shown for comparison. $CaCO_3$ particles have three strong intensity peaks at 1420 cm^{-1} indicating the asymmetric stretch vibration, 875 cm^{-1} of the out-of-plane bending adsorption vibration and 712 cm^{-1} of the in-plane bending vibration for $–CO_3^{2–}$ [15]. The characteristic bands observed for $CaCO_3$ can be seen also in the FT-IR spectra of untreated and treated egg shells which proves that they are composed mainly of calcium carbonate in the form of calcite. The absorption bands appearing at 2874 and 2982 cm^{-1} were assigned to the stretching vibration of $–CH_2$, $–CH_3$ and a broadband at around 3420 cm^{-1} might be attributed to stretching of –OH groups [16].

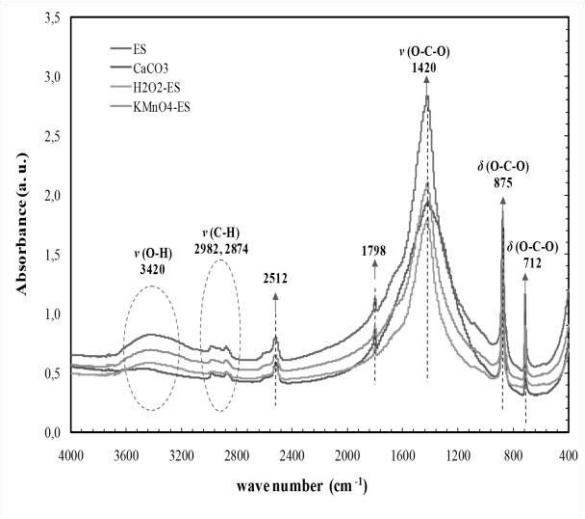

Fig. 3. FT-IR spectra of commercial calcium carbonate and waste egg shells before and after chemical treatment

The FT-IR spectra of treated egg shells are similar to those of the initial ES (Fig. 3). This means that calcite did not undergo structural changes after the treatment of the ES surface was carried out. After the treatment with H_2O_2 and $KMnO_4$, the intensities of the bands registered at 1420, 875 and 712 cm^{-1} decreased, which indicated that the reagents used react with the surface of the raw ES particles. FT-IR results are in good agreement with XRD results.

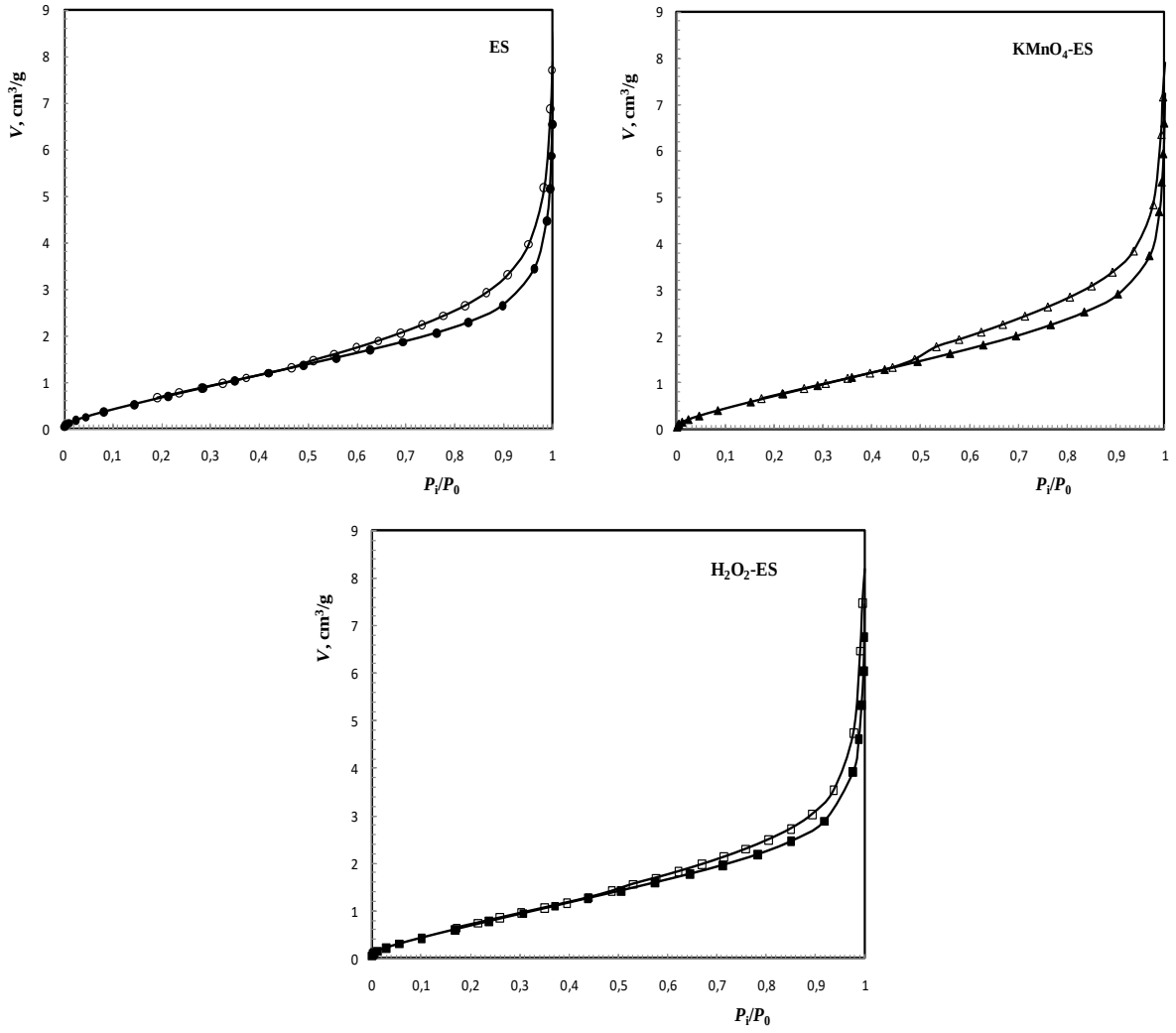

Fig. 4. N_2 adsorption-desorption isotherms of ES, $KMnO_4$-ES and H_2O_2-ES powders

Table 1. Textural porous parameters of untreated and treated egg shells

Parameters	Egg shell samples		
	ES	H_2O_2-ES	$KMnO_4$-ES
BET surface area, m^2/g	3.6654	3.4631	3.8206
Total pore volume, cm^3/g	0.0064	0.0062	0.0062
Average pore radius (B.J.H.), nm	3.3236	3.5429	3.1360
Cumulative pore volume (B.J.H.), cm^3/g	0.0054	0.0058	0.0066

The nitrogen adsorption-desorption isotherms at –196°C of untreated and treated egg shells are shown in Fig. 4. The isotherms of all samples are of type II according to the IUPAC classification having H_3 type hysteresis loop, an indication that the products have a nonporous or macroporous structures. Regardless of the surface treatments with various reagents, the latter do not affect the structure of egg shell powders.

Table 1 shows the Brunauer-Emmett-Teller surface area (m^2/g), total pore volume (cm^3/g), Barrett-Joyner-Halenda average pore radius (nm) and cumulative pore volume (cm^3/g) of egg shells before and after chemical treatment with H_2O_2 and $KMnO_4$. For untreated egg shells the determined

Brunauer-Emmett-Teller surface area is 3.6654 m^2/g and pore volume is 0.0064 cm^3/g. The results obtained are in accordance with these reported in the literature for pore volume from 0.00022 to 0.0065 cm^3/g [17]. After treatment with $KMnO_4$ porous characteristics remained almost unchanged and the surface area and pore volume for $KMnO_4$-ES were 3.8206 m^2/g and 0.0062 cm^3/g, respectively. For egg shell powders treated with H_2O_2 the BET surface area is 3.4631 m^2/g and 0.0062 cm^3/g for pore volume. The results obtained showed that the porous characteristics of the treated powders do not differ significantly and the values of the surface area and total pore volume were low. This means that it is necessary to use other modifying agents to improve the porous characteristics or carry out additional treatment of ES powders.

CONCLUSIONS

Surface treatment of waste egg shells was carried out with two different modifying reagents. The resulting powders were characterized by SEM, XRD and FT-IR analyses, the porous characteristics were determined and compared to these of untreated egg shells and commercial calcium carbonate. It was found out that the initial egg shells consist of irregularly shaped particles of different sizes. After the treatment, the samples showed identical particle morphology. When $KMnO_4$ was used, depositions of particles were observed on the surface while the use of H_2O_2 resulted in change of the surface roughness of the treated egg shell powders. The XRD analysis confirmed that no new phases were formed after the treatment showed that the relative crystallinity of the $KMnO_4$ treated samples was higher than that of the initial and the H_2O_2-treated egg shells. After the treatment, the intensities of the IR absorption bands registered at 1420, 875 and 712 cm^{-1} were found to decrease, which indicated that the reagents used reacted with the surface of raw egg shell particles. The N_2 adsorption-desorption isotherms at –196°C of all the samples showed that they are of type II which means that the products have a nonporous or macroporous structures. For the untreated egg shells, the BET surface area was determined to be 3.6654 m^2/g and pore volume was 0.0064 cm^3/g. It was established that the porous characteristics of the obtained treated powders did not differ significantly and the values of the surface area and total pore volume were low.

REFERENCES

1. Baláž, M., E. V. Boldyreva, D. Rybin, S. Pavlović, D. Rodríguez-Padrón, T. Mudrinić and R. Luque. *Front. Bioeng. Biotechnol.*, **8**, (2021), 612567.
2. Nakano, T., N. I. Ikawa and L. Ozimek. *Poult. Sci.*, **82**, (2003), p. 510.
3. Mittal, A., M. Teotia, R. K. Soni and J. Mittal. *J. Mol. Liq.*, **223**, (2016), p. 376.
4. Mohan, T.P. and K. Kanny. *J. Compos. Mater*., **52**, (2018), p. 3989.
5. Stadelman, W. J. *Egg and egg products,* In: *Encyclopedia of Food Science and Technology*, 2nd Edn., Ed. by F. J. Francis, John Wiley & Sons, New York, 2000, p. 593.
6. Owuamanam, S. and D. Cree. *J. Compos. Sci*., **4**, (2020), p. 70.
7. John-Jaja, S.A., U. H. Udoh and S. C. Nwokolo. *J. Basic Appl. Sci*., **5**, (2016), p. 389.
8. Boronat, T., V. Fombuena, D. Garcia-Sanoguera, L. Sanchez-Nacher and R. Balart. *Mater. Des*., **68**, (2015), p. 177.
9. Zhao, Y. H. and Y. J. Chi. *Biotechnol.*, **8**, (2009), p. 254.
10. Hincke, M. T., Y. Nys, J. Gautron, K. Mann, A. B. Rodriguez-Navarro and M. D. Mckee. *Front. Biosci*., **17**, (2012), p. 1266.
11. Kaweewong, K., W. Garnjanagoonchorn, W. Jirapakkul and S. Roytrakul. *Protein J*., **32**, (2013), p. 297.
12. Pliya, P. and D. Cree. *Constr. Build. Mater*., **95**, (2015), p. 1.
13. Intharapat, P., A. Kongnoo and K. Kateungngan. *J. Polym. Environ*., **21**, (2013), p. 245.
14. Luo, X., X. Song, Y. Cao, L. Song and X. Bu. *RSC Adv.*, **10**, (2020), p. 7976.
15. Laskar, I. B., K. Rajkumari, R. Gupta, S. Chatterjee, B. Paul and L. Rokhum. *RSC Adv*., **8**, (2018), p. 20131.
16. Joshi, G., D. S. Rawat, B. Y. Lamba, K. K. Bisht, P. Kumar, N. Kumar and S. Kumar. *Energy Convers. Manag*. **96**, (2015), p. 258.
17. Liao Dexiang, D., W. Zheng, X. Li, Q. Yang, X. Yue, L. Guo and G. Zeng, *J. Hazard. Mater*., **177**, (2010), p. 126.

ANNUAL OF ASSEN ZLATAROV UNIVERSITY, BURGAS
BULGARIA, 2022, v. LI(1)

DETERMINATION OF THE ANTIMICROBIAL EFFECTIVENESS OF THE ANTIBIOTIC CIPROFLOXACIN

Dimitrina Krasteva, Katya Gabrovska, Yavor Ivanov
E-mail: dida_burgas@mail.bg

ABSTRACT

*The inhibitory efficiency of the antibiotic **Ciprofloxacin** on the bacterial growth of two gram-positive strains (S. aureus and B. subtilis) and two gram-negative strains (E. coli and Micrococcus sp.) was determined. For this purpose, two methods were used: the disc-diffusion method with the measurement of the diameter of the inhibited zone and the dilution method for determining the minimum inhibitory concentration (MIC) of the antimicrobial agent. At 25 mg/L Ciprofloxacin, the diameter of the zone of inhibition of S. aureus was 19 mm. The MIC of the antibiotic against Staphylococcus aureus was 0.59 mg/L Ciprofloxacin, determined from an incubation time of 24 hours. The antibiotic efficiency of Ciprofloxacin against Bacillus subtilis was determined. The measured diameter of the inhibition zone formed at 25 mg/L **Ciprofloxacin** was 16 mm. The MIC of the antibiotic against Bacillus subtilis was 37.5 mg/L **Ciprofloxacin**, determined from an incubation time of 24 hours. The third microorganism analyzed was E. coli. A disk with 25 mg/L Ciprofloxacin resulted in a zone of inhibition with a diameter of 13 mm. The MIC of the antibiotic against E. coli was identical to that determined against Bacillus subtilis. The sensitivity of the antibiotic to Micrococcus sp. was the weakest one. After incubation for 24 hours of the samples, a weak cell growth was measured in all samples containing different concentrations of the antibiotic.*

Key words: *disk diffusion method, minimum inhibitory concentration, Ciprofloxacin, Staphylococcus aureus, Escherichia coli, Bacillus subtilis, Micrococcus sp.*

INTRODUCTION

Antibiotic resistance is a global health problem. Antibiotics are often called "miracle" drugs, but their overuse and misuse lead to an increased incidence of resistance. The adaptation of bacteria is so successful that some bacterial infections are almost untreatable with antibiotics. In each resistance mechanism, the bacterium changes its ability to withstand the drug as well as its interaction with the host and environment [1]. The growing resistance of bacteria to antibiotics and the frequent failed treatments of infections, on the one hand, require the identification of the main causes of this problem, and the search for ways to reduce and improve the effectiveness of therapies, on the other. One of the reasons for unsuccessful therapies is the choice of drugs, especially when they are chosen incorrectly, as well as when they are administered in too small doses. This leads to the survival of a resistant bacteria population and resistance to antibiotics [2]. Therefore, when having bacterial infections, it is important to use antibiotics in doses that guarantee therapeutic effectiveness. Administration of antibiotics should be preceded by sampling for microbiological studies. In bacterial infections, the identification of the pathogen and the antibiogram suggest the choice of a drug expected to be clinically effective. Typically, antibiograms contain a qualitative assessment of the strain's susceptibility or resistance to antibiotics, as well as information on the mechanisms of resistance detected. For many infections, such parameters are sufficient to stop the use of already administered antibiotics in case of resistance of the strain and replace it with a drug to which the strain is sensitive. In the case of critically ill patients suffering from chronic infections treated with a broad spectrum of antibiotics having a history of failed therapies, much more precise guidelines are needed to facilitate the selection of an optimal (i.e, effective) antibiotic. Among these microbiological parameters is the minimum inhibitory concentration (MIC) of the antimicrobial agent [3- 4]. MIC is considered the "gold standard" for determining the susceptibility of microorganisms to antimicrobial agents. Another method for determining the antibiotic sen-

sitivity of microorganisms is the diffusion method [4-7].

Ciprofloxacin is fluoroquinolone antibiotic structurally related to nalidixic acid. The primary mechanism of action of ciprofloxacin is inhibition of bacterial DNA gyrase. It is a broad spectrum antibacterial drug to which most Gram-negative bacteria are highly susceptible in vitro and many Gram-positive bacteria are susceptible or moderately susceptible [8]. The aim of the present study was to determine the antimicrobial effectiveness of the antibiotic **Ciprofloxacin** on the bacterial growth of two gram-positive strains (*S. aureus and B. subtilis*) and two gram-negative strains (*E. coli and Micrococcus sp.*).

EXPERIMENT

Materials and methods reagents

Nutrient media Mueller Hinton Agar, Nutrient broth were purchased from Sigma - Aldrich, Germany. Unwetted chromatographic paper discs (d = 6 mm) were purchased from Bul Bio-NCZPB, Bulgaria. The antibiotic Ciprofloxacin and the reagent NaCl were provided by Sopharma, LTD, Bulgaria. The microorganisms: *Staphylococcus aureus (ATCC 6538), Escherichia coli (ATCC 8739), Bacillus subtilis (ATCC 19659)* and *Micrococcus sp. (ATCC 4698)* are from the microorganism bank of the Department of Biotechnology, Prof. Dr Assen Zlatarov University, Burgas.

Antibiotic solutions

A stock solution of the antibiotic Ciprofloxacin with a concentration of 600 mg/L was prepared. An appropriate range of concentrations of the antibiotic under research (from 0.04 to 150 mg/mL) was selected for testing the microorganisms. Serial dilution of the antibiotic solution was performed with 0.9% NaCl solution. The lowest dilution concentration depended on the possible minimum inhibitory concentration [4-5].

Preparation of bacterial inoculum

With the help of an inoculating loop, cells of the respective investigated microorganisms (*S. aureus, E. coli, B. subtilis and Micrococcus sp.*) were introduced into 3 mL of Nutrient broth and incubated overnight on a shaker, 220 rpm at 37°C. The optical density of the solution at 650 nm (OD_{650nm}) was measured using a spectrophotometer (Jenway 7205, Germany). The bacterial solution was then diluted with Nutrient broth liquid medium to obtain a suspension with OD_{650}nm = 0.3-0.5, corresponding to a cell concentration of 5 x10^5 CFU/mL [6].

Disk diffusion method

In the disc-diffusion method, the antibiotic sensitivity of microorganisms is determined using paper discs impregnated with different concentrations of the antibiotic under research. First, the solid culture medium (Mueller Hinton agar) was prepared as follows: 36 g of agar were dissolved in 1 L d.H2O and the solution was autoclaved for 15 min at 121°C (BIOBASE, Model BKM-XD35D). The medium (25 mL) was poured into a 9 cm diameter petri dish and allowed to solidify. Then, 250μL of the bacterial suspension with a concentration of 5 x 10^5 CFU/mL was evenly spread over the solid culture medium [4-7]. Sterile paper discs (6 mm diameter) impregnated with different concentrations of antibiotic are placed on the surface of the agar: 0; 1.56; 6.25 and 25 mg/L. For comparison, a disk without antibiotic impregnated with 0.9% NaCI was inserted. Petri dishes were left for 30 minutes at room temperature to diffuse the antibiotic into the solid culture medium. They were then incubated in a thermostat at 37°C for 24 h. Placing a filter disc on the inoculated agar was accompanied by the simultaneous development of two events: 1) diffusion of the antibiotic from the disc into the agar and 2) growth of the microorganism. Zones of suppressed bacterial growth can be seen around some of the discs. The diameter of the inhibition zones was measured in mm [9]. These values determine the antibiotic sensitivity of the microorganisms to the researched antibiotic.

Determination of the minimum inhibitory concentration of the antibiotic

The determination of MIC was carried out by the dilution method. 2 mL of Ciprofloxacin solution with a concentration of 600 mg/L and 6 mL of a bacterial solution of the corresponding microorganism (5 x10^5 CFU/mL) were mixed. Then, using the serial dilution method, solutions with different antibiotic concentrations (0 ÷ 150 mg/L) were obtained. The tubes were incubated in a thermostat at 37°C, and the optical density of the bacterial suspension was measured at 650 nm at 0, 5, 24 and 48 h. The lowest concentration at which no visible bacterial growth was recorded at 24 hours was the minimum inhibitory concentration of the antibiotic.

RESULTS AND DISCUSSION

The aim of the present study was to determine the inhibitory effect of the antibiotic **Ciprofloxacin** on the bacterial growth of two gram-positive strains (*S. aureus and B. subtilis*) and two gram-negative strains (*E. coli and Micrococcus sp.*). *Staphylococcus aureus* is a gram-positive bacterium that is carried by about one-third of the population and is responsible for common serious illnesses. These diseases include food poisoning and toxic shock syndrome, which are caused by exotoxins produced by *S. aureus*. A recognized problem in clinical practice is the emergence of multidrug-resistant strains of *S. aureus* and they are a cause for concern [10]. The antimicrobial potential of **Ciprofloxacin** was investigated by two methods: by the disk diffusion method and by the dilution method. First, the antimicrobial potential of the antibiotic against *Staphylococcus aureu*s was investigated. In the disc-diffusion method, the antibiotic applied to paper discs was in a concentration range of 1.56 to 25 mg/L.

For comparison, an experiment was carried out with a disk without an antibiotic. It was found out that two inhibitory zones were formed only at the concentrations of 6.25 and 25 mg/L **Ciprofloxacin** (Fig. 1A). The inhibitory effect increased with increasing amount of antibiotic. At 6.25 mg/L **Ciprofloxacin**, a zone of inhibition with a diameter of 12 mm was measured. At 25 mg/L **Ciprofloxacin**, the diameter of the zone of inhibition was 19 mm. The minimum inhibitory concentration of the antibiotic against *Staphylococcus aureus* was also determined by the dilution method. The antibiotic concentration in these experiments ranged from 0.04 to 150 mg/L. For comparison, a sample without antibiotic was made. The results are presented in Fig. 1B.

At the 5th hour, a visible retardation of cell growth was observed in the samples loaded with 2.35, 9.38, 37.5 and 150 mg/L. At the 24th hour, growth retardation was present at concentrations of 0.04 and 0.15 mg/L antibiotic, while at the other higher concentrations there was no growth. The lowest concentration of **Ciprofloxacin** at which no growth was observed was 0.59 mg/L antibiotic (Fig. 1B). Therefore, the MIC for *Staphylococcus aureus* is 0.59 mg/L **Ciprofloxacin**. At the 48th hour of incubation, there was no cell growth in the antibiotic-containing samples, only the antibiotic-free sample showed cell growth.

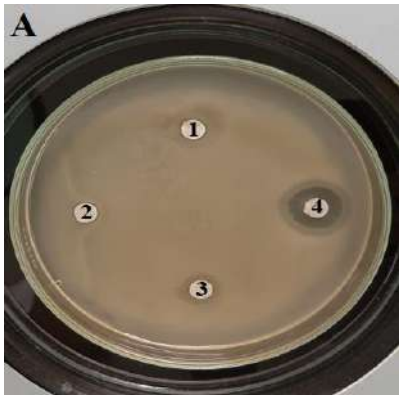

Fig. 1 A) Antibacterial activity of **Ciprofloxacin** against *Staphylococcus aureus* (5×10^5 CFU/mL). Image of disc diffusion assay at different concentrations of antibiotic 1, 2, 3, 4, 0, 1.56, 6.25, 25 mg/L, respectively.

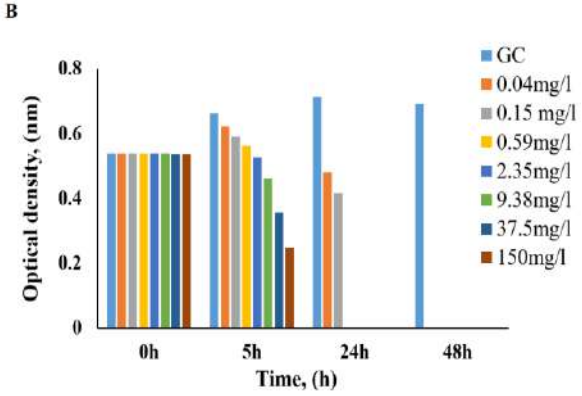

Fig. 1 B) Determination of the minimum inhibitory concentration of **Ciprofloxacin** when varying the concentration of the antibiotic and different incubation times.

Bacillus subtilis is a ubiquitous microorganism. In laboratory conditions, it is easy to grow and handle [11]. This Gram-positive bacterium is a facultative aerobe that was originally classified as a soil bacterium, but its ability to grow in many different terrestrial and aquatic environments, from the root surface of some plants to the gastrointestinal tract of some animals, is now well known. This ability to adapt to different environments is mainly due to spore formation, which occurs under certain conditions of stress and nutrient deficiency [12]. The antibiotic efficiency of **Ciprofloxacin** against *Bacillus subtilis* was determined. Using to the disk diffusion method, it was found out that only at a concentration of 25 mg/L **Ciprofloxacin**, a zone of cell inhibition was observed. The measured diameter of the inhibition zone formed was 16 mm (Fig. 2A). The minimum inhibitory concentration of **Ciprofloxacin** against *Bacillus subtilis* was also determined, Fig. 2B. At 24 h, no visible growth

was observed at 37.5 and 150 mg/L antibiotic (Fig. 2B). Therefore, the MIC is 37.5 mg/L **Ciprofloxacin** against *Bacillus subtilis* and it is higher than that against *Staphylococcus aureus*. At 48 hours of incubation of the cells in the samples containing the antibiotic, there was no cell growth. The results show that *Bacillus subtilis* is less sensitive to the tested antibiotic compared to *Staphylococcus aureus.*

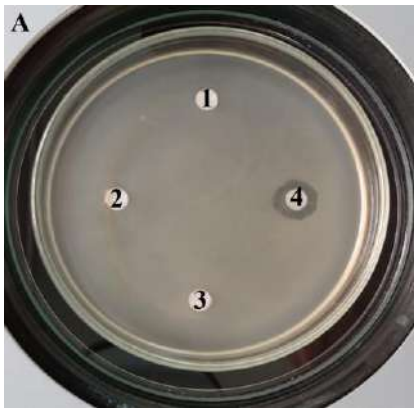

Fig. 2 A) Antibacterial activity of **Ciprofloxacin** against *Bacillus subtilis* (5×10^5 CFU/mL). Image of disc diffusion assay at different concentrations of antibiotic 1, 2, 3, 4, 0, 1.56, 6.25, 25 mg/L, respectively.

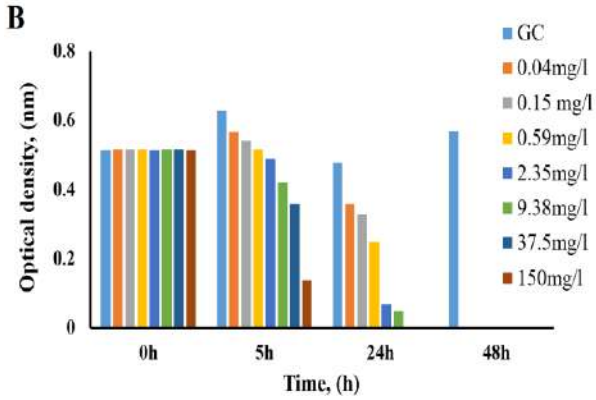

Fig. 2 B) Determination of the minimum inhibitory concentration of **Ciprofloxacin** when varying the concentration of the antibiotic and different incubation times.

The third microorganism analyzed was *E. coli*. It is part of the intestinal microflora in both humans and warm-blooded animals. However, pathogenic strains can cause intestinal and extraintestinal infections. These microorganisms can be found in the environment, food and water contaminated with faeces. The presence of *E. coli* is used as an indicator of faecal contamination [13]. Antibiotics can be an effective treatment for *E. coli* infections, but sometimes long-term use poses a risk of complications such as haemolytic uremic syndrome. It is clear from Fig. 3 that a disc with 25 mg/L **Ciprofloxacin** resulted in a zone of inhibition with a diameter of 13 mm (Fig. 3A). The minimum inhibitory concentration of **Ciprofloxacin** against *E. coli* was also determined, Fig. 3C. At a **Ciprofloxacin** concentration of 2.35 mg/L at the 24^{th} hour, the least cell growth was observed. No visible growth was observed at 24 h at 37.5 and 150 mg/L antibiotic (Fig. 3B). Therefore, the MIC against *E. coli* is 37.5 mg/L **Ciprofloxacin.**

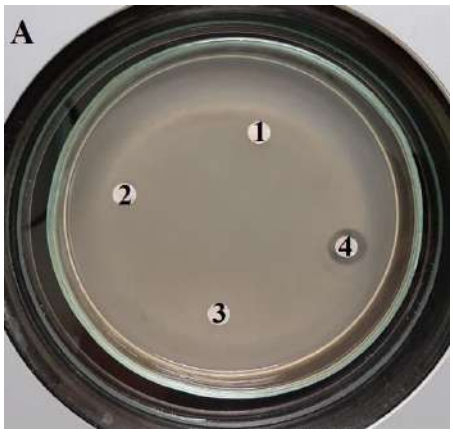

Fig. 3 A) Antibacterial activity of **Ciprofloxacin** against *E. coli* (5×10^5 CFU/mL). Image of disc diffusion assay at different concentrations of antibiotic 1, 2, 3, 4, 0, 1.56, 6.25, 25 mg/L, respectively.

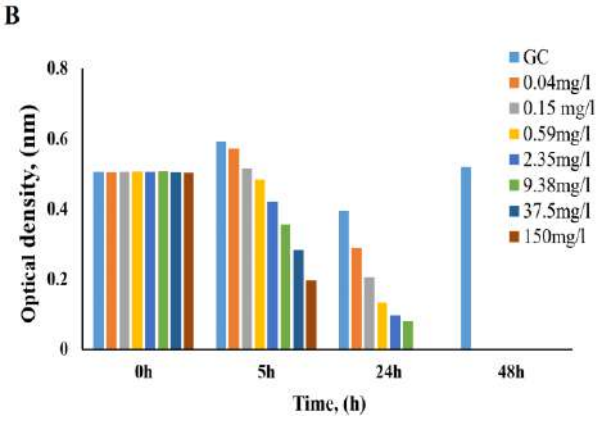

Fig. 3 B) Determination of the minimum inhibitory concentration of **Ciprofloxacin** when varying the concentration of the antibiotic and different incubation times.

Micrococcus sp. belongs to the harmless saprophytes that inhabit or contaminate the skin, mucous membrane, and oropharynx. However, they can be opportunistic pathogens for immunocompromised patients [14- 15]. They are associated with a variety of infections, including bacteremia, peritonitis in long-term ambulatory peri-

toneal dialysis, and infections associated with venous catheters [14]. In Figure 4A it can be seen that **Ciprofloxacin** does not affect *Micrococcus sp.* because there is no inhibition zone around the discs impregnated with the antibiotic. The minimum inhibitory concentration of **Ciprofloxacin** against *Micrococcus sp.* by the dilution method was also determined (Fig. 4B). When the samples were incubated for 24 hours, cell growth was measured in all samples, with the higher concentrations of the antibiotic showing weaker growth. At the 48th hour, however, growth was reported only in the samples containing 0.04 and 0.15 mg/L **Ciprofloxacin**. The lowest concentration of **Ciprofloxacin** at which no visible growth was observed was 0.59 mg/L, but at the 48th hour of incubation of *Micrococcus sp.* bacterial cells (Fig. 4B). Therefore, the MIC is 0.59 mg/L **Ciprofloxacin,** but at the 48th hour.

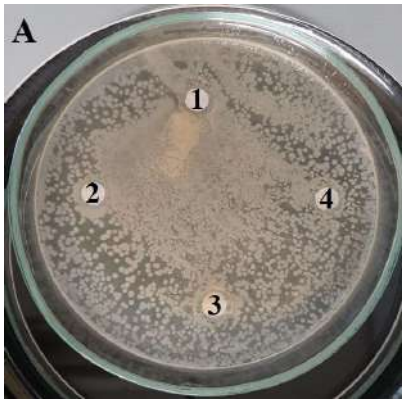

Fig. 4 A) Antibacterial activity of **Ciprofloxacin** against *Micrococcus sp.* (5×10^5 CFU/mL). Image of disc diffusion assay at different concentrations of antibiotic 1, 2, 3, 4, 0, 1.56, 6.25, 25 mg/L, respectively.

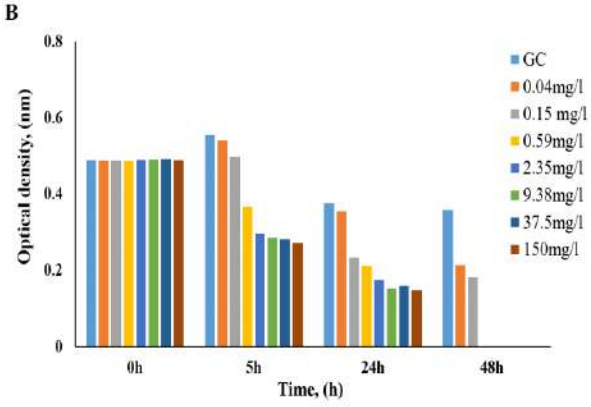

Fig. 4 B) Determination of the minimum inhibitory concentration of **Ciprofloxacin** when varying the concentration of the antibiotic and different incubation times.

CONCLUSIONS

To evaluate the effectiveness of the antibiotic preparation **Ciprofloxacin**, the disc-diffusion method and the dilution method were applied to determine the minimum inhibitory concentration of the antibiotic. The tested antibiotic was found to be most effective against *Staphylococcus aureus* and least effective against *Micrococcus sp*. The minimum inhibitory concentration for *Staphylococcus aureus* bacteria was determined to be 0.59 mg/L **Ciprofloxacin**.

REFERENCES

1. Andersson, D., (2003). Persistence of antibiotic resistant bacteria. Current Opinion in Microbiology (pp. 452-456). Elsevier. DOI 10.1016/j.mib.2003.09.001.
2. Cantón, R., Morosini, M.I., (2011). Emergence and spread of antibiotic resistance following exposure to antibiotics. FEMS Microbiol (pp. 977–991). doi.org/10.1111/j.1574-6976.2011.00295.x.
3. Kowalska-Krochmal, B and B. Dudek-Wicher, (2021). The Minimum Inhibitory Concentration of Antibiotics: Methods, Interpretation. Clinical Relevance, Pathogens, (pp.165). doi.org/10.3390/pathogens10020165.
4. Andrews, J.M., (2001). Determination of Minimum Inhibitory Concentrations, J Antimicrob Chemother (pp. 5-16) DOI: 10.1093/jac/dkf083.
5. Lin, M.F., Lin, Y.Y. and C.Y. Lan, (2014). Minimal Inhibitory Concentration (MIC) Assay for Acinetobacter baumannii, http://www.bio-protocol.org/e1308 Vol 4, Iss 23.
6. International Standard ISO 20776-1 (2019). Susceptibility Testing of Infectious Agents and Evaluation of Performance of Antimicrobial Susceptibility Test Devices—Part 1: Broth Micro-Dilution Reference Method for Testing the In Vitro Activity of Antimicrobial AGENTS Against Rapidly Growing Aerobic Bacteria Involved in Infectious Diseases, 2nd ed.; International Organization for Standardization: Geneva, Switzerland.
7. European Committee for Antimicrobial Susceptibility Testing (EUCAST) of the European Society of Clinical Microbiology and Infectious Diseases (2000). Determination of minimum inhibitory concentrations (MICs) of antibacterial agents by agar dilution. Clin.

Microbiol. Infect. (pp. 509–515). doi.org/10.1046/j.1469-0691.2003.00790.x.
8. Campoli-Richards D.M., Monk J.P., Price A., Benfield P., (2021). Ciprofloxacin. doi.org/10.2165/00003495-198835040-00003.
9. Zhu M.J., Olsen S.A., L. Sheng, Xue Y., Yue W., (2015). Antimicrobial efficacy of grape seed extract against Escherichia coli O157:H7 growth, motility and Shiga toxin production, Food Control (pp.177-182). doi.org/10.1016/j.foodcont.2014.11.024.
10. Pinchuk, I.V., Beswick, E.J., Reyes, V.E. (2010). Staphylococcal Enterotoxins. Toxins (pp. 2177-2197). doi:10.3390/toxins2082177.
11. Martinez, R.M. (2013). Bacillus subtilis, Brenner's Encyclopedia of Genetics (Second Edition) (pp.246-248). doi.org/10.1016/B978-0-12-374984-0.00125-X.
12. Freyre-González, J.A., Manjarrez-Casas, A.M., Merino, E., Martinez-Nuñez, M., Perez-Rueda, E., Gutiérrez-Ríos, R.M. (2013). Lessons from the modular organization of the transcriptional regulatory network of Bacillus subtilis. BMC Systems Biology, 7:127 http://www.biomedcentral.com/1752-0509/7/127
13. Luna-Guevara, J. J., Arenas-Hernandez, M. M. P., Martınez de la Peña, C., Silva, J.L., Luna-Guevara, M. L. (2019). The Role of Pathogenic E. coli in Fresh Vegetables: Behavior, Contamination Factors, and Preventive Measures. International Journal of Microbiology (pp.10).doi.org/10.1155/2019/2894328.
14. Bannerman, T. L., & Peacock, S. J. (2007). Staphylococcus, Micrococcus sp., and Other Catalase- Positive Cocci. Manual of Clinical Microbiology (pp. 390-404). Washington, USA: ASM Press.
15. Kocur, M., Kloos, W. E., Schleifer, K. H. (2006). The Genus Micrococcus sp. The Prokaryotes (3rd ed., pp. 961-971). New York: Springer.

ANNUAL OF ASSEN ZLATAROV UNIVERSITY, BURGAS
BULGARIA, 2022, v. LI(1)

OPERATIONAL RELIABILITY IN A SMART GRID

Mehmed Hasan
e-mail: Mehmedkadirhsn70@gmail.com

ABSTRACT

The paper proposes a methodology for evaluating the operational reliability of a smart grid. The peculiarities of the smart grid operation and the main requirements toward them are taken into account. The presented results concern the evaluation of the operational reliability of a smart grid based on available data and at power source redundancy in a medium voltage distribution network.

***Keywords**: smart grid, operational reliability*

INTRODUCTION

Electrical networks are intended to deliver the generated electricity from energy sources to consumers. In recent years, the construction of smart grids improving the conventional electrical grids has begun [1, 2]. Many technical devices are implemented in the modern smart grids nowadays, such as computerized equipment, communication systems and automation devices, which allows them to use the energy resources rationally and achieve optimal operating conditions [3÷7]. Together with the new technologies entering the smart grid, the requirements toward the electrical networks are changing.

The networks for transmitting high and ultra-high voltage meet the requirements and have a high degree of readiness for operation as part of a smart grid. They are equipped with digital relay protections, anti-emergency and technological automation, tele-mechanics and automated control systems. Moreover, these transmission networks have a ring structure and provide a two-way power supply to the consumers, which is one of the prerequisites for building a smart grid [2].

Unlike the high voltage distribution networks, the medium and low voltage ones are not ready for direct transition to operation within a smart grid. They do not satisfy the basic preconditions of a smart grid: observability of the mode parameters, two-way power supply for the users, automated control and diagnostics systems. The distribution networks for medium and low voltage are usually open branched. Provision of emergency connections, redundancy and reconfiguration of the power grid are the first step to achieving a two-way power supply to consumers. The introduction of decentralized energy sources (DES) creates conditions for bilateral power supply of the branch to which they are connected.

In traditional networks, there is no provision for accumulating the excess amount of electricity. A smart grid, however, provides for the introduction of powerful storage systems to accommodate the excess of electric power and, accordingly, for its consumption when a shortage of power occurs during an increase in consumption. Thus, the modes of operation of the generating sources are stabilized within a day: in the hours of low consumption accumulation takes place, while in the hours of peak loads consumption of the accumulated electricity begins. Combining the work of DES with powerful storage systems creates conditions for continuous electricity supply to hybrid consumers.

These features of the smart grid require a new approach in evaluating its operational reliability, according to the requirement for two-way power supply of the users in the distribution networks.

The aim of this paper is to present a methodology for evaluating the operational reliability of a smart grid.

METHODOLOGY, EXPERIMENT AND RESULTS FOR EVALUATING THE OPERATIONAL RELIABILITY OF A SMART GRID

Reliability is basically the property of an object to perform its functions while keeping its operational indicators within pre-set limits during the period of operation [1]. Reliability is evaluated according to 4 indicators: infallibility, durability, repairability and storability. Safety and power

supply continuity are added to these indicators for the electric power facilities.

The choice of a reliability indicator to be assessed depends on the type of the evaluated reliability: parametric, functional, a priori, operational, structural.

To assess the operational reliability, it is appropriate to examine the infallibility indicator, this is the property of the object to maintain its operability continuously for a certain period of time.

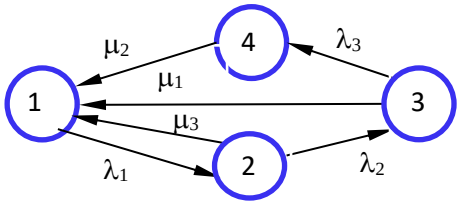

Fig. 1. State diagram: λ_i - failure intensity; μ_i – recovery intensity

The following states are considered in the process of evaluating the operational reliability of a smart grid (Fig. 1):

1 – state of trouble-free operation of all the elements in the smart grid;

2 – state of unsustainable failure of a smart grid element (which self-removes during the diagnostic process);

3 – state of sustainable failure of a smart grid element with successful automatic circuit recloser (ACR) and restoration of the power supply to consumers;

4 – state of failure of a smart grid element.

The following system of equations is obtained for the graph of states in Fig. 2:

$$\begin{cases} P_2(\mu_1+\lambda_2)-P_1\lambda_1=0; \\ P_3(\mu_2+\lambda_3)-P_2\lambda_2=0; \\ P_4\mu_3-P_3\lambda_3=0; \\ \sum_{i=1}^{4}P_i=1. \end{cases} \quad 1)$$

The probabilities P_i (i=1÷4) for the corresponding *i* states are expressed for the diagram in Fig. 2 and the system of equations (1) as it follows:

$$P_1 = P_4\frac{\mu_3}{\lambda_3}\cdot\frac{\lambda_3+\mu_2}{\lambda_2}\cdot\frac{\lambda_2+\mu_1}{\lambda_1}; \quad (2)$$

$$P_2 = P_4\frac{\mu_3}{\lambda_3}\cdot\frac{\lambda_3+\mu_2}{\lambda_2}; \quad (3)$$

$$P_3 = P_4\frac{\mu_3}{\lambda_3}; \quad (4)$$

$$P_4 = \frac{1}{1+\frac{\mu_3}{\lambda_3}\left[1+\frac{\lambda_3+\mu_2}{\lambda_2}\left(1+\frac{\lambda_2+\mu_1}{\lambda_1}\right)\right]}\cdot \quad (5)$$

In order to estimate the probabilities $P_{i,}$, data on failure intensity λ_i and recovery intensity μ_i are needed. The obtained results of the performed calculation are presented in Fig. 2.

The more the probability P_1 approaches 1, the better the smart grid performs its functions.

A states diagram concerning a situation in which the users of a smart grid are power supplied by a main source S and a backup source G is shown in Fig. 3.

Failure intensity λ_1	**0,63**
Failure intensity λ_2	**0,21**
Failure intensity λ_3	**0,12**
Recovery intensity μ_1	**27,3**
Recovery intensity μ_2	**0,24**
Recovery intensity μ_3	**0,18**
• **Results**	
Probability P_4	**0,008**
Probability P_3	**0,012**
Probability P_2	**0,02**
Probability of failure-free operation P_1	**0,96**

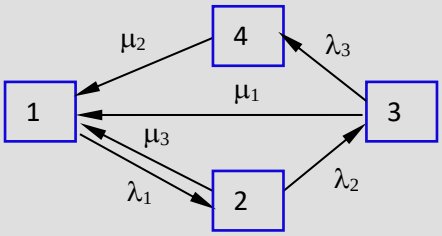

States:

1 – failure-free operation of all elements;
2 – unsustainable failure of an element
3 – sustainable failure of an element with successful ACR;
4 – failure of a Smart grid element.

Fig. 2. Calculation of the probability of failure-free operation

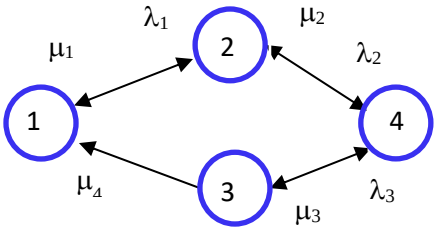

Fig. 3. State diagram: λ_i - failure intensity; μ_i – recoveries intensity

This is a case of redundancy of power supply to users in a branch of a distribution smart grid. The states shown in Fig. 3 are:

1 – trouble-free operation of the main and backup power sources;

2 – failure of power supply from S and functioning of the element G;

3 – functioning of power supply from S and failure of the element G;

4 – power cut from both S and G.

If in a normal mode the power source S supplies the consumers, then after its emergency shutdown, the backup source G is turned on. Hence, as the backup source G is not in operation during the normal period, its failures are not taken into account. Therefore, no direct transition from state 1 to state 4 is possible. When the supply from S is on and the backup source G is in a state of emergency repair, the transition from state 1 to state 3 is impossible. State 4 is a failure of one of the power sources when the other one is turned off and in such a case the consumers are left with no power supply.

The probability of failure-free operation $P_1 \approx 1$ and the probability of a failure state of both power supplying sources P_4 are expressed for the diagram in Fig.3 in the following way:

$$P_4 \approx \frac{\lambda_1 \lambda_2}{(\mu_1 + \mu_2)\mu_1}. \qquad (6)$$

The results of the calculation are presented in Fig. 4.

CONCLUSIONS

- The operational reliability increases with the construction of a smart grid, as the modern technical means allow to control electricity generation at any moment of time according to the magnitude of the load, as well as to accumulate the surplus of energy and use it if necessary.
- The proposed approach and the developed software for evaluating the operational reliability of smart grids based on operational data allows to estimate the probability of failure-free operation, which, for a real smart grid, should be close to 1.
- For a system with redundancy of the power sources, the probability of failure-free operation and the probability of failure are determined using the developed software, based on the application of the mathematical method of states definition.

Failure intensity λ_1	**0,06**	
Failure intensity λ_2	**0,01**	
Failure intensity λ_3	**0,058**	
Recovery intensity $\mu_1 = \mu_3$	**0,7**	
Recovery intensity $\mu_2 = \mu_4$	**0,1**	
• **Results**		
Probability P_4	**0,0007**	
Probability of failure-free operation P_1	**0,9993**	

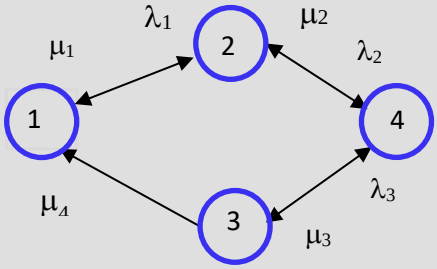

States:

1 – failure-free operation of S and G;
2 – failure of S and operation of G;
3 – operation of S and failure of G;
4 – failure of both S and G.

Fig. 4. Calculation of the probability of failure-free operation of a system with power redundancy

REFERENCES

1. Notov P.P., S.I. Nedelcheva. Electric Power Engineering, Part One. ISBN 978-954-438-821-8, Sofia, TU-Sofia Publishing House, 2009.
2. Hasan M.K. Evaluation of the operational reliability of a smart electric grid. World Wide Journal of Multidisciplinary Research and Development (November-2022). Vol. 8(11), E-ISSN:2454-6615, (WWJMRD).
3. Notov P.P., S.I. Nedelcheva. Electric power engineering. Smart electrical grids. Part three. ISBN 978-619-167-119-9. Sofia, TU-Sofia Publishing House, 2014.
4. Raykov. K.V. Energy efficiency of smart electric grids. Monograph. ISBN 978-619-167-490-9, Sofia, TU-Sofia Publishing House, 2022.
5. Bakardjieva J.N., K.V. Raykov. Design of a distribution smart grid. 2022 8th International Conference on Energy Efficiency and Agricultural Engineering (EE&AE), Scopus, 30 June - 2 July 2022, Ruse, Bulgaria.
6. Nedelcheva S.I., Y.N. Bakardzhieva. Designing smart electrical networks. ISBN 978-619-167-235-6. Sofia, TU-Sofia Publishing House, 2015.
7. Raykov K.V. Peculiarities and priority directions in the construction of smart electrical grids. ISSN 1312-3920, TU-Sliven News, No. 4, 2022, pp. 3-7.

ANNUAL OF ASSEN ZLATAROV UNIVERSITY, BURGAS
BULGARIA, 2022, v. LI(1)

SYNERGISTIC ACTION OF PRESERVATIVES ON DIFFERENT TYPES OF MICROORGANISMS

Ruska Nenkova, Galina Yordanova, Galina Grigorova
E-mail: rdnenkova@abv.bg

ABSTRACT

The aim of the present work was to investigate the antimicrobial effect of sodium benzoate, sodium nitrite and sulfurous acid and their synergistic action (sodium benzoate and sodium nitrite, sodium benzoate and sulfurous acid, sodium nitrite and sulfurous acid) on selected bacteria, yeast and fungi, for a potential use in the food industry. The following species of microorganisms were tested: Staphylococcus aureus, Saccharomyces cerevisiae and Aspergillus oryzae. The most sensitive microorganism against sodium benzoate is Staphylococcus aureus and the MIC is 4 mg/ml. The strongest antimicrobial effect was exerted by sulfurous acid (no growth) in relation to the species Staphylococcus aureus. MIC of sulfurous acid to the yeast Saccharomyces cerevisiae and the fungi Aspergillus oryzae is 18 mg/ml. The combination of sodium benzoate with sulfurous acid and sodium nitrite with sulfurous acid has an inhibitory effect on the growth of the tested yeasts and fungi.

Key words: *Staphylococcus aureus, Saccharomyces cerevisiae, Aspergillus oryzae, sodium benzoate, sodium nitrite, sulfurous acid*

INTRODUCTION

Following the EU regulation, preservatives are food additives that protect against the action of microorganisms (fungi and/or bacteria) and thereby extend the shelf life of foodstuff. The inhibitory effect of preservatives varies, depending on the concentration and type of preservative, pH of the medium and the species of microorganism. Inhibition of growth and activity of microorganisms can be achieved by lowering pH of the medium or by increasing the concentration of preservatives [1]. The effectiveness of use of preservatives is often dictated by limitations in their action or by the sensitivity of the microorganisms [2].

Various preservatives may also be used separately or simultaneously. The antimicrobial properties of sodium nitrite, sodium benzoate, and potassium sorbate have been described in [3] and have been tested in a variety of combinations to improve forage conservation [4, 5, 6]. Stanojevic et al. [7] investigated the antimicrobial effects of sodium benzoate, sodium nitrite and potassium sorbate and their synergistic action in vitro on selected food- spoiling bacteria and fungi.

The activity of the benzoic acid and the alkali metal salts of benzoic acid is exerted on the cell membranes, and also inhibits enzymes of the citric acid cycle and of the oxidative phosphorylation. Some studies [8] show that a daily dose of less than 0.5 g sodium benzoate (E211) is harmless for man, but a lesser dose than 0.4 g a day^{-} has no risk of accumulation. This additive is renally eliminated as hippuric acid ($C_6H_5CONHCH_2COOH$) and (in case of high doses) as glucuronic acid derivatives ($C_6H_{10}O_7$) [9]. Sodium nitrite is known to be responsible for the production of the desirable heat-stable pink colour in cured meats. It has also been used as an inhibitor of bacterial spoilage of fish. Masarin and Ferraz reported that the use of wood chips (Eucalyptus grandis) washed with 3.2 mM sulfurous acid (pH 2.5) for biotreatment with white rot fungi under non-sterile conditions decreased the level of contaminant fungi, and resulted in fibrillation improvements similar to samples subjected to the standard biotreatment process using wood chips autoclaved at 121°C for 15 min [10].

The aim of the present work is to study the antimicrobial action of sodium benzoate, sodium nitrite and sulfuric acid, and to evaluate the effectiveness of their synergistic effect on selected bacteria and fungi and thus to expand the possibilities for more efficient preservation of food products. The following species of microorganisms were

tested: *Saccharomyces cerevisiae, Staphylococcus aureus* and *Aspergillus oryzae*.

MATERIALS AND METHODS

The preservatives used in the experiment were as follows: sodium benzoate, sodium nitrite and sulfurous acid. Different concentrations of preservatives were created by dissolving them in MPB and wort.

The antimicrobial activity of preservatives was tested in relation to the bacteria *Staphylococcus aureus,* the yeast *Saccharomyces cerevisiae* and the fungi *Aspergillus oryzae*. All microorganisms were obtained from stock cultures of the Laboratory of Microbiology in the Department of Biotechnology. Prior to testing, fresh bacterial cultures grew on an MPA substrate (35°C/24 h), while fungal and yeast cultures grew on Beer agar for 2 and 7 days at 28°C. The minimal inhibitory concentration (MIC) was defined as the lowest concentration of an antimicrobial agent at which there was no visible growth of the microbe.

The concentrations of preservatives were as follows: sodium benzoate — from 2.4 to 6.4 mg/ml; sodium nitrite — from 2 to 16 mg/ml; sulfurous acid — from 6 to 30 mg/ml. Each test tube was given 0.1 ml of the fabricated inoculums. The test tubes were incubated at 35°C for 24 h for bacteria (*Staphylococcus aureus*); and at 28°C for 48 h for yeast (*Saccharomyces cerevisiae)* and fungi for 168 h (*Aspergillus oryzae*).

Synergism of the preservatives was assessed by testing the following combinations of preservatives: sodium benzoate and sodium nitrite, sodium benzoate and sulfurous acid, sodium nitrite and sulfurous acid.

RESULTS AND DISCUSSION

The inhibitory concentration varied, depending on the kind of preservative and taxonomic characteristics of the species of microorganism tested. Table 1 presents the results of the inhibitory effect of sodium benzoate on *Staphylococcus aureus*, *Saccharomyces cerevisiae*, *Aspergillus oryzae.* The most sensitive microorganism against sodium benzoate is *Staphilococcus aureus* and the MIC is 4 mg/ml. In the studied range *Aspergillus oryzae* does not show any sensitivity to sodium benzoate.

The inhibitory effect of sodium nitrite (Table 2) and sulfurous acid (Table 3) was investigated on the three tested microorganisms. The most sensitive microorganism to sodium nitrite was found to be *Staphylococcus aureus* (MIC is 8 mg/ml). The strongest antimicrobial effect was exerted by sulfurous acid (no growth) in relation to the species *Staphylococcus aureus*. MIC of sulfurous acid to the yeast *Saccharomyces cerevisiae* and the fungi *Aspergillus oryzae* is 18 mg/ml.

Table 1. Growth of *Staphylococcus aureus*, *Saccharomyces cerevisiae*, *Aspergillus oryzae* at different concentrations of sodium benzoate

Microorganism tested	Concentration of sodium benzoate, mg/ml					
	2.4	3.2	4	4.8	5.6	6.4
Staphilococcus aureus	+	+	-	-	-	-
Saccharomyces cerevisiae	+	+	+	+	+	-
Aspergillus oryzae	+	+	+	+	+	+

Table 2. Growth of *Staphylococcus aureus, Saccharomyces cerevisiae* and *Aspergillus oryzae* at different concentrations of sodium nitrite

Microorganism	Concentration of sodium nitrite, mg/ml				
	2	**4**	**8**	**12**	**16**
Staphylococcus aureus	+	+	-	-	-
Saccharomyces cerevisiae	+	+	+	+	-
Aspergillus oryzae	+	+	+	+	-

Table 3. Growth of *Staphylococcus aureus, Saccharomyces cerevisiae* and *Aspergillus oryzae* at different concentrations of sulfurous acid

Microorganism tested	Concentration of sulfurous acid, mg/ml				
	6	**12**	**18**	**24**	**30**
Staphylococcus aureus	-	-	-	-	-
Saccharomyces cerevisiae	+	+	-	-	-
Aspergillus oryzae	+	+	-	-	-

Table 4. Combined action of preservatives on the tested microorganisms: *Staphylococcus aureus, Saccharomyces cerevisiae* and *Aspergillus oryzae*

Preservative, mg/ml	Microorganism						
	Staph. aureus	***Saccharomyces cerevisiae***			***Aspergillus oryzae***		
Sodium nitrite	4	12		12	12		12
Sodium benzoate	3.2		6.4	6.4		3.2	3.2
Sulfurous acid		12	12		12	12	
Growth after 48 h	-	-	-	+	-	-	+
Growth after 72 h	-	-	-	+	-	-	+

It is known that the effectiveness of individual or combined action of preservatives depends not only on their concentration and type, but also on the species of microorganism on which they act [7]. In the present work we have combined the three used preservatives in different combinations to study the synergistic and additive effect on tested microorganisms. The combinations and the results are presented in Table 4.

The results show that the tested microorganisms *Saccharomyces cerevisiae* and *Aspergillus oryzae* are not sensitive to the combination of preservatives sodium benzoate and sodium nitrite, with the exception of *Staphylococcus aureus*. However, it is significant that the combination of sodium benzoate with sulfurous acid and sodium nitrite with sulfuric acid has an inhibitory effect on the growth of the tested yeasts and fungi.

CONCLUSION

The results of this study demonstrate a more effective antimicrobial action of the preservatives when used in combination with other preservatives than when used individually, a finding that can contribute to a more effective conservation of food. Synergism was recorded at low levels of preservatives, which indicates the possibility of avoiding the use of higher concentrations of sodium benzoate, sodium nitrite and sulfurous acid which could lead to accumulation of toxic products in conserved food.

REFERENCES

1. Restaino, L. K., K. Komatsu and M. J. Syracuse, 1981. Effects of acids on potassium sorbate inhibition on food–related microorganisms in culture media. *J. Food Sci*., 47: 134-143.
2. Stickler, D. J. and B. Tomas, 1982. Intrinsic resistance to nonantibiotic antibacterial agents, *Principles and Practice of Disinfection, Preservation and Sterilization* (A.D. Russell, W.B. Hugo and G.A.J. Ayliffe, eds.), Blackwell Scientific Publications, Oxford, pp. 186-198.
3. Woolford, M. K. 1990. The detrimental effects of air on silage. J. Appl. Bacteriol. 68:101–116.
4. Lättemäe, P., and P. Lingvall. 1996. Effect of hexamine and sodium nitrite in combination with sodium benzoate and sodium propionate on fermentation and storage stability of wilted and long cut grass silage. Swed. J. Agric. Res. 26:135–146.
5. Lingvall, P., and P. Lättemäe. 1999. Influence of hexamine and sodium nitrite in combination with sodium benzoate and sodium propionate of fermentation and hygienic quality of wilted and long cut grass silage. J. Sci. Food Agric.

79:257–264.
6. Knicky, M., and R. Spörndly. 2014. Silage additives—Assessment of their efficiency to improve aerobic stability of silages. Page 55–56 in Proc. 16th Int. Symp. Forage Conserv. Mendel Univ., Brno, Czech Republic.
7. D. Stanojevic, L. Comic, O. Stefanovic and SL. Solujic-Sukdolak, 2009. Antimicrobial effects of sodium benzoate, sodium nitrite and potassium sorbate and their synergistic action in vitro, Bulgarian journal of agricultural science, 15 (no 4), 307-311.
8. Voss, C., Tsikriktsis, N. and Frohlich, M. 2002. Case Research in Operations Management. International Journal of Operations & Production Management, 22, 195-219.
9. Silva M. M., F. C. Lidon, 2016, Food preservatives – An overview on applications and side effects, Emirates Journal of Food and Agriculture 28(6): 366-373.
10. Masarin F. and A. Ferraz. 2008. Evaluation of *Eucalyptus grandis* Hill ex Maiden biopulping with *Ceriporiopsis subvermispora* under non-aseptic conditions, Hozforschung., 62, pp. 1-7

ANNUAL OF ASSEN ZLATAROV UNIVERSITY, BURGAS
BULGARIA, 2022, v. LI(1)

PROBABILITY MODELING USING LOGISTIC REGRESSION AND MAPREDUCE

Stanislav Popov, Todor Petkov, Veselina Bureva
E-mail: stani_popov@yahoo.com

ABSTRACT

As the amount of information available for data mining grows larger, the time needed to train models on those huge volumes of data also grows longer. MapReduce programming method is easily applicable to many different learning algorithms. Machine learning is at the core of data analysis. Traditional machine learning algorithms speed up at a time to fit the statistical query model on multicore components. MapReduce programming model enables easy development of scalable parallel applications to process large clusters of data. Therefore, when combined with logistic regression algorithm it can be very successfully used for prediction analysis.

Key words: *big data, MapReduce, machine learning*

INTRODUCTION

As the number and type of data acquisition devices grow annually, the sheer size and rate of data being collected is rapidly expanding. These big data sets can contain gigabytes or terabytes of data, and can grow on the order of megabytes or gigabytes per day. While the collection of this information presents opportunities for insight, it also presents many challenges. Most algorithms are not designed to process big data sets in a reasonable amount of time or with a reasonable amount of memory. MapReduce allows us to meet many of these challenges to gain important insights from large data sets.

The aim of this research is to analyze the process of the MapReduce algorithm step by step and make program realization of prediction model on patient data using logistic regression in MATLAB.

BIG DATA DEFINTION AND HOW IT WORKS

The definition of big data is data that contains greater variety arriving in increasing volumes and with higher velocity. This is also known as the three Vs [1].

Put simply, big data are larger, more complex data sets, especially from new data sources [2]. These data sets are so voluminous that traditional data processing software is not able to manage them. But these massive volumes of data can be used to address scientific problems that it was not possible to tackle before.

Big data provide new insights that open up new opportunities and models. Getting started involves three key actions: integrate, manage, analyze and the following text describes each of them:

1) Integrate - Big data brings together data from many disparate sources and applications. Traditional data integration mechanisms, such as extract, transform, and load (ETL) are generally not up to the task. It requires new strategies and technologies to analyze big data sets at terabyte, or even petabyte, scale. During integration, the data must be brought in, processed and formatted in order to be available in a form that data analysts can get started with.
2) Manage - Big data requires storage. The storage solution can be in the cloud, on premises, or both. The important aspect is to bring the desired processing requirements and necessary process engines to those data sets on an on-demand basis. The choice of storage solution depends mostly on where the data are currently residing. The cloud is gradually gaining popularity because it supports your current compute requirements and enables you to spin up resources as needed.
3) Analyze - The investment in big data pays off when the data are analyzed. This includes getting new clarity with a visual analysis of the varied data sets, building

data models with machine learning and artificial intelligence.

The rest of the article focuses on the MapReduce algorithm and its program realization in MATLAB.

MAPREDUCE ALGORITHM IN MATLAB

MapReduce is a programming technique for analyzing data sets that do not fit in memory [3]. MATLAB provides a slightly different implementation of the MapReduce technique with the *mapreduce* function.

The *mapreduce* function uses a data store to process data in small blocks that individually fit into memory. Each block goes through a Map phase, which formats the data to be processed. Then the intermediate data blocks go through a Reduce phase, which aggregates the intermediate results to produce a final result. The Map and Reduce phases are encoded by *map* and *reduce* functions, which are primary inputs to *mapreduce*. There are endless combinations of *map* and *reduce* functions to process data, so this technique is both flexible and extremely powerful for tackling large data processing tasks.

Mapreduce lends itself to being extended to run in several environments. The utility of the *mapreduce* function lies in its ability to perform calculations on large collections of data. Thus, *mapreduce* is not well-suited for performing calculations on normal sized data sets which can be loaded directly into the computer memory and analyzed with traditional techniques. Instead, MapReduce is used to perform a statistical or analytical calculation on a data set that does not fit in memory [4].

Each call to the *map* or *reduce* function by *mapreduce* is independent of all others. For example, a call to the *map* function cannot depend on inputs or results from a previous call to the *map* function. It is best to break up such calculations into multiple calls to *mapreduce*.

Fig. 1 presents the MapReduce architecture.

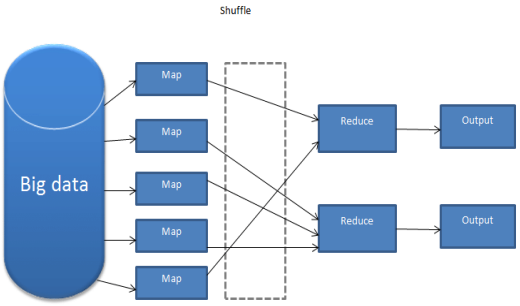

Fig. 1 MapReduce architecture

The algorithm has the following steps [5]:

1) *mapreduce* reads a block of data from the input datastore using [data,info] = read(ds), and then calls the *map* function to work on that block.
2) The *map* function receives the block of data, organizes it or performs a precursory calculation, and then uses the add and *addmulti* functions to add key-value pairs to an intermediate data storage object called a KeyValueStore. The number of calls to the *map* function by *mapreduce* is equal to the number of blocks in the input datastore.
3) After the *map* function works on all of the blocks of data in the datastore, *mapreduce* groups all of the values in the intermediate KeyValueStore object by unique key.
4) Next, *mapreduce* calls the *reduce* function once for each unique key added by the *map* function. Each unique key can have many associated values. *Mapreduce* passes the values to the *reduce* function as a ValueIterator object, which is an object used to iterate over the values. The ValueIterator object for each unique key contains all the associated values for that key.
5) The *reduce* function uses the *hasnext* and *getnext* functions to iterate through the values in the ValueIterator object one at a time.
6) Then, after aggregating the intermediate results from the *map* function, the *reduce* function adds final key-value pairs to the output using the *add* and *addmulti* functions. The order of the keys in the output is the same as the order in which the r*educe* function adds them to the final KeyValueStore object. That is, *mapreduce* does not explicitly sort the output.

LOGISTIC REGRESSION AND MAPREDUCE

Logistic regression is a way to model the probability of an event as a function of another variable [6]. The operation is included in MapReduce by connecting multiple calls to *mapreduce* to execute an iterative algorithm. Because each iteration requires a separate pass through the data, the anonymous function passes information from one iteration to the next to provide the information directly to the *mapper*. To complete the logistic regression, the *map* and *reduce* functions must perform a weighted linear regression based on the current coefficient values and the vector product of the input data blocks.

The *map* function used in the software implementations presented in the next section, in addition to the standard parameters, contains additional ones (gender, weight, age, smoker / non-smoker), through which only the necessary information is extracted from the data store. These parameters may change depending on what data need to be calculated. Also, the function contains the condition that the least squares forecasting and calculation must meet. The other elements of the map function are described as comments in the code. They are standard and can be used repeatedly in different implementations of the algorithm.

USING MAPREDUCE TO FIT A LOGISTIC REGRESSION MODEL

The following section describes a method of predicting the probability of women/men to be smokers as they age. The range of the predictor variable (age) is between 25 and 50 years. The data are taken from hospital patient records. Below are presented the three functions in MATLAB needed to perform the prediction: Mapreduce.m, mapper_fit_all.m and Reducer_fit.m. What follows is the program realization of the prediction model.

1) Mapper_fit_all.m

```
function Mapper_fit_all(b,t,~,intermKVStore,
active_gnr)
  t = t(strcmp(t.gnr,active_gnr),:);
  y = t.smoke;
  x = t.age;
  t = ~isnan(x) & ~isnan(y);
  x = x(t);

  if ~isempty(b)
    xb = b(1)+b(2)*x;
    mu = 1./(1+exp(-xb));
  else
    mu = (y+.5)/2;
    xb = log(mu./(1-mu));
  end

  w = (mu.*(1-mu));
  z = xb + (y - mu) .* 1./w;

  X = [ones(size(x)),x,z];
  wss = X' * bsxfun(@times,w,X);

  add(intermKVStore, 'key', wss);
end
```

2) Mapreduce.m

```
ds = datastore('hospitalC.csv');
ds.SelectedVariableNames = {'gnr', 'age',
'smoke'};

 b = [];

for iteration = 1:5
    b_old = b;
    iteration;

    mapper = @(t,ignore,intermKVStore)
Mapper_fit_all(b,t,ignore,intermKVStore,'m');
    result = mapreduce(ds, mapper, @Reducer_fit,
'Display', 'off');

    disp(result)
    tbl = readall(result);
    b = tbl.Value{1};

      if ~isempty(b_old) && ...
      ~any(abs(b-b_old) > 1e-6 * abs(b_old))
      break
    end
end
xx = linspace(25,50);
yy = 1./(1+exp(-b(1)-b(2)*(xx)));
b = [];

for iteration = 1:5
    b_old = b;
    iteration;
mapper = @(t,ignore,intermKVStore)
Mapper_fit_all(b,t,ignore,intermKVStore, 'f');
    result = mapreduce(ds, mapper, @Reducer_fit,
'Display', 'off');
    disp(result)
    tbl = readall(result);
    b = tbl.Value{1};

    if ~isempty(b_old) && ...
      ~any(abs(b-b_old) > 1e-6 * abs(b_old))
      break
    end
end

figure()
xx2 = linspace(25,50);
yy2 = 1./(1+exp(-b(1)-b(2)*(xx)));
plot(xx2,yy2, xx,yy);
title('MapReduce probability for smoking');
legend('Men', 'Women')
xlabel('Age');
ylabel('Prob[smoking]')
```

3) Reducer_fit.m

```
function Reducer_fit(~,intermValI-
ter,outKVStore)
  old = 0;
```

```
while hasnext(intermValIter)
  new = getnext(intermValIter);
  old = old+new;
end

N = old;

XtWX = N(1:end-1,1:end-1);
XtWY = N(1:end-1,end);
        b = XtWX\XtWY;
add(outKVStore, 'key', b);
end
```

After finishing the five iterations the result is shown in Fig. 2.

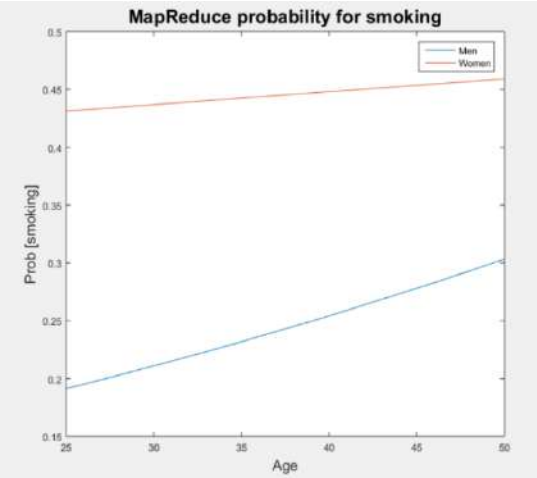

Fig. 2 Probability model of patient data

The result shows that in both sexes, with increasing the age between 25 and 50 years, the likelihood of having smokers also increases. With men, the curve is steeper, but in general the probability grows slower. With women, the curve is flatter and the probability values are higher.

CONCLUSION

The current research develops a probability model using logistic regression and MapReduce algorithm. Both are implemented into a practical example that contains patient data with different attributes from which the age of the patients is used as a predictor. The calculated probability is for the patients to be smokers or not. After the program realization of the algorithm finishes its iterations, the result is shown in an aggregate graphics for both men and women.

REFERENCES

1. Riahi Y., Big Data and Big Data Analytics: Concepts, Types and Technologies, 2018, pp. 524-528.
2. De Mauro A., Marco M., A Formal Definition of Big Data Based on its Essential Features, Library Review, 2016, pp.122-135.
3. Vaidya M., The Map Reduce Framework: Analysis and The Research Perspectives, 2013, p. 124.
4. Miner D., Shook A., MapReduce Design Patterns, 2013, O'Riley, pp. 45-46.
5. Dean J., Ghemawat S., MpReduce: Simplified Data Processing on Large Clusters, Sixth Symposium on Operating System Design and Implementation, San Francisco, CA, 2004, pp.137-150.
6. Sperandei S., Understanding logistic regression analysis. Biochema medica, 2014, p. 24.

ANNUAL OF ASSEN ZLATAROV UNIVERSITY, BURGAS
BULGARIA, 2022, v. LI(1)

SOME FEATURES OF GASOIL OXIDATION

Yordanka Tasheva, Aleksander Dimitrov, Milena Dimitrova
E-mail: jtasheva_2006@abv.bg

ABSTRACT

The thermodynamic characteristics of the oxidation of two gasoil fractions were investigated. The calculated thermodynamic parameters were: Gibbs energy, enthalpy and entropy of the separate systems gas oil fraction: oxidizing mixture. It was found out that in all studied systems the oxidation process is thermodynamically possible.

Key words: *gasoil, middle distilled fractions, oxidation, Gibbs energy*

INTRODUCTION

Desulfurization of fuels has become a topic of recent concern with the increased environmental hazards sulfur emissions are having on the atmosphere, such as photochemical smog and acid rain. In the case of acid rain, the sulfurous gases mix with water vapor in clouds and condense with them in the form of rain as the atmosphere in the cloud becomes saturated. The resultant acid rain can irreversibly damage ecosystems by disturbing the pH of the groundwater and absorption by plants [1].

In the case of photochemical smog, sulfurous gases accumulate in the troposphere, thus blocking sunlight from reaching the Earth's surface, which is needed for plant photosynthesis. The combustion of fuels typically used in automobiles is a large contributor to SOx production. Sulfur in the form of compounds, such as dibenzothiophene, become SOx compounds in combustion. The simplest solution for minimizing this emission is removing the sulfur containing compounds from fuels prior to combustion. The Environmental Protection Agency (EPA) is decreasing the allowable sulfur standard in response to more information on the SOx problem [2].

This measure would minimize the largest anthropogenic producer of sulfonated gases and, in turn, allow for the recovery of ecosystems not already occupying land near natural SOx producers, such as volcanoes [1]. In an attempt to tackle this problem, several mechanisms of sulfur extraction have been proposed, including standard thermochemical treatment (hydrotreating) and biodesulfurization [3-5].

Hydrotreatment is the most commonly used process for sulfur extraction prior to combustion. In this process the petroleum fuel is contacted with the Ru2+ compound (L)Ru(H2O) at temperatures between 560< T(K)<670 [6]. L in this compound is a ligand which solubilizes ringed sulfur containing structures in the fuel such as thiols, thioethers and dibenzothiophenes. The resultant complex (L)Ru(DBT) is then pressurized to remove the DBT for incineration or sonochemical decomposition. This step regenerates the Ru, thus enabling large quantities of low-sulfur fuel feedstock for a small amount of extractant [6, 7].

The major problem with this system is that the ligands required to successfully complex with the DBT are fairly expensive and unstable. The ligands typically used in this complex include: cyclopentadiene, phosphines, and carbon monoxide. Any losses within the fuel are not only costly to replace, but can also add worse chemicals to the fuels than those targeted for removal. Furthermore, the instability of these compounds guarantees some contamination to occur. Work has been conducted to try more stable and less expensive ligands, however these results have not yielded similar removals as their currently used less stable counterparts. Due to this lack of information, much emphasis has been placed on finding a replacement process capable of removing large quantities of sulfurous compounds without contaminating the fuel.

Biodesulfurization is a relatively new approach to sulfur treatment that utilizes enzymes to decompose and remove dibenzothiophene. In this process, the sulfur containing fuel feedstock is fed into a tank, oxidized, and decomposed

using *Rhodococcus* biocatalysts. The advantage that this process has over hydrotreating is that it can be carried out at ambient temperature which reduces the operating costs. The removal involves partially oxidizing the fuel and decomposing the DBT with liquid-liquid extractions, which can take up to 8 hours for full sulfur removing efficiency. The sulfur reduction potential of this process seems to match that of the hydrotreatment process. However, its lack of fuel contamination and ability to be run at ambient conditions are not enough to offset the increased equipment cost and longer treatment times. Since neither of these methods has proved to be economically efficient in complete sulfur removal, there is still a need for alternative mechanisms. Utilization of RTIL provides one potential solution. Desulfurization of fuels using oxidation processes has been attempted by Bosmann and co-workers, as well as Petkov and co-workers in Bulgaria [8-10].

EXPERIMENT

Gas oil fractions named A1 and A2 from Bulgarian oil were used as raw materials. The physicochemical properties of A1 and A2 are given in [8]. Formic acid, acetic acid and hydrogen peroxide were used as oxidation mixture. All reagents were purchased from Sigma-Aldrich. All technological tests were performed in laboratory conditions.

The methodology of the oxidation process was as follows: a mixture of 50 - 150 ml of the studied raw material, 200 - 350ml oxidation mixture (hydrogen peroxide - carboxylic acid (formic or acetic acid) in a ratio of 1: 4 to 4: 1) and 30 mg 0.1 % potassium permanganate solution, which serves as a catalyst, was stirred continuously in a reflux flask at constant temperature for 60 minutes. After completion of the reaction, the test sample was separated from the acid phase of the oxidation mixture by means of a separatory funnel. The resulting gas oil fraction was washed with 5% calcium carbonate solution or only with distilled water to remove acidic products, air-dried and filtered by known conventional methods. Thermodynamic parameters were calculated according to well-known physicochemical equations. The calculation methodology is described in previous works [8, 9]. The obtained results are presented in Fig. 1 to 8.

RESULTS AND DISCUSSION

The dependences of the distribution coefficient /ln K/ on the temperature /1 / T/ of the investigated oxidized blends are shown in Fig. 1-4. Fig. 5-8 present the dependences of the Gibbs energy, enthalpy and entropy of the middle distilled raw materials A1 and A2 subjected to oxidation with formic and acetic acids in the presence of a potassium permanganate catalyst.

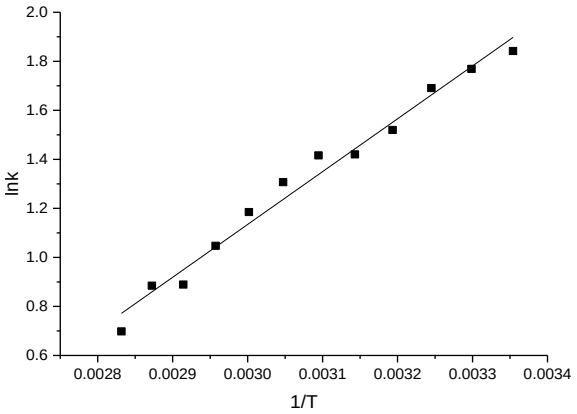

Fig. 1. Dependence of the distribution coefficient on temperature (1 / T) of oxidized sample A1 with acetic acid

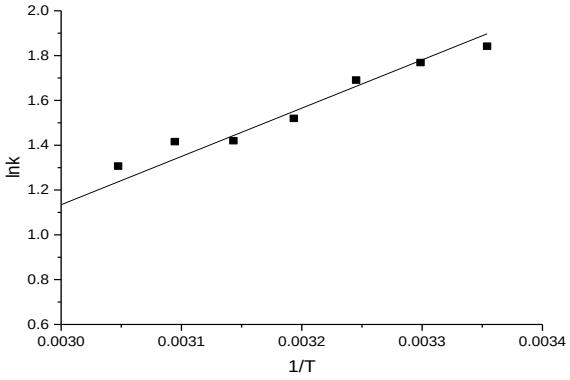

Fig. 2. Dependence of the distribution coefficient from temperature (1/T) of oxidized sample A1 with formic acid

The negative values obtained for the free Gibbs energy for all studied systems middle distillate fraction : oxidative mixture confirm the experimental data for the oxidation process of the studied raw materials A1 and A2, while showing that this process for all systems studied by us is thermodynamically possible.

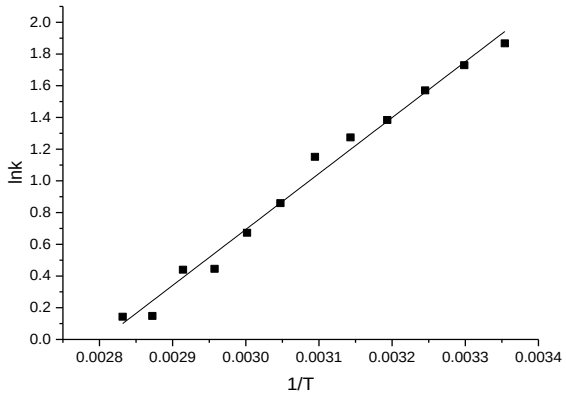

Fig. 3. Dependence of the distribution coefficient from temperature (1/T) of oxidized sample A2 with acetic acid

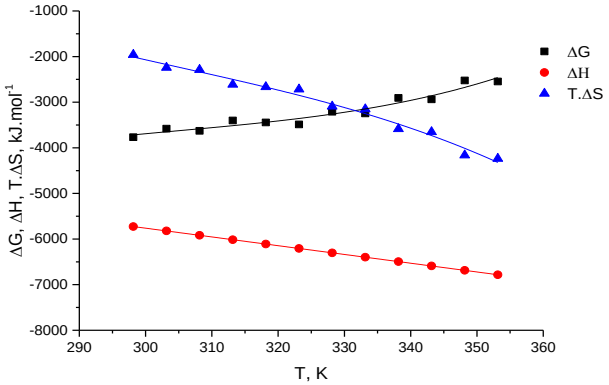

Fig. 6. Dependence of Gibbs energy, entropy and enthalpy from temperature of system A1: formic acid (in presence of 0,1% $KMnO_4$)

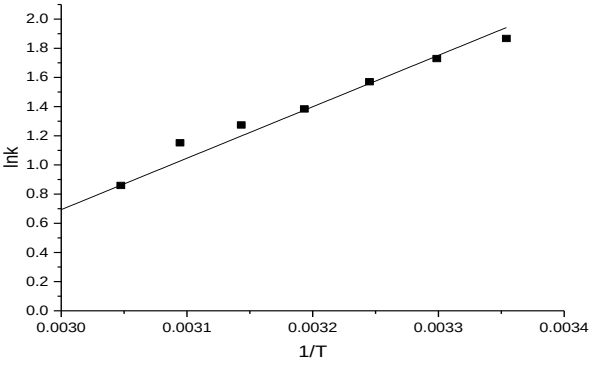

Fig. 4. Dependence of the distribution coefficient from temperature (1/T) of oxidized sample A2 with formic acid

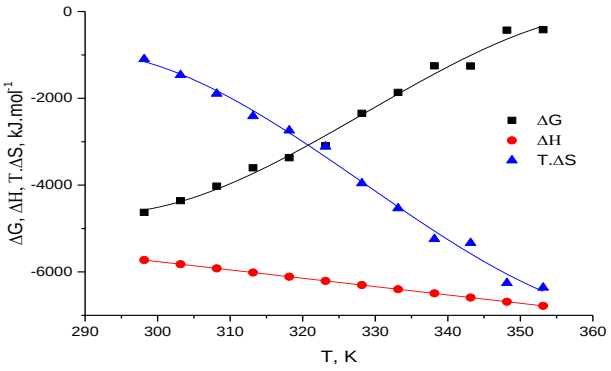

Fig. 7. Dependence of Gibbs energy, entropy and enthalpy from temperature of system A2:acetic acid (in presence of 0,1% $KMnO_4$)

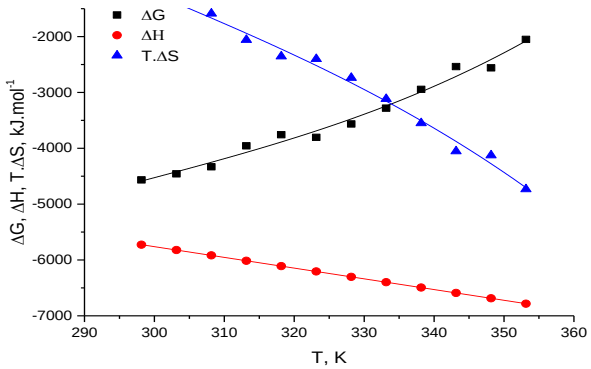

Fig. 5. Dependence of Gibbs energy, entropy and enthalpy from temperature of system A1:acetic acid (in presence of 0.1% $KMnO_4$)

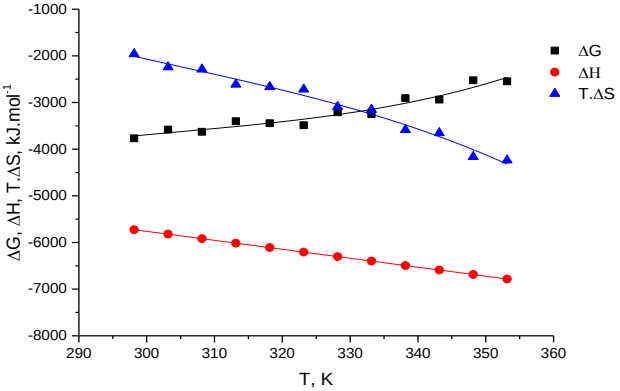

Fig. 8. Dependence of Gibbs energy, entropy and enthalpy from temperature of system A2: formic acid (in presence of 0.1% $KMnO_4$)

From the obtained data on the entropy of distribution of the individual systems, it can be seen that in the process of oxidation of the gas oil fractions studied by us, an intermolecular interaction of the most noticeable thermal effect is most likely to take place.

The application of the process of oxidation of gas oil fractions in order to purify them from sulfur and arene hydrocarbons was studied. The dependences of the distribution coefficients on the temperature were determined. The thermodynamic parameters of the process were calculated: Gibbs energy, enthalpy and entropy of the separate systems gas oil fraction: oxidizing mixture. It was found out that in all studied systems, the oxidation process is thermodynamically possible. From the obtained data on the entropy of distribution of the individual systems, it can be seen that in the process of oxidation of the gas oil fractions studied by us, an intermolecular interaction of the most noticeable thermal effect is most likely to take place.

REFERENCES

1. Wang L., S. Baode, Fr. Yang et all. *Chemical Engineering Science,* Denitrification of simulated oil by extraction with H_2PO_4-based ionic liquids, **73**, (2012), p. 208.
2. Wang F., Zh. Zhang, J. Yang et all., Oxidative desulfurization of dibenzothiophene using ozone and hydrogen peroxide in ionic liquid, *Fuel*, **107,** (2013), p. 394.
3. De Luna M., M. Samaniego, D. Ong et all. Kinetics of mixing-assisted oxidative desulfurization of dibenzothiophene in toluene using a phosphotungstic acid/hydrogen peroxide system: effects of operating conditions, *Journal of Cleaner Production,* **178,** (2018), p. 468.
4. Fallah R., S. Azizian, G. Reggers et all. Rapid and facile desulphurization of liquid fuel by carbon nanoparticles dispersed in aqueous phase, *Fuel Processing Technology,* **119,** (2012), p. 278.
5. Gao Sh., G. Yu, R. Abro et all. Extractive desulfurization of fuel using 3-methylpyridinium-based ionic liquids, *Fuel*, **173** (2016).
6. Saleh A., I. Danmaliki. Adsorptive desulfurization of dibenzothiophene from fuels by rubber tyres-derived carbons: kinetics and isotherms evaluation, *Process Saf. Environ. Prot.*, **102**, (2016), p.16.
7. Ma X., A. Zhou, Ch. Song. A novel method for oxidative desulfurization of liquid hydrocarbon fuels based on catalytic oxidation using molecular oxygen coupled with selective adsorption**,** *Catal. Today*, 123 (2007).
8. Guttierez J., G. Fuentez, M. Hernandez-Teran et all. Deep oxidative desulfurization with task-specific ionic liquids: an experimental and computational study, *Appl Catal A-Gen*., **305** (2006).
9. Tasheva Y., A some features of gasoil extraction, Remolval of sulfur compounds by adsorption, *Annual of Assen Zlatarov University,* **XLVIII** (2019).
10. Tasheva Y., Al. Dimitrov, M. Dimitrova, *Annual of Assen Zlatarov University*, **XLVIX** (2020).

ANNUAL OF ASSEN ZLATAROV UNIVERSITY, BURGAS
BULGARIA, 2022, v. LI(1)

ENTROPICAL THERMODYNAMIC DESCRIPTION OF HUMANS AND HEALTH AS A UNIQUE FUNCTIONAL ELEMENT IN THE CONCEPT OF HEALTH ECOLOGY AND THE BIOSPHERE[1]

Mihai Petrov
E-mail: mihpetrov@abv.bg

ABSTRACT

The aim of this study is to develop a quantitative description of human being by the application of the integrative bioeconophysical concept of the thermodynamic parameter entropy as a result of the complex human interaction with the Biosphere and Technosphere (the sphere of material products). Human metabolism needs energy from the environment, as well as from the Technosphere of the average 12,000 kJ per day and is described by the laws of thermodynamics and contains the weight of the human body, effective molar mass of the human body, and mass of substances intake by the body. The change in entropy over time contains two components: the sphere of material products (technosphere) and the biosphere. The extreme case of the gradual consumption of products containing pollutants leads to the development of pathological cases with higher entropy of human being.

Key words: *bioeconophysical concept, free energy of Gibbs, molar masses, entropy, Biosphere, Technospere*

INTRODUCTION

The econophysical and bioeconophysical conceps that were developed in papers [1–5] with the quantitative expression of Gibbs free energy of human being lie in the basis of this recent study on their application in the case of consumption of medicals with therapeutic effect, oxygen, nutrients, etc., and based on that, the conception of human entropy is suggested as a result of the reciprocal interaction between the Biosphere and the Technosphere.

EXPERIMENT

The modern human being is in permanent interaction with the elements of the Biosphere to ensure a normal physiological state as well as with the elements of the Technosphere without which it is also impossible to ensure a normal state of comfort and development. The general scheme of the interaction of the human being with the elements of the Biosphere and the Technosphere is presented in Fig. 1.

A large part of the Technosphere components are produced as a result of the direct consumption of the elements of the Biosphere. The current state of the Biosphere is characterized by the accumulation of pollutants with a negative effect on human health, as well as the limited natural energy resources of the Biosphere.

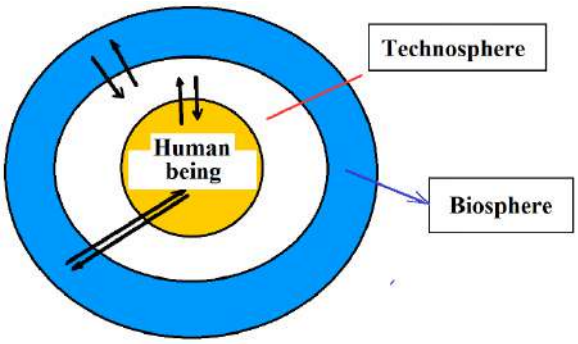

Fig. 1 A general diagram of the interaction of the complex system Human being-Biosphere-Technosphere

The corresponding Gibbs free energy ΔG_{mol}, which was developed in the above-mentioned papers, as the dependence of mass, time and the amount of intake moles is:

[1] The article was presented at the Challenges for Medical Science and Practice in the 21st Century Congress of Medicine, Burgas, 1-3 September 2022

$$\Delta G_{mol} = \frac{2.M.R.T.m_{org}}{m_f.M_{org}.\ln 2}.\ln\left(\frac{A.\tau}{4.\ln 2}\right); \text{[J/mol]} \quad (1)$$

where, M is molar mass of the intake substances (food, medical or oxygen); m_f is the respective mass of the intake substances (food, medical or oxygen); R is universal constant of gases; T is absolute temperature (T ≈ 310K); m_{org} is the mass of respective organ, receptor or the whole human body; M_{org} is the respective molar mass (for the whole human body is ≈ 20 g/mol); τ is interval of time in hours (*h*) for the food intake, administration of medical doses, oxygen; A is pre-exponential factor (h^{-1}) (It has the meaning of the elimination rate constant λ for the case of very small molecules with molar masses M→0) [4].

RESULTS AND DISCUSSION

The application of the expression (1): $\Delta G = \Delta G_{mole} \cdot \nu$; ($\nu = m_f/M$) on the human body of various weight, age and height is compared with the well-known values of energy E_{tab} that are found by the biocalorimetric method. There are tables for the basic metabolism of the biocalorimetric method [6] and the values of energy E_{tab} of the weight, age and height of the human body are presented.

The corresponding energies in kilojoules $\Delta G = \Delta G_{mole} \cdot \nu$ in comparison with the data E_{tab} from the table of metabolism are presented in the following graph (Fig. 2):

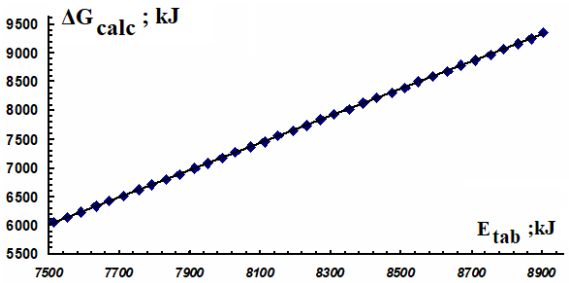

Fig. 2 Comparison of the calculated values of Gibbs free energy with the tabular data from calorimetric method

In order to validate the corresponding method of the energy calculation based on the values of Gibbs free energy, firstly we will calculate the time interval τ from (1):

$$\tau_{calc} = \frac{4.\ln 2}{A}.e^{\frac{E_{tab}.M_{body}.\ln 2}{2.R.T.m_{body}}}, \quad (2)$$

where, m_{body} is the mass of human body; $M_{body} \approx$ 20 g/mol is the molar mass of human body.

The values of ΔG are calculated for the empirical theoretical value of the time interval τ = 5.5 (h) and are presented in Table 1. The aim is to observe if the average value $<\tau_{calc}>$ matches the theoretical value of 5.5 hours.

There are statistical criteria to check if the average value of a sample matches the real theoretical value 5.5 (*h*). One of them is the T-test. The statistical program BIOSTAT gives the answer that the average value of 5.84 (h) is similar to the theoretical value 5.5 hours with a probability *p=0.84* and then the conclusion is that these values are matching.

Table 1. Energy values of metabolism and dose time intervals

m_{body}; kg	E_{tab}; kJ	ΔG_{calc}; kJ	τ_{calc}; h
40	6554.24	3778.723	6.628968
42	6633.66	3967.659	6.524358
44	6713.08	4156.595	6.430691
46	6792.5	4345.531	6.346345
48	6871.92	4534.467	6.269999
50	6951.34	4723.403	6.200572
52	7030.76	4912.339	6.137169
54	7114.36	5101.275	6.080306
56	7193.78	5290.212	6.026766
58	7273.2	5479.148	5.977343
60	7352.62	5668.084	5.93158
62	7432.04	5857.02	5.889087
64	7511.46	6045.956	5.849527
66	7590.88	6234.892	5.812606
68	7670.3	6423.828	5.778069
70	7753.9	6612.764	5.746618
72	7833.32	6801.701	5.716178
74	7912.74	6990.637	5.687531
76	7992.16	7179.573	5.660525
78	8071.58	7368.509	5.635023
80	8151	7557.445	5.610902
82	8230.42	7746.381	5.588053
84	8309.84	7935.317	5.566379
86	8393.44	8124.253	5.546517
88	8472.86	8313.19	5.526917
90	8548.1	8502.126	5.507565
92	8631.7	8691.062	5.49046
94	8711.12	8879.998	5.473477
96	8790.54	9068.934	5.457251
98	8869.96	9257.87	5.441733
			$<\tau_{calc}>$=5.84

The importance and the role of this expression consist in the fact that it is possible to estimate what the dose interval of time is, if we know the mass of the human body.

For the well-known medical product Analgin in the form of tablets, the mass of one tablet is 500 mg and the molar mass is 333.34 (g/mol). It is usually administered four times a day with an interval of 4-6 hours. The respective quantity of moles of one tablet of Analgin is:

$$\nu = \frac{m}{M} = \frac{0.5(g)}{333.341(g/mol)} = 0.001499(mol)$$

The bounding of drugs with receptors takes place by the mechanism of G-protein-coupled receptors, GPCR [7]. The activation energy between the molecule of metamizole sodium and the GPCR receptors is about 20 kJ/mol [8].

$$\tau = \frac{4.\ln 2}{A}.e^{\frac{\Delta G_{mol}.\nu.M_{body}.\ln 2}{2.R.T.m_{body}}} = \frac{4.\ln 2}{0.5}.e^{\frac{20000.0,0015.20.\ln(2)}{2.8,31.310.80000}} =$$

$$= \frac{4.\ln(2)}{0.5}.e^{10^{-7}} = \frac{4.0,693}{0.5} \approx 5.5(h) \to 6(h)$$

In this way one tablet of Analgin can be taken approximately four times a day.

Generally, the human being consumes nutrients together with water of the order of 2500 grams per day (≈2000 is water and ≈500 grams of total mass for proteins, carbohydrates and fats) and the respective amount of moles of nutrients per day is 2500/500=5 moles and this quantity of 5 moles ensures the production of 100-150 moles of ATP per day, which is required for the process of hydrolysis. Then, the total energy of 12 (MJ) divided by 5 moles gives the result of the order 2.56 (MJ/mol) and the corresponding time interval can be recalculated as:

$$\tau = \frac{4.\ln 2}{A}.e^{\frac{\Delta G_{mol}.\nu.M_{body}.\ln 2}{2.R.T.m_{body}}} = \frac{4.\ln 2}{0.5}.e^{\frac{2,56.10^6.5.20.\ln 2}{2.8,31.310.80000}} =$$

$$= \frac{4.\ln 2}{0.5}.e^{0.430509} = 2.4963(h) \to 3(h)$$

In this way, the person intakes the corresponding meals and water during a day with an interval of two or three hours (about 4-5 times per day).

Regarding the concept of entropy, it has been shown that the human chemical potential is of the order of 2.75 - 3 (kJ/mol) [5]. The total amount of the moles that the human body contains as the dependence of the mass of the body is of the order of 4000-5000 moles. The effective molar mass of the human being is about 20 (g/mol). The corresponding variation of Gibbs free energy is of the order of 10 (MJ)-13 (MJ), which is actually the required amount of the energy per day as a result of the consumption of nutrients. The corresponding variation of the entropy of the human being is defined as:

$$\Delta S = -\frac{\Delta G}{T}; \qquad [J/K] \tag{3}$$

If the human entropy changes by a value of ≈35 (kJ/K) during one day and if the World's population is ≈7 billion, then the total entropy of the humanity sphere ΔS_h is of the order:

$\Delta S_h = 35 \cdot 10^3 \cdot 7 \cdot 10^9 = 245 \cdot 10^{12}(J/K)= 2.45 \cdot 10^{14}$(J/K)

$\approx 2.5 \cdot 10^{14}(J/K)\equiv 2.89 \cdot 10^9$ (W/K)

The value of a similar approximate order $2.58 \cdot 10^9$ (W/K) was obtained in paper [9]. The current state of the Biosphere is characterized by the presence of dangerous pollutants: nitrates, nitrites, sulfur dioxide, ozone, nitrogen oxide, nitrogen dioxide, sulfuric acid rains, fine micron sized particles of lead, metals and other oxides of metals, particles of carbons and particles of plastic materials suspended in the atmosphere and waters, etc. The largest share refers to carbon dioxide (75%) [10]. Every year the atmosphere accumulates carbon dioxide with the corresponding amount of heat $3 \cdot 10^{20}$ (J). Accordingly, there is a heat accumulation during one day: $8 \cdot 10^{17}$ (J) [10]. The corresponding entropy variation of the biosphere during one day is:

$$\Delta S_{bios-re} = \frac{8 \cdot 10^{17}}{300(K)} = 2,7 \cdot 10^{15}(J/K) \equiv 3 \cdot 10^{10}(W/K)$$

The state of the biosphere is influenced by the state of the humanity sphere as well as by the sphere of materials that are consumed and produced by the industry (Technosphere). In this way, the entropy variation of the biosphere is the sum of the entropy variations of the Technosphere and of the humanity sphere.

$$\Delta S_{bios-re} = \Delta S_{Tech-re} + \Delta S_h \tag{4}$$

The respective variation of the entropy of the Technosphere is:

$$\Delta S_{Tech\text{-}re} = \Delta S_{Bios\text{-}re} - \Delta S_h =$$

$$= 3 \cdot 10^{10}(W/K) - 0.289 \cdot 10^{10}(W/K) = 2.71 \cdot 10^{10}(W/K)$$

It is necessary to check this result of $2.71 \cdot 10^{10}$ (W/K) with the real one. When we describe the Technosphere, the main focus is on the consumption of electricity, which is used to produce almost all products for the consumption and use by human beings [11].

It is calculated that, on average, 28 kWh of electrical energy is spent for each person per day. If we take into account the energy for the production of all goods in all factories and if they are distributed evenly for whole World's population, then indeed the expenses are of the order 28 kWh per day for each person [11]. If this result is multiplied by 7 billion population, then the total energy consumption is:

$28 \cdot 7 \cdot 10^9$(kW·h)=$196 \cdot 10^9$(kW.h)=$196 \cdot 10^{12}$ (W.h)=$196 \cdot 10^{12}$(J/s)·3600(s)=$705600 \cdot 10^{12}$(J)= =$7 \cdot 10^{17}$ (J).

The corresponding entropy change of the Technosphere during one day is:

$7 \cdot 10^{17}$(J)/(24·3600(s)·300(K))=$2.7 \cdot 10^{10}$(W/K)

In such a way, it is proved that the real result of electrical consumption coincides with the calculated value within the minimal limits of errors.

This complex system Human being-Biosphere-Technosphere could be considered a "closed" system with respect to very remote cosmic space [12]. The entropy obtains the maximal value over time and the state of the equilibrium is reached for this "closed" system. The increase of the entropy of this complex system takes place due to the increase of the gaseous pollutants in the atmosphere. The evolution of the entropy with time of this complex system is described as:

$$\frac{dS}{dt} = \frac{dS_h}{dt} + \frac{dS_{tech-re}}{dt} + \frac{dS_{bios-re}}{dt} \qquad (5)$$

where, $\frac{dS}{dt} = 0$ is the case of stationary state and it means that there is no variation of the entropy over time. Then:

$$\frac{dS_h}{dt} = -\frac{dS_{tech-re}}{dt} - \frac{dS_{bios-re}}{dt} \qquad (6)$$

If the entropy of the Biosphere increases due to the increase of gaseous pollutants and if the entropy of the Technosphere increases due to the application of new technologies in greater quantities, then a situation could happen where the sphere of humanity could be in decline by entropy: $\frac{dS_h}{dt} < 0$. In general, the entropy also depends on the quantity of its constituent structural elements and for the case of humanity with the population of 7 billion it could be the beginning of the decline of the population due to diseases and epidemics which are related to the increase of pollutants. The opposite situation $\frac{dS_h}{dt} > 0$ could happen when $\frac{dS_{bios-re}}{dt} < 0$. This situation could be a result of the increase of the rate of photosynthesis with an increasing rate of production of oxygen and glucose. Regarding the Technosphere, the same decrease could be $\frac{dS_{tech-re}}{dt} < 0$, meaning that this component reaches the situation of high order of the quality of the products with high efficiency. So, if the values are $\frac{dS_{bios-re}}{dt} < 0$; $\frac{dS_{tech-re}}{dt} < 0$, then the entropy of humanity is $\frac{dS_h}{dt} > 0$, meaning that the World's population increases over time. But in general, the Technosphere can be characterized by two components: 1) effective part and 2) ineffective part.

$$\frac{dS_{tech-re}}{dt} = \frac{dS_{eff}}{dt} + \frac{dS_{ineff}}{dt} \qquad (7)$$

The effective part ensures the decrease of the entropy of the Technosphere due to the high order of the quality of the products with high efficiency and also the normal physiological development of human beings:

$$\frac{dS_h}{dt} = \frac{dS_{eff}}{dt} \qquad (8)$$

The ineffective part refers to such elements that are not consumed by the human being. For example, plastic bottles are referred to as ineffective components that could be accumulated accidentally in the Biosphere, especially in water areas or in the atmosphere in the form of plastic micrometric particles with dangerous effect on the human being, especially on the respiratory tract [13]. The environmental protection Agency (EPA) has the function of monitoring and control of the state of ecosystems [14]. So, in general, the Biosphere accumulates ineffective wastes and the entropy component of the Biosphere will consists of two terms: one is related to the previous state of the biosphere and the other is related to pollutants (ineffective part):

$$\frac{dS'_{bios-re}}{dt} = \frac{dS_{bios-re}}{dt} + \frac{dS_{ineff}}{dt} \qquad (9)$$

Then, the entropy of the Biosphere increases over time due to the increase of pollutants: $\frac{dS'_{bios-re}}{dt} > \frac{dS_{bios-re}}{dt}$. For example, if the ineffective part consists only of carbon dioxide – CO_2, then a certain amount of this gas can be used

during the process of photosynthesis. In an ideal stationary state when all momentary emitted carbon dioxide is used for photosynthesis, then: $\frac{dS^{/}_{bios-re}}{dt}=0$ and the following expression is obtained $\frac{dS_{bios-re}}{dt}=-\frac{dS_{ineff}(CO_2)}{dt}$. Here it is important to mention that when the quantity of the ineffective part is decreased $\left(\frac{dS_{ineff}(CO_2)}{dt}<0\right)$, the Biosphere has the possibility to recover $\left(\frac{dS_{bios-re}}{dt}>0\right)$ due to forest areas. So, if the ineffective part of CO_2 increases over time, then $dS_{bios\text{-}re} < 0$, which means the disappearance of many components over time (disappearance of animal population and forests). It is obvious that the entropy depends not only on the aggregation state of the substance but also on the quantity. The gaseous aggregation state has larger entropy than the solid state [15]. Great quantity in kilograms of the same substance gives the result of larger entropy [15]. In the special case when $\left|\frac{dS_{ineff}}{dt}\right|>\left|\frac{dS_{bios-re}}{dt}\right|$, then $dS^{/}_{bios-re}>0$ and it means excessive accumulation of pollutant gases with dangerous destructive effect on the nature. Paper [16] describes the same situation of increase of entropy of the Biosphere. If we substitute (7) and (8) in (5), then the following expression is obtained:

$$\frac{dS}{dt}=2.\frac{dS_h}{dt}+\frac{dS_{ineff}}{dt}+\frac{dS_{bios-re}}{dt} \qquad (10)$$

Expression (9) gives:

$$\frac{dS_{bios-re}}{dt}=\frac{dS^{/}_{bios-re}}{dt}-\frac{dS_{ineff}}{dt} \qquad (11)$$

The substitution of (11) in (10) gives:

$$\frac{dS}{dt}=2.\frac{dS_h}{dt}+\frac{dS^{/}_{bios-re}}{dt} \qquad (12)$$

The case of stationary state $\frac{dS}{dt}=0$ gives:

$$\frac{dS_h}{dt}=-\frac{dS^{/}_{bios-re}}{2.dt} \qquad (13)$$

Expression (13) has the following result: if the entropy of the Biosphere is increased with the increase of pollutants, then the entropy of humanity is decreased. Paper [17] gives the following information about the entropy of humanity: "However, more commonly, these compounds give up their free energy by “working” on ecosystems and human populations to break us down and expedite entropic maximum for the environment. By reacting with these products, our low entropy systems are pushed closer to thermal equilibrium and ultimately toward death." So, inundations and other natural cataclysms that result from pollutants excess in the atmosphere lead to the death cases in humanity and, in its turn, the entropy of humanity that is dependent on the quantity of population could lead to its decrease.

The state of pathology and diseases of individual human beings is characterized by high values of entropy [18]. The increase of entropy is explained by the fact that the value of Gibbs free energy from expression (1) is increasing due to the fact that the effective part ($m_f \rightarrow 0$) of the consumed substances decrease gradually. A lot of pollutants in the form of particulate matter could exist in food products and vegetables. The effective part therefore decreases and allergic states could lead to more complicated pathological states. Also, polluted air leads to the development of respiratory and lung diseases.

CONCLUSIONS

The concept of entropy that is proposed in this paper allows us to make predictions about the further evolution of the state of humanity, the Biosphere and the Technosphere. Healthy ecology is the major task of Humanity to improve the states of ecosystems. The state of ecosystems in symbiosis with the human being is in an evolutionary state with the change of the entropy of both the Biosphere and the human being. Nowadays, the number of new diseases is increasing over time. New epidemics with unknown etiologies appear and all these new epidemics are related somehow to the current state of the ecosystem which is polluted with an increasing quantity of ineffective elements. Human health is influenced by a number of very complex factors and the major task of all committees of environmental protection is to find ways to improve ecosystems.

REFERENCES

1. Mihai Petrov, The research of the principle of Pareto in the pharmaceutical activity, VI-th Congress of Pharmacy with International Participation, October, 2016, Republic of Bulgaria https://m.wasteels.bg/en/event/6th-congress-pharmacy-international-participation

2. Mihai Petrov, The basis of pharmaceutical bioeconophysics of drug's administration, VII-th Congress of Pharmacy with International Participation, November, 2019, Republic of Bulgaria// eprints.ugd.edu.mk › abstract_book_en
3. Mihai Petrov, "The Thermodynamical Processes of the Model of Ideal Gas for the Description of the Activity of the Microeconomical Systems", European Journal of Business and Management, Vol 10, No 26 (2018) www.iiste.org › EJBM › article › download
4. Mihai Petrov, 2021. Aspekti na bioikonofizichna farmakologiya v lechenieto na zaharen diabet. – *Upravlenie i Obrazovanie . 2021, Vol. 17 Issue 6*, 198-205. https://web.s.ebscohost. com/ abstract?direct=true
5. Mihai Petrov, The Bioeconophysical Aspect of The Description of The Ecological State By The Symbiosis of Human being-Biosphere-Technosphere , Econophysics Colloquium (August 24-26, 2022, Online, 36.pdf - Google Drive, Econophysics Colloquium 2022 (auth.gr)
6. Mtaweh H, Tuira L, Floh AA, Parshuram CS. Indirect Calorimetry: History, Technology, and Application. Front Pediatr. 2018 Sep 19;6:257. doi: 10.3389/fped.2018.00257. PMID: 30283765; PMCID: PMC6157446.
7. Kristiansen K. Molecular mechanisms of ligand binding, signaling, and regulation within the superfamily of G-protein-coupled receptors: molecular modeling and mutagenesis approaches to receptor structure and function. Pharmacol Ther. 2004 Jul;103(1):21-80. doi: 10.1016/j.pharmthera.2004.05.002. PMID: 15251227.
8. O. Kocak, E. Simsek, Proliferative effects of metamizole sodium on u-87 mg glioblastoma cell line: a pain killer or a killer? World Cancer research Journal 2021; 8: e1987.
9. Shi, Weifang. 2017. "Entropy Analysis of the Coupled Human–Earth System: Implications for Sustainable Development" Sustainability 9, no. 7: 1264. https://doi.org/10.3390/su9071264
10. Mihai Petrov, Major contribution of carbon dioxide excess in atmosphere to the green house effect, Oxidation Communications 44, No 4, 870–907 (2021)
11. https://www.encyclopedie-energie.org/en/energy-consumption-and-entropy-release-in-the-biosphere/
12. Gulia Rispoli, The Biosphere and the Earth system, https://pure.mpg.de/rest/items/item_3401188/component/file_3401189/content
13. Vianello, A., Jensen, R.L., Liu, L. et al. Simulating human exposure to indoor airborne microplastics using a Breathing Thermal Manikin. Sci Rep 9, 8670 (2019). https://doi.org/10.1038/s41598-019-45054-w
14. Environmental protection act, https://www.moew.government.bg/en/environmental-protection-act-7628/
15. Stephen Lower, Entropy Rules - Chemistry LibreTexts,2022, ttps://chem.libretexts.org › 15.02:_Entropy_Rules
16. Carlo Bianciardi, Sergio Ulgiati, Entropy, in Encyclopedia of Energy, 2004.
17. Tao, James L., "Pollution in Light of Entropy" (2016). Undergraduate Honors Theses. Paper 1142.
18. Houck PD. Should negative entropy be included in the fundamental laws of biology? OA Biology 2014 May 10;2(1):7.

ANNUAL OF ASSEN ZLATAROV UNIVERSITY, BURGAS
BULGARIA, 2022, v. LI(1)

INVESTIGATION OF THE INFLUENCE OF AEROSOL AND GAS POLLUTANTS ON ECOSYSTEMS, THE RESPIRATORY SYSTEM AND HUMAN HEALTH[1]

Mihai Petrov
E-mail: mihpetrov@abv.bg

ABSTRACT

Air quality is influenced by polluting particles and gases with a negative effect on human health. Depending on air pollution, respiratory tract diseases such as COPD and asthma are developed. The mechanism of the pathogenesis of respiratory diseases as well as the medical therapy is explained, showing that the half-life depends on the molar mass. It is shown that the activation energy of receptors with beta-2 agonists depends on the molar masses. Depending on the physicochemical composition of the human body, the result of the value of chemical potential of human being responsible for the maintaining of the metabolism is obtained.

Key words: *biosphere, molar masses, half-life, beta-2 agonists, receptors, chemical potential*

INTRODUCTION

The biosphere, which includes important elements such as water basins, and the atmosphere that ensures the life and existence of living organisms, including humans, have lately been subject to the influence of polluting factors and polluting particles suspended in the atmosphere in the form of aerosols. Ecosystems that are part of the biosphere, and humanity is thoroughly dependent on the state of the biosphere, are important from the point of view of cleanliness and of the small impact of pollutants. The major part of the ecosystems consists of water basins. Water, which is a vital element for various types of animals and humans, needs to be clean in order to ensure the life of the inhabitants of these ecosystems. Human activity usually leads to the pollution of water basins – oceans, seas, lakes, rivers, groundwater, etc. The great importance of water is that it ensures the existence of life. Nowadays, various chemicals, bacteria and other anthropogenic pollutants have already started to affect our water having a negative impact on living habitants resulting in the disappearance of species of plants and animals.

Aerosols are fine particles that float in the atmosphere. The aerosols from human activities are emitted by smokestacks, car exhausts, wildfires and have increased rapidly, most of them at the same rate as the greenhouse gases responsible for climate change. Aerosol pollution kills 4 million people a year. Aerosol sizes are of the order of micrometres. These include sulphate crystals, globules of almost pure black carbon (soot), droplets of nitric or sulphuric acid. Discarded plastic shopping bags release micro plastic fibbers and they are able to be suspended in the atmosphere in the form of aerosols.

This study aims to describe how pollutants influence the respiratory system and the overall human health, as well as the types of diseases of the respiratory system caused by these pollutants and the respective support medical therapy.

EXPERIMENT

Air quality in Bulgaria causes serious concerns: the measurements show that citizens throughout the country breath air that is assessed as harmful to health. For example, the concentration of PM2.5 and PM10 is much higher than the values prescribed by the European Union and the World Health Organization (WHO) for health protection. Concentrations of PM2.5 in urban areas of Bulgaria were the highest of all 28 EU member states as average values over a three-year period [1]. Bulgaria has the strongest pollution among the countries with an average daily concentration of 77 $\mu g/m^3$ (the EU limit value is

[1] The article was presented at the Challenges for Medical Science and Practice in the 21st Century Congress of Medicine, Burgas, 1-3 September 2022

50 μg/m^3). According to the World Health Organization, 60% of Bulgaria's urban population is exposed to dangerous (unhealthy) levels of particulate matter (PM10) [1], according to the Air Quality Index (AQI), the concentration of PM2.5 in the air of Sofia is 6.1 times higher than the annual World's Health Organization recommended value.

RESULTS AND DISCUSSION

Recently, a wide range of respiratory health consequences associated with air pollution have been identified and they are considered harmful, ranging from death from respiratory disease to reduced quality of life, including some irreversible changes in physiological functions [2]. The exposure to air pollutants leads to the development of asthma, worsen pre-existing respiratory disease, and the development or progression of chronic diseases, including chronic obstructive pulmonary disease, emphysema, and lung cancer. Chronic obstructive pulmonary disease (COPD) is a life-threatening lung disease that makes it difficult to breathe normally. The number of deaths from COPD has increased by more than 60% in the last 20 years, with air pollution being an important risk factor for the inflammation as an immunological response [3]. The inflammatory response is known as chronic bronchitis. It leads to tissue destruction in the lung alveoli or the development of emphysema [3]. Other types of diseases which are related to the cardiovascular system are also observed and their aetiology points to air pollutants. The consequences include: altered cardiac autonomic function, myocardial infarction, angina pectoris, increased blood pressure, atherosclerosis, hypertension, increased cerebrovascular ischemia [4].
The major pollutants of air are particulate matter (PM), ozone (O_3), sulfur dioxide (SO_2), nitrogen dioxide (NO_2), carbon monoxide (CO), and lead (Pb) [5]. The pollutants in the ambient air can be divided into primary and secondary types [6]. To offer guidance in reducing the impacts of air pollution on human health, WHO air quality groups (AQGs) released air quality guidelines in which four pollutants, namely PM, O_3, NO_2, and SO_2, were listed as indices of air pollution [6]. These four pollutants are major factors for the development of COPD and bronchial asthma [7]. Asthma is a complex disorder characterized by airway inflammation and reversible airflow obstruction resulting in a symptom complex of wheezing, dyspnoea, or cough (or combination of these) [8]. Typical airway changes include an increase in eosinophils and thickening of the lamina reticularis [9]. Mast cell activation occurs when allergens (PM or pollutant gases) interact with immunoglobulin IgE and are fixed on the surface of mast cells in bronchial asthma. When activated, they release mediators (histamine, cysteinyl leukotrienes, prostaglandin D2) that lead to the bronchospasm [10]. Consequently, the arachidonic acid and thrombocyte activating factor are formed from the phospholipids of the mast cell membrane. In turn, leukotriene and prostaglandin are formed from arachidonic acid [10].

Regarding the therapy of asthma, the interaction of therapeutical substances with the receptors is based on the description of the mechanism with the targets G-protein couple receptors (GPCR). Beta adrenoreceptors refer to this class of GPCRs [11]. Beta 2 receptors (β_2AR) are present in the airway smooth muscle. They also exist on the cardiac muscle, uterine muscle, alveolar type II cells, mast cells, mucous glands, epithelial cells, vascular endothelium, eosinophils, lymphocytes, and skeletal muscle, i.e. in almost the whole human organism [12]. The therapeutical molecules of medical substances are of two types: agonists and antagonists. The agonists amplify the therapeutical effects and the antagonists inhibit the effect [13]. The β-Agonists are the medicals of first line treatment for both asthma and COPD. They exert their bronchodilator effects via β_2 adrenoreceptors (β_2AR) located on the airway smooth muscle cells. The activation of these receptors leads to the relaxation of the airways and the corresponding expansion of the lumen of the bronchi (Fig. 1).

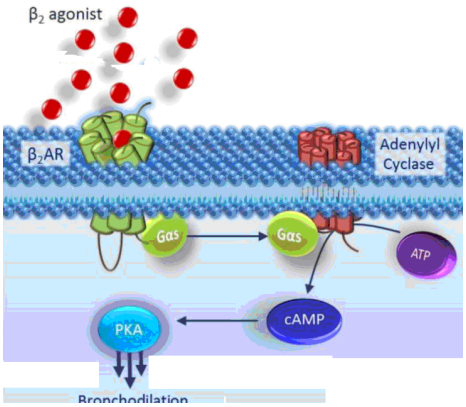

Fig. 1 The classic β_2AR signalling pathway

Binding of β_2-agonist to β_2AR induces a conformational change allowing the α-subunit of the G-protein to dissociate and bind to ade-

nylyl cyclase. Adenylyl cyclase is thus activated and catalyses the formation of cyclic AMP (cAMP) from ATP. The (cAMP) molecules bind to PKA which induces the dissociation of the catalytic and regulatory subunits from each other. Once released, the PKA catalytic subunits phosphorylate and hence activate myriad cellular targets, which results in the airway smooth muscle relaxation and hence bronchodilation [14].

There are quantitative expressions based on modern integrative platforms of bioeconophysics and pharmaceutical bioeconophysics which are developed in [15–17] and show the interdependence between the price of one gram of therapeutic substance, molar mass, activation energy of receptors, and half-life time. The data related to the cost of one gram of therapeutic substance are taken from Drug's database [18]. The drug's bank database shows the values of half-life of antiasthmatic molecules and are presented in Table 1 below.

Table 1. The values of half-life of antiasthmatic molecules (agonists)

Molecule	M; g/mol	$T_{1/2}$; h
Vilanterol	486.43	26
Fluticasone	444.5	24
Mometasone	427.36	5.8
Salmeterol	415.47	5.5
Olodaterol	386.44	7.5
Formoterol	344.4	3.5
Salbutamol	239.31	5
Terbutaline	225.28	3.5
Isoprenaline	211.25	2
Ephedrine	165.24	4.5
Levosalbutamol	239.31	3.5
Ritodrine	287.36	2
Orciprenaline	211.25	6
Arfomoterol	344.17	7
Pirbuterol	240.29	2
Bambuterol	367.44	16
Doxophylline	266.25	2.5
Etafedrine	193.29	2

The respective dependence of half-lives as the function of molar masses are presented in Fig. 2.

The respective dependence of $lnT_{1/2} = f(M)$ is presented in Fig 3.

The linear regression of the dependence $\ln T_{1/2} = f(M)$ gives the results of correlation coefficients a and b of the linear dependence, which are presented in Fig. 3.

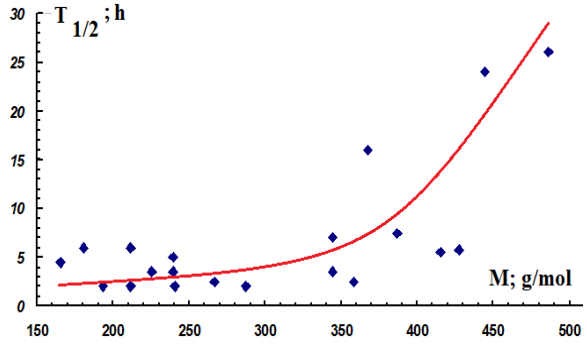

Fig. 2 The dependence of half-life time on molar masses of $\beta_2 AR$ agonists

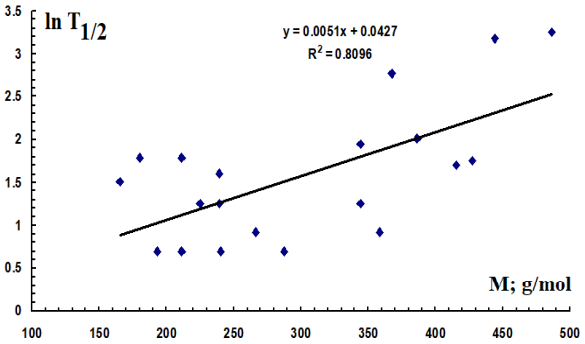

Fig. 3 The dependence of $lnT_{1/2}=f(M)$

$$b \equiv \ln\left(\frac{\ln 2}{A}\right) = 0.0427; \quad a \equiv \frac{\ln 2 \cdot N \cdot P_p}{RTm_p N_A v_{rec}} = 0.0051;$$

Numerical results a and b give the possibility to calculate the pre-exponential factor A [15–17] of these molecules:

$$\ln\left(\frac{\ln 2}{A}\right) = 0.0427; \quad \Rightarrow \quad \frac{\ln 2}{A} = e^{0.0427} \approx 1.0436$$

$$\Rightarrow A = \frac{\ln 2}{1.0436} = \frac{0.693}{1.0436} \cong 0.66(h^{-1})$$

The meaning of A is coincident with the constant rate of elimination of metabolic products of medicals λ for the case of very small molecules. (M→0) [15–17]. The calculated value a = 0.0051 makes it possible to calculate the activation energies of one mole of receptors E_{mol} by the formula: $E_{mol} = a.M.R.T$ and these values of energies are presented in Table 2.

Table 2. The activation energies of β_2AR receptors by agonists

Molecule	M; g/mol	half-life; h	Emole; J/mole
Vilanterol	486.43	26	6390.7708
Fluticasone	444.5	24	5839.8898
Mometasone	427.36	5.8	5614.702
Salmeterol	415.47	5.5	5458.4905
Olodaterol	386.44	7.5	5077.0912
Formoterol	344.4	3.5	4524.7650
Salbutamol	239.31	5	3144.0811
Terbutaline	225.28	3.5	2959.7534
Isoprenaline	211.25	2	2775.4257
Ephedrine	165.24	4.5	2170.9412
Levosalbutamol	239.31	3.5	3144.0811
Ritodrine	287.36	2	3775.367
Orciprenaline	211.25	6	2775.4257
Arfomoterol	344.17	7	4521.7433
Pirbuterol	240.29	2	3156.9564
Bambuterol	367.44	16	4827.46713
Doxophylline	266.25	2.5	3498.0217
Etafedrine	193.29	2	2539.4652

The respective dependence of the activation energies of the receptors as the function of molar masses is presented in Fig. 4.

It can be seen from Fig. 4 that the activation energies range from 2 to 6 kJ/mol. Papers [19, 20] present the value of the activation energy of the order of 4 (kJ/mol) of β_2AR receptors. The price of one gram (Pgr) of medicals as the function of the mass of one medical form (tablets, capsules, aerosols, injections, etc.) gives the information of the quantity of activated receptors in moles [15–17].

The amount of receptors can be calculated by the graph $lnP_{gr} = f(ln(m_f))$. It is expected that the price of one gram decreases with the increase in the mass of one form (dosage form). The data about the prices are extracted from the database [18]. The dependence of the price of one gram as the function of the price of one form of β_2AR agonists is represented in Fig. 5.

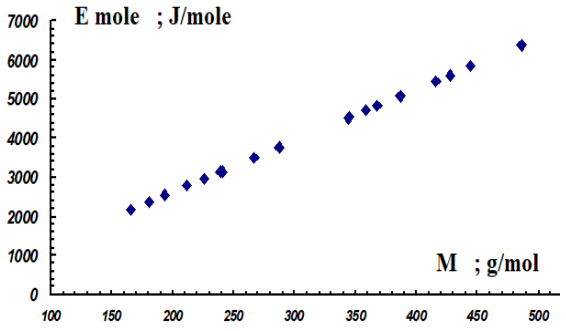

Fig. 4 The dependence of activation energies $E_{mol} = f(M)$ of the β_2AR receptors as the function of molar masses of β_2-agonists

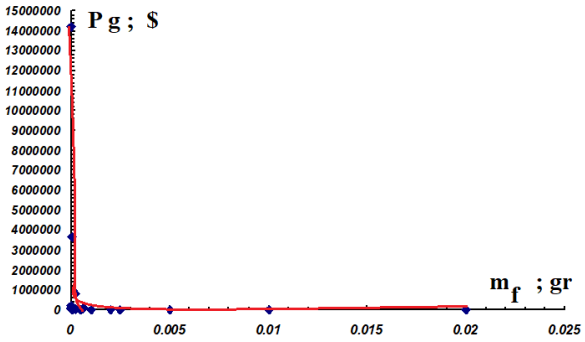

Fig. 5 The dependence of the price of one gram as the function of the price of one form of β_2AR agonists

Smaller prices with increase of the masses is one of the principles of microeconomics that is based on the supply-demand processes [17].

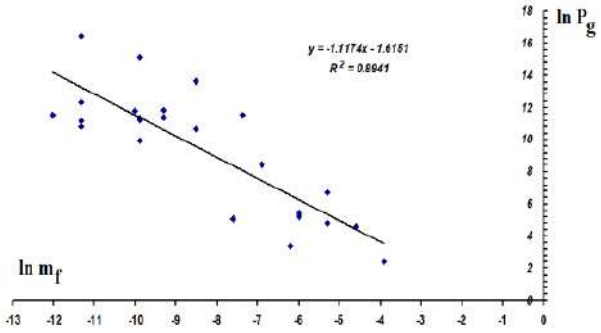

Fig. 6 The dependence of $lnP_{gr} = f(ln(m_f))$ of β_2AR agonists

The correlational calculations of the dependence $lnP_{gr} = f(ln(m_f))$ give the following result:

$$\ln\left[\frac{E_{mole}\cdot\nu_{rec}}{\ln 2}\right]=-1.6151$$

$$\frac{E_{mole}\cdot\nu_{rec}}{\ln 2}=e^{-1.6151}\Rightarrow$$

$$\nu_{rec}=\frac{\ln 2\cdot e^{-1.6151}}{E_{mole}}\cong\frac{0.693\cdot 0.1988}{E_{mole}}=\frac{0.1377}{E_{mole}}$$

The calculated values of the activation energies are presented in Table 3.

Table 3. The activation energies E_{mol} of β_2AR agonists

molecule	M; g/mol	E_{mol}; J/mol	ν_{rec}; moles
Vilanterol	486.43	6390.770	2.15E-05
Fluticasone	444.5	5839.889	2.35E-05
Mometa-sone	427.36	5614.702	2.45E-05
Salmeterol	415.47	5458.490	2.52E-05
Olodaterol	386.44	5077.091	2.71E-05
Formoterol	344.4	4524.765	3.04E-05
Salbutamol	239.31	3144.081	4.37E-05
Terbutaline	225.28	2959.753	4.65E-05
Iso-prenaline	211.25	2775.425	4.96E-05
Ephedrine	165.24	2170.941	6.34E-05
Ritodrine	287.36	3775.367	3.64E-05
Orci-prenaline	211.25	2775.425	4.96E-05
Arfomoterol	344.17	4521.743	3.04E-05
Pirbuterol	240.29	3156.956	4.36E-05
Bambuterol	367.44	4827.467	2.85E-05
Doxophyl-line	266.25	3498.021	3.93E-05
Etafedrine	193.29	2539.465	5.42E-05

The dependence of the quantity of activated receptors ν_{rec} as the function of molar masses of medications is presented in Fig. 7.

It is observed that the quantity of the activated receptors decreases with the increase of molar masses of medicals. The therapeutical effect is stronger for medicals with high molar masses.

The representation of both quantities of moles of medical form and the moles of receptors on the same plot as the function of molar masses of medicals is shown in Fig. 8.

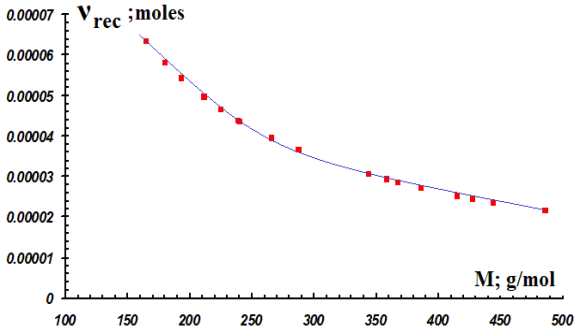

Fig. 7 The dependence of quantity of activated receptors ν_{rec} as the function of molar masses of β_2AR agonists

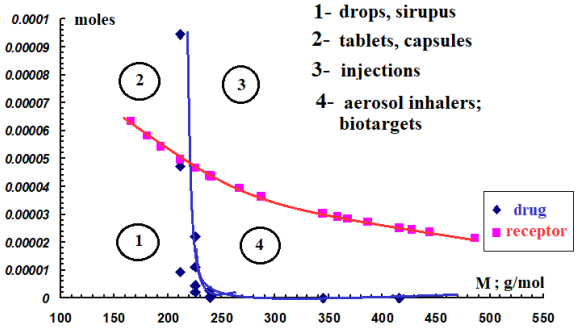

Fig. 8 The quantity of moles of medical form and the moles of receptors as the function of molar masses of medicals

The intersection point can be seen in Fig. 8 and the respective value of the molar mass is 240 (g/mol) with the respective activation energy 3 (kJ/mol). In fact, this energy coincides with the chemical potential of the metabolism process in human beings [17].

About 70% of the human mass consists of water. For example, if the human mass is 80 kg, then 56 kg is only water. Then, the amount of moles of water is ≈3000 moles inside the body. It was mentioned in [17] that the total amount of moles together with all other structural elements of the human is in the order of 4000-5000 moles with the effective molar mass of the human being 20 g/mol.

The average total amount of energy to maintain human metabolism is of the order of 12 MJ per day and is maintained by intake of food and water. If we divide this value by 4000 moles, then we get 3 kJ/mol, which is the chemical potential of the human being.

Regarding Fig. 8, there are four regions for the classification of medical forms. Small molar masses up to 240 g/mol and masses of small

forms are referred to syrups and drops. The second region of relatively high masses of the form refers to tablets and capsules. The third region refers to the form of injections. Finally, the fourth region refers to aerosols and nano-biotechnologies that interact directly with the receptor targets.

CONCLUSIONS

The symbiotic unity of the human being with nature is confirmed by the application of bioeconophysics platform. Human health is impossible without the normal good state of the biosphere. Cases of pollution can lead to chronic diseases. Maintaining metabolism in a normal state requires to improve the state of the Biosphere: clean air, clean waters, and healthy ecosystems being humanity's primary tasks.

REFERENCES

1. Air pollution and Health in Bulgaria, Facts, figures and recommendations, 2018, Air Quality, https://www.env-health.org/wp-content/uploads/2018/11/HEAL-Brief-Pos_AIR_Bulgaria.pdf.
2. Ioannis Manisalidis, Elisavet Stavropoulou, Agathangelos Stavropoulos and Eugenia Bezirtzoglou, Environmental and Health Impacts of Air Pollution: A Review, Frontiers in Public Health, 2020, doi: 10.3389/fpubh.2020.00014.
3. Devine JF. Chronic obstructive pulmonary disease: an overview. Am Health Drug Benefits. 2008 Sep;1(7):34-42. PMID: 25126252; PMCID: PMC4106574.
4. Lee BJ, Kim B, Lee K. Air pollution exposure and cardiovascular disease. Toxicol Res. 2014 Jun;30(2):71-5. doi: 10.5487/TR.2014.30.2.071. PMID: 25071915; PMCID: PMC4112067.
5. American Thoracic Society. What constitutes an adverse health effect of air pollution? Official statement of the American Thoracic Society. Am J Respir Crit Care Med 2000; 161:665-73.
6. Sivertsen B. Air Quality Guidelines Global Update 2005. 2006. Available online: http://www.euro.who.int/pubrequest
7. Jiang XQ, Mei XD, Feng D. Air pollution and chronic airway diseases: what should people know and do? J Thorac Dis. 2016 Jan; 8(1): E31-40. doi: 10.3978/j.issn.2072-1439.2015.11.50. PMID: 26904251; PMCID: PMC4740163.
8. Volcheck GW. Asthma. Clinical Allergy. 2008 Aug 27:189–278. doi: 10.1007/978-1-59745-315-8_6. PMCID: PMC7120997.
9. Shifren A, Witt C, Christie C, Castro M. Mechanisms of remodeling in asthmatic airways. J Allergy (Cairo). 2012; 2012:316049. doi: 10.1155/2012/316049. Epub 2012 Jan 19. PMID: 22315625; PMCID: PMC3270414.
10. Kaliner M. Asthma and mast cell activation. J Allergy Clin Immunol. 1989 Feb; 83(2 Pt 2): 510-20. doi: 10.1016/0091-6749(89)90031-6. PMID: 2645347.
11. Stacy Gelhaus Wendell, Hao Fan and Cheng Zhang, Pharmacology of GPCRs in Asthma Therapy and Drug Action, Pharmacological Reviews January 1, 2020, 72 (1) 1-49; DOI: https://doi.org/10.1124/pr.118.016899
12. Abosamak NER, Shahin MH. Beta 2 Receptor Agonists/Antagonists. In: StatPearls [Internet]. Treasure Island (FL): StatPearls Publishing; 2022 Jan-. Available from: https://www.ncbi.nlm.nih.gov/books/NBK559069/
13. Negus SS. Some implications of receptor theory for in vivo assessment of agonists, antagonists and inverse agonists. Biochem Pharmacol. 2006 Jun 14;71(12):1663-70. doi: 10.1016/j.bcp.2005.12.038. Epub 2006 Feb 7. PMID: 16460689; PMCID: PMC1866283.
14. Billington CK, Penn RB, Hall IP. β2 Agonists. Handb Exp Pharmacol. 2017;237:23-40. doi: 10.1007/164_2016_64. PMID: 27878470; PMCID: PMC5480238
15. Mihai Petrov, The basis of pharmaceutical bioeconophysics of drug's administration, VII-th Congress of Pharmacy with International Participation, 2019, Republic of Bulgaria with the paper // eprints.ugd.edu.mk › abstract_book_en
16. Mihai Petrov, 2021. Aspekti na bioikonofizichna farmakologiya v lechenieto na zaharen diabet. – *Upravlenie i Obrazovanie . 2021, Vol. 17 Issue 6*, 198-205. https://web.s.ebscohost.com/abstract?direct=true
17. Mihai Petrov, The Bioeconophysical Aspect of The Description of The Ecological State By The Symbiosis of Human being-Biosphere-Technosphere, Econophysics Colloquium (August 24-26, 2022, Online,

36.pdf - Google Drive, Econophysics Colloquium 2022 (auth.gr))
18. Wishart DS, Feunang YD, Guo AC, Lo EJ, Marcu A, Grant JR, Sajed T, Johnson D, Li C, Sayeeda Z, Assempour N, Iynkkaran I, Liu Y, Maciejewski A, Gale N, Wilson A, Chin L, Cummings R, Le D, Pon A, Knox C, Wilson M. DrugBank 5.0: a major update to the DrugBank database for 2018. Nucleic Acids Res. 2017 Nov 8. doi: 10.1093/nar/gkx1037.
19. Rajan Lamichhanea, Jeffrey J. Liua, Goran Pljevaljcica, Kate L. Whiteb , Edwin van der Schansa , Vsevolod Katritcha, Raymond C. Stevensa, Kurt Wüthricha, and David P. Millar ,"Single-molecule view of basal activity and activation mechanisms of the G protein-coupled receptor β2AR" https://www.pnas.org/doi/pdf/10.1073/pnas.1519626112
20. Sijia S. Dong, William A. Goddard, Ravinder Abrol, Conformational and Thermodynamic Landscape of GPCR Activation from Theory and Computation, Biophysical Journal, Volume 110, Issue 12, 2016, Pages 2618-2629, ISSN 0006-3495, https://doi.org/10.1016/j.bpj.2016.04.028. (https://www.sciencedirect.com/science/article/pii/S0006349516302314)

.

ANNUAL OF ASSEN ZLATAROV UNIVERSITY, BURGAS
BULGARIA, 2022, v. LI(1)

PHYSICAL ACTIVITY IN TYPE 2 DIABETES – A KEY ROLE IN TREATMENT[1]

Nikolay Kostadinov
e-mail: n.kostadinov_m.d@abv.bg

ABSTRACT

Physical activity is a key element in the prevention and overall management of type 2 diabetes. Despite the growing body of evidence establishing the importance of exercise in diabetes, many people with chronic diabetes do not become regularly active. Regular physical activity keeps blood sugar under control and can prevent or delay type 2 diabetes. Most of the benefits of physical activity in the management of diabetes are realized through improvements in insulin action. The treatment of type 2 diabetes aims not only to achieve optimal metabolic control of the disease, but also to improve the quality of life of the affected people. Engaging in physical activities has a positive effect on the physical aspect of the quality of life of patients with type 2 diabetes mellitus.

Key words: *Type 2 diabetes, physical activity, metabolic control, quality of life*

INTRODUCTION

Diabetes mellitus (DM) is a metabolic disease characterized by hyperglycaemia resulting from impaired insulin secretion, insulin action, or both [1]. Diabetes is a global problem that also affects our country. There are currently about 426,000 people with diagnosed diabetes in Bulgaria, which represents 7.9% of the population aged 20 to 79 (57% men and 43% women).

The incidence of diabetes in Bulgaria (diagnosed and undiagnosed) of 7.9% in 2006. reached 9.55% in 2012, p=0.06. There was an increase in diabetes prevalence of 20.88% over a 6-year period, or an annual average of about 3.5%. Age, especially 50 to 59, is a major risk factor for a significant increase in diabetes, where an increase from 9.4% in 2006 to 15.7% in 2012, $p<0.02$ was observed [1].

Diabetes mellitus is one of the most progressively growing chronic diseases of the 21st century. Modern medical practice defines the disease as an important risk factor for the development of severe debilitating complications that limit the physical activity of the affected persons, worsen the quality of life, and incur significant economic costs.

Exercise therapy through physical activity plays an essential role in the management of diabetes. By developing a structured and individualized regimen, exercise can help improve lean muscle strength, gait pattern, and balance, and above all, improve glycaemic control. Therefore, engaging in physical activities has a positive effect on the physical aspect of the quality of life of individuals with diabetes.

REVIEW

Diabetes often leads to the development of physical disabilities, which in turn can have a detrimental effect on the patient's quality of life.

Like any other chronic disease, DM is associated with many personal, family, social and financial problems and even higher mortality. Problems such as elevated blood glucose, dietary and physical restrictions, repeated insulin injections, musculoskeletal complications, physical disabilities, sexual dysfunction, and vascular disorders are some examples that negatively affect the lives of DM patients.

Therapeutic goals in the treatment of type 2 DM include control of hyperglycaemia and acute symptoms, as well as prevention of late complications of diabetes. Physical activity and therapeutic nutrition are part of the complex treatment of the patient. Moreover, in diabetes mellitus, strict adherence to a certain nutritional and exer-

[1] The article was presented at the Congress of Medicine "Challenges for medical science and practice in the 21st century'' in Burgas, 1-3 September, 2022

cise regimen are even more important than drug therapy [2].

Approaches to the treatment of diabetes mellitus should be aimed primarily at eliminating a sedentary lifestyle, preparing an individual and feasible daily program of physical exercises. All this, in combination with an appropriate diet, aims at reaching and maintaining an optimal body weight.

Physical activity should include daily efforts to be more physically active. The duration and frequency of physical activity should reach up to 30 - 45 minutes 3 to 5 days/week or up to 150 minutes/week of moderately intense aerobic physical activity, 50-70% maximum heart rate, with no more than two consecutive days without physical activity [3]. In the absence of contraindications, muscle strength/resistance exercises should be done twice a week [3].

A gradual increase in physical activity is recommended based on individual wishes, capabilities and set goals. Diet and physical activity are partners in the fight against diabetes. The balance between them is key to optimal effectiveness of diabetes therapy. Properly dosed and planned physical activity plays an important role in controlling the disease and improving the quality of life of patients, reducing the risk of accidents and diabetic complications. Depending on the general condition of the patient and the type of diabetes, the most appropriate type and intensity of physical activity is selected.

Regular physical activity improves the body's sensitivity to insulin and helps manage blood sugar levels, maintain a healthy weight and improve the insulin sensitivity of cells. Moderate physical activity also helps avoid other risk factors associated with diabetes, such as high blood pressure and cardiovascular disease. Physical activity should be dosed strictly individually and should take the general condition of the patients into account. Every 60 minutes of physical activity improves insulin sensitivity, weight, cardiovascular risk and self-esteem. It has the same effect on blood sugar up to 12-14 hours after that, including at night, and improves HbA1C 30-37% [4]. Physical activity burns calories, which helps maintain a healthy weight and lower blood sugar levels. This lowers the risk of complications, high blood pressure and cardiovascular disease, which are common in people with diabetes. Regular exercise, including both aerobic activity and resistance training, offers distinct and significant health benefits for people with type 2 diabetes [5].

The intensity of exercise in diabetics largely depends on whether complications are present. The presence of some of the chronic complications of diabetes is not an indication to stop physical activity, but it should be tailored to the specific complication:

- in case of peripheral neuropathy – ergometer and swimming;
- proliferative retinopathy – walking on the bottom of a pool, ballroom dancing, moderate cycling. Avoid blood pressure rise, yoga, weight lifting.;
- nephropathy – light to moderate loads.

Diet, physical activity, and medication are partners in the battle to achieve and maintain low-risk levels of blood sugar, lipids, and blood pressure [1].

Physical activity improves blood circulation in the hands and feet, which are problem areas for people with diabetes, and reduces stress, which can be the cause of high blood sugar levels.

It has been proven that light and regular physical activity helps to reduce the overall level of blood sugar and the resistance of cells to insulin. This is precisely why, in type 2 diabetes, physical activity appears to be a very important factor in the treatment and prevention of complications due to the fact that people with type 2 diabetes often have multiple co-morbidities and are overweight. Light to moderate exercise that is daily and planned is recommended. This helps improve overall metabolism and protect against many diabetic complications. Exercise is a safe and effective treatment modality to help control glucose levels and reduce complications in individuals. with type 2 diabetes. However, there are numerous challenges that must be overcome for both general practitioners and their patients to initiate and maintain regular exercise as part of a treatment plan [6].

Physically inactive people are at risk of type 2 diabetes, especially those over the age of 40. Therefore, adequate activity is mandatory to reduce the prevalence of developing type 2 DM among urban residents [7].

Physical activity over the age of 70 is associated with good disease knowledge and positive attitudes toward DM2 self-care. Therefore, physical activity may benefit the treatment and control of glucose levels in older people with T2DM.

Therefore, prevention and treatment programs for type 2 DM should focus on changes in dietary habits and physical activity. In addition,

courses providing information about DM2 are needed so that older people can change their attitudes about the disease [8].

Healthcare professionals need to individualize their approach when advising and supporting physical activity engagement in those with type 2 DM with or without complications. After taking into account the presence of co-morbidities and complications where possible, individual preferences and motivation should primarily inform the decision-making regarding modality (aerobic vs resistance). Although recommending a single activity regimen (eg, aerobic) is unlikely to address the multidomain deficits often present in those with type 2 DM, the HCP should also be pragmatic about realistic goals, particularly if the individual is sedentary /inactive. An approach combining both aerobic and resistance activity provides the most benefit, but actually the type of activity is far less important than deciding whether to be active at all [9].

There is a real relationship between physical activity and demographic characteristics. This relationship indicates that demographic characteristics (such as education and employment) are important for physical activity intervention and promotion. Governments should organize appropriate exercise programs for diabetic patients. Patients should begin exercise with a warm-up session (i.e., stretching in the neck, triceps, chest, upper back, torso, and lower back). It is important that exercise should be started slowly and gradually (from light to heavy). One should start with normal walking for 10 minutes to running for 15 minutes [10].

MATERIAL AND METHODS

In a prospective analysis, I observed 40 patients with DMT2 in my practice from January 2020 until January 2021, as shown in Table 1.

Table 1

40 patients	19 men and 21 women
mean age	58.47 +/– 18.47
mean duration of DMT2	8.85 +/– 7.15
mean HbA1c %	7.26% +/– 0.27

Mean BMI was 29.3 kg/m2. Most participants were hypertensive (60%), and mean systolic/diastolic BP was 145.2/85.0 mmHg. None of the 40 patients followed a strict dietary and exercise regimen.

The antidiabetic therapy of the patients remained unchanged and was as follows: Metformin: 8 patients, SUP and Metformin: 4 patients, DPP4 ihb. Metformin: 6 patients, GLP-1 RA: 10 patients, SGLT-2 inh: 12 patients.

All patients with AH were monitored and checked over time by a cardiologist with appropriate antihypertensive therapy. Given the slightly deteriorated glycaemic control in all 40 patients, the initial treatment was left, with the only change being in the preparation of a motor regimen consistent with the general condition, accompanying diseases and complications of diabetes.

RESULTS

After 24 weeks, the patients had an average reduction of body weight of 6 kg. After six months of group activities with purposeful physical activity, control studies were carried out. All patients with type 2 diabetes reduced initial high HbA1C values by an average of 0.53%.

CONCLUSIONS

Correctly dosed and individually planned physical activity plays an important and irreplaceable role in the control of diabetes and its complications. Depending on the general condition of the patient, the most suitable type and intensity of physical activity is selected. The complex treatment of diabetes includes nutrition, medication and physical activity. The balance between these three components is key to the optimal effectiveness of diabetes therapy and improving the patients' quality of life.

The ultimate goal of diabetes treatment is to improve people's quality of life. The physical complications of diabetes can take the form of muscle weakness, pain, loss or balance, and dysfunction of the lower extremities, all of which can ultimately affect an individual's quality of life. Physical activity plays a critical role in managing many of the symptoms of diabetes. By incorporating individualized physical activity and patient education into diabetes management, complications can be prevented.

People with diabetes have a worse quality of life than those without diabetes, especially in the areas of physical functioning and well-being.

Better glucose control generally improves quality of life, and some psychosocial factors (health-related beliefs, social support, coping style, and personality) have a powerful effect on quality of life either directly or through their ability to buffer the negative effects of diabetes.

As a powerful tool, physical activity is crucial for predicting the condition of patients, for disease management, improving their health status and quality of life, and long-term health care. Physical activity is undoubtedly one of the cornerstones of comprehensive patient care.

REFERENCES

1. Recommendations for good clinical practice in ZD-BDE-2019.
2. Stanchev P., Orbetsova M., Incretins in diabetes mellitus. Journal of Endocrinology, 2016, 4, page 147.
3. American Diabetes Association, 2016.
4. Cuenca-Garcia M.Et all-Diabet.Med 29, e369--e376/2012/ ISPAD Clinical Practice Consensus Guidelines 2014 Pediatric diabetes 2014-15, ISPAD Guidelines, 2018.
5. Angela M. Bell, MD The benefits of physical exercise for people with type 2 diabetes, FACP — Written by Mary West on October 18, 2021.
6. Jan Radford,Jane O'Brien,Kade Davison--AJGP>2020>April>Type 2 diabetes and the medicine of exercise. Volume 49, Issue 4, April 2020. Type 2 diabetes and the medicine of exercise: The role of general practice in ensuring exercise is part of every patient's plan Andrew Williams.
7. Ahmad I,Aung MN,Ueno S,Khin ET,Latt TS,Moolphate S,Yuasa M -Physical Activity of Type 2 Diabetes Mellitus Patients and Non-Diabetes Participants in Yangon, Myanmar: A Case-Control Study Applying the International Physical Activity Questionnaires (IPAQ-S) Authors Published20 April 2021 Volume 2021:14 Pages 1729—1739 DOI https://doi.org/10.2147/DMSO.S291468
8. Alisson Padilha de LimaTânia Rosane Bertoldo Benedetti Luma Zanatta de Oliveira Suzane Stella Bavaresco Cassiano Ricardo Rech Journal of Physical Education-30•2019•https://doi.org/10.4025/jphyseduc.v30i1.3017-Physical Physical activity is associated with knowledge and attitudes to diabetes type 2 in elderl
9. Deirdre Harrington PhD, Joe Henson PhD - Practical Diabetes Physical activity and exercise in the management of type 2 diabetes: where to start? First published: 04 October 2021 https://doi.org/10.1002/pdi.2361
10. Thailand Jiriya Intana, Phenchamat Khamthana, Issara Siramaneerat,Chalit Chaowilai, The Open Public Health Journal-The Effect of Physical Exercise Program in Patients with Type 2 Diabetes Mellitus in Ratchaburi Province

ANNUAL OF ASSEN ZLATAROV UNIVERSITY, BURGAS
BULGARIA, 2022, v. LI(1)

GEODES UNUSUAL MANIFESTATION OF UROLITHIASIS. TWO CASES OF BLADDER AND KIDNEY PRESENCE OF GEODES[1]

Zlatka Cholakova, Nikolay Mirinchev
Department of Urology, University Hospital for Active Treatment, Burgas
E: mail: z_cholakova@yahoo.com

ABSTRACT

Geodes are hollow rock masses of spherical shape and of various sizes. They are formed in sedimentary or volcanic rocks. Their formation takes a long time. There are very few reported cases of geode-like hollow stones in the human body. We present cases of geodes found in the genitourinary tract in two patients. The aims are to present the two cases of unusual manifestation of geodes in patients with urolithiasis admitted to the Urology Department for endoscopic mini-invasive treatment and to examine the scientific publications related to geodes established in humans. Patient evaluation included medical history, physical examination, urinalysis, complete blood count, serum biochemistry, coagulation test, and chemical analysis of stones.

Case 1: Geodes found in the bladder of a patient with lower urinary tract symptoms and prostate cancer. Vesical lithiasis was established and the patient was referred for endoscopic laser cystolithotripsy. During cystoscopy, three elliptical, yellow-orange calculi with a smooth surface were found. During the laser lithotripsy, all three stones had a cavity. The cavity had a grainy surface with a mottled appearance. There were distinct irregular areas on the inner surface of the cavity with a dark brown and a light brown color. The wall of stone had with a layered structure and a yellow-orange color.

Case 2: Geode found in pyeloureteral segment of the right kidney of a woman with renal colic. A stone in the pyeloureteral segment of the right kidney was detected using native tomography. A retrograde flexible ureterorenoscopy was performed, which revealed a stone with a pale-yellow color and an uneven crystalline surface with small spikes on its surface. During the lithotripsy, it was found that the stone had a central cavity filled with darker colored brown crystals. After disintegration of the stone, 4.5Fr ureteral stent was placed and the nephrostomy tube was removed.

In very rare cases, geodes are found in the human body. There is no scientifically based theory or mechanism for their in-vivo formation. There is a lack of data on the frequency of distribution of geodes in the human body. Most likely, their formation is related to a multifactorial pathological process similar to their formation in nature.

Key words: *geodes, people, urolithiasis, endoscopic lithotripsy*

INTRODUCTION

Geodes are hollow rock masses, with a spherical shape and of different sizes. Their inner surface is lined with crystals that have grown towards the center of the cavity. The most common crystals growing within a geode are quartz, calcite, or fluorite, although other minerals are also found. Geodes are usually characterized by an outer shell made of chalcedony, which is a dense microcrystalline form of quartz. The hard outer shell of a geode can usually be separated from the surrounding rock material. Geodes are most often formed in limestone or volcanic rocks. The mineralogy of the geode and the rock in which it formed is usually different. Because chalcedony is harder and more resistant to weathering, hollow spheres resist erosion unlike a host that erodes more easily. The initial requirement for geode formation is the presence of a cavity in the host rock. In volcanic rocks, such cavities often result from the release of gases from the molten

[1] The article was presented at the Challenges for Medical Science and Practice in the 21st Century Congress of Medicine, Burgas, 1-3 September 2022

lava. As the lava solidifies, the gas bubbles are preserved as holes in the rock. In the case of sedimentary rocks, such as limestone, a cavity may form from groundwater dissolving the rock itself or as a result of biological material becoming buried by sediment. Groundwater carries dissolved minerals, including silica, that pass through the host rock and reach the cavity. The chalcedony shell is formed first, requiring a long period of time to completely harden. Groundwater bearing minerals leads to additional deposition of mineral layers in a geode. These crystals initially form on the walls of the geode and then grow towards its center [4]. There are very few reported cases of geode-like hollow stones in the human body. We present cases of geodes in the genitourinary system of two patients found incidentally.

AIMS

To present two cases of an unusual manifestation of urolithiasis with geodes – hollow stones of different localization. To examine the scientific publications related to geodes established in humans.

MATERIALS AND METHODS

We describe 2 cases of accidentally discovered geode-hollow calculi in patients with urolithiasis admitted to the Urology Department for monoscopic mini-invasive treatment. Patient evaluation included medical history, physical examination, urinalysis, complete blood count, serum biochemistry, coagulation test. Imaging studies were performed, preoperative ultrasound of kidneys, ureters and bladder (BUM) in the first case and native computed axial tomography (CT) preoperatively in the second case. A respiratory and cardiovascular evaluation (chest radiograph and electrocardiogram) was performed. Both patients were treated conservatively and operatively. An endoscopic mini-invasive operative approach was adopted. In case 1, a single stage Holmium cystolithotripsy was performed, and in case 2, a two-stage approach was adopted, which included the placement of a percutaneous nephrostomy under ultrasound control and debridement of the infectious episode as the first stage. The second stage consisted of performing retrograde flexible ureterorenoscopy with holmium laser lithotripsy. The chemical composition of stones was investigated (Tables 2 and 3).

RESULTS

CASE 1: Geodes found in bladder. A 65-year-old man with prostate cancer on hormonal therapy was admitted to the Department of Urology with lower urinary tract symptoms: dysuria, hesitancy, interruption of the stream, frequent urination. The patient reported that he suffered from frequent urinary infections. Two years earlier he had undergone endoscopic lithotripsy for vesical lithiasis. From the digital rectal examination, an enlarged prostate gland with a hard-elastic consistency in both lobes was found. The clinical-laboratory preoperative investigations are indicated in Table 1.

Table 1 Clinical and laboratory studies of the reported case 1 pre- and post-operatively

Lab. studies	***Case 1*** before / after
Hemoglobin*(120-160g/l)*	105/ 109
Leukocytes*(3,5-10,5.10^9/l)*	4.2/4.0
Platelets*(140-440.10^9/l)*	217/208
CRP*(0-6.0mg/l)*	19.6/10.0
Glucose (s)*(2.78-5.55mmol/l)*	7.55/5.20
Potassium*(3.5-5.5mmol/l)*	5.00/4.5
Calcium*(2.12-2.62mmol/l)*	2.34/2.17
Creatinine*(74-127mmol/l)*	92.0/98.0
LDH*(125-220mmol/l)*	178.0
Urea(3.2-8.2mmol/l)	8.8/5.4
Prothrombin time*(11.5-13.5sec.)*	14.1
Prothrombin activity*(70-120%)*	97.5
INR*(1.0-1.05)*	1.02
tPSA*(0-4ng/ml)*	35.09
Sediment - Leukocytes	16/ 6 per HPF
Sediment-Erythrocytes	8/ 5 per HPF
Sediment- Bacteria	Postitive/ *
Uroculture	*/Negative

Preoperative chest x-ray and electrocardiogram showed no pathological abnormalities. The ultrasound of the kidneys and bladder revealed the presence of three vesical stones with longitudinal dimensions of *10mm, 15mm, 12mm*. Enlarged prostate gland. No residual urine after micturition. Kidneys - without urostasis. The patient underwent urethrocystoscopy with holmium cystolithotripsy. During the cystoscopy, three elliptical, yellow-orange calculi with a smooth surface were found. During the laser lithotripsy, all three stones had a cavity (Fig. 1).

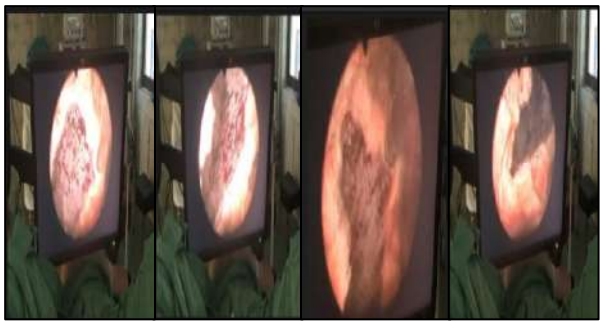

Fig. 1 Endoscopic morphology of vesical geode during endoscopic Holmium cystolithotripsy Stone cavity is demonstrated

The cavity had a grainy surface with a mottled appearance. There were distinct irregular areas on the inner surface of the cavity colored in a darker brown color and such with a light brown color (Fig. 2).

Fig. 2 Endoscopic image of the inner surface of vesical geode

Fig. 3 Fragments of geodes extracted after endoscopic Holmium cystolithotripsy

The wall of stone was found to have a layered structure and a yellow-orange color. After the complete disintegration of stones, the fragments were removed with an Ellik evacuator (Fig. 3). The patient was fitted with a three-way urethral catheter and placed on bladder irrigation for 6 hours. The urethral catheter was removed on the first postoperative day. No complications, such as hematuria, fever, or pain, were observed in the postoperative period. The patient was discharged with improvement of symptoms after 48 hours.

The fragments obtained from the lithotripsy were sent for chemical analysis as two samples – one containing parts of the outer shell of the stone and the second containing parts of the inner part of the wall of the stone. The results are shown in Table 2.

Table 2 Composition of the wall forming the bladder geodes

Composition	***Outer part***	***Inner part***
Carbonates	*	*5%*
Phosphates	5%	5%
Oxalates	49%	42%
Uric acid	45%	46%
Ammonium	*	1%
Magnesium	1%	1%

CASE 2: Geode found in the pyeloureteral segment of the ureter of the right kidney. A 62-year-old woman with pain in the right lumbar region for 6 months accompanied by nausea, vomiting and low-grade fever. For two weeks, the pains had intensified and become unbearable. She underwent conservative treatment with success. A native CAT of the BUM was performed in outpatient conditions, where hydronephrosis II degree of the right kidney, multiple nephrolithiasis and a stone in the pyeloureteral segment of the right kidney with a longitudinal size of *15 mm* were found. 12 years earlier, a pyelolithotomy had been performed on the right kidney due to a coralliform stone occupying the entire pyelocalyx system of the kidney. At the time of hospitalization, the patient had febrile-intoxication syndrome.

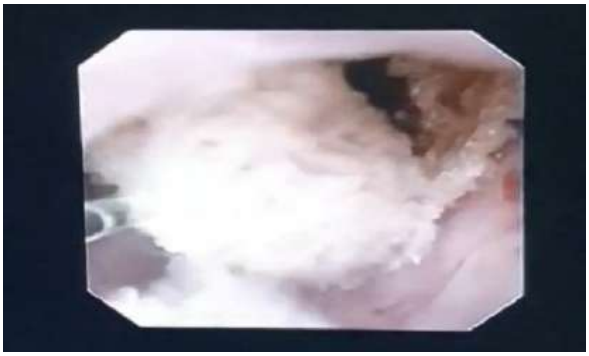

Fig. 4 Endoscopic renal cavity geode morphology during endoscopic retrograde flexible holmium lithotripsy. Stone cavity filled with darker brownish crystals is demonstrated

Table 3 Clinical and laboratory studies of the reported case 2 pre- and post-operatively

Lab. studies	***Case 2*** before / after First stage	***Case 2*** before / after Second stage
Hemoglobin*(120-160g/l)*	135/ 131	125/116
Leukocytes*(3,5-10,5.10^9/l)*	11.5/12.9	8.4/10.1
Platelets*(140-440.10^9/l)*	325/578	331/274
CRP*(0-6.0mg/l)*	161.8/11.1	9.2/21.9
Glucose (s)*(2.78-5.55mmol/l)*	6.83/4.69	6.37
Potassium*(3.5-5.5mmol/l)*	4.20/4.40	4.40/4.50
Calcium*(2.12-2.62mmol/l)*	2.32/2.36	2.59/2.39
Creatinine*(74-127mmol/l)*	72.0/69.0	99.0/84.0
Uric acid*(214-410mmol/l)*	307.0/369.0	646.3/314.0
Urea*(3.2-8.2mmol/l)*	11.7/19.1	18.0/6.4
Prothrombin time*(11.5-13.5sec.)*	13.4	14.2
Prothrombin activity*(70-120%)*	84.1	96.3
INR*(1.0-1.05)*	1.10	1.02
Sediment - Leukocytes	605/20 per HPF	13/1 per HPF
Sediment-Erythrocytes	69/5 per HPF	5/3 per HPF
Uroculture	Negative	Negative

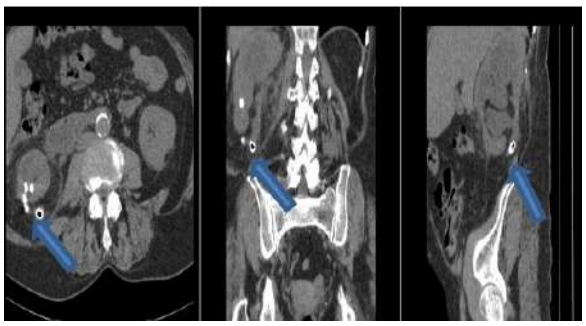

Fig. 5 Preoperative CAT of case 2 showing a geode (cavity in the center of the stone filled with gas - blue arrow) in the pyelourethral segment of the ureter of the right kidney

Fig. 6 Antegrade pyelography of case 2 in the prone position through the placed nephrostomy performed during the first stage of treatment

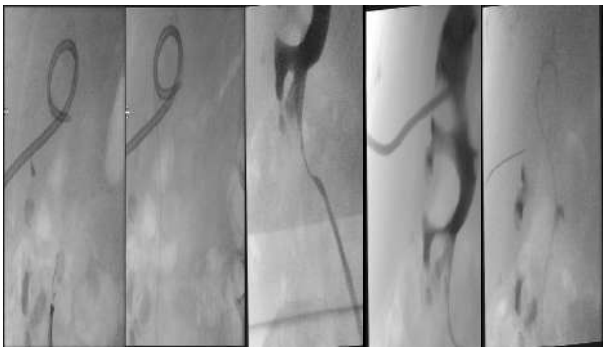

Fig. 7 Intraoperative radiographs and retrograde ureteropyelography of case 2 in the supine position during the second stage of treatment

The treatment approach included conservative treatment until relief of symptoms and percutaneous drainage of the right kidney (Fig. 6). At the second stage, a retrograde flexible ureterorenoscopy was performed (Fig. 7).

Intraoperative retrograde ureteropyelography showed ureteral deviation and proximal ureteral calcification. A hydrophilic guide was placed in the right ureter and a 7.5 Fr. flexible ureterorenoscope was mounted on it. The proximal ureter was reached, where a stone with a pale yellow color and an uneven crystalline surface with small spikes on its surface was found. During the lithotripsy, it was found that the stone had a central cavity filled with darker colored brown crystals (Fig. 4). After disintegration of the stone, a 4.5Fr ureteral stent was placed and the nephrostomy tube was removed (Fig. 7). No complications, such as hematuria, fever, or pain, were observed in the postoperative period. The patient was discharged with improvement of symptoms. The fragments obtained after lithotripsy were sent for chemical analysis (Table 4).

Table 4 Geode composition found in the pyeloureteral segment of the urethra of the right kidney

Composition	
Carbonates	10%
Phosphates	5%
Oxalates	30%
Uric acid	55%

CONCLUSION

Geodes, also called hollow stones, are found in nature. In very rare cases, they are found in the human body. There is no scientifically based theory or mechanism for their in-vivo formation. There are no data on the frequency of distribution of geodes in the human body. Most likely, their formation is related to a multifactorial pathological process similar to their formation in nature. From our search for scientific publications similar to ours, we have found out that there are only three publications about geodes found in the human body. The scientific publications about a geode formed around a paraurethral sling [2], a geode formed in the kidney of a patient suffering from pyelonephritis complicated to pyonephrosis [3] and geodes formed in a patient with benign prostatic hyperplasia and diabetes mellitus with hyperuricemia [1]. From the published articles on established geodes in humans in the past and our two cases, we can draw the following conclusions: Geodes are a very rare form of urolithiasis. There is no published theory about their formation in the urinary-excretory system in humans. Hyperuricemia may play a role in the formation of geodes. Some metabolic (gout) and autoimmune (diabetes mellitus) diseases may play a role in the pathogenesis of geodes. Uroinfections and the presence of certain types of bacteria can be a factor in the formation of geodes. The localization of geodes can be vesical, ureteral or renal, as well as in unusual places - paraurethral. In the composition of the geodes we examined, we found a predominant urate component (*45% to 55%* of the composition). The second predominant component of the composition of geodes are oxalates (*30% to 40%* of the composition). The carbonate component in the composition of stones represented from *5% to 10%*. Phosphates were encountered in 5% of the samples. Ammonium and magnesium were found in *1%* of the composition of the studied geodes. As composition, they are mixed stones. The composition of the geodes from our samples showed the presence of varying percentages of uric acid, oxalates, carbonates, phosphates, ammonium and magnesium. They can have a smooth or uneven surface with a yellow-orange or pale yellowish color. They consist of a solid shell and a cavity filled with crystals. In our study, we examined the two parts of the wall of bladder geodes. We found a difference in the composition of the outer and inner part of the wall (Table 2) of bladder geodes. Carbonates and ammonium were found only in the inner part of the investigated fragments. These are components of the composition of inflammatory stones. Geodes vary in size and shape. Predisposing factors for the formation of geodes can be conditions leading to stagnation of urine in the urinary system (US) - postoperative adhesions, kinks, strictures, tumor processes, congenital anomalies of the US, frequent uroinfections, presence of foreign bodies, etc. The time for the formation of the established geodes according to anamnestic data of cases 1 and 2 can be assumed to be over 1 year. In his publication on a hollow kidney stone [3], Howard reported that stones that have remained for a long period of time in the ureter sometimes have cavities. The case described by him shows the presence of a hollow stone in an afunctioning sclerotic kidney. The anamnestic data of severe trauma in the area of the kidney, the pyelolithotomy performed in the past, severe infection of the kidney and the hypothesis expressed by the author about the formation of the hollow stone - the presence of coagulum in the cavity system of the kidney and the deposition of salts on the coagulum leading to the formation of a stone with cavity over time. In our reported second case, we observed a similar scenario with frequent infections, presence of a stone removed by pyelolithotomy, and then recurrence of a stone with the presence of a cavity. We assume that the described events can play an important role in the formation of hollow stones. The composition of the stone found by Howard was predominantly phosphatic. In our case, we found a mixed stone with mainly a urate component, and the phosphate component presented in a very low percentage. The time interval from pyelolithotomy to the symptoms of renal colic is about 12 years, from which we can possibly assume the formation of a stone with a cavity in case 2. We have no evidence of the presence of blood clots in the cavitary system of the kidney in case 2, but an operation such as pyelolithotomy suggests the presence of some amount of blood-coagulum during the operative intervention in the cavitary system of the kidney, but we

have no definite evidence of this to confirm the hypothesis of the lithogenesis of the hollow stones reported by Howard.

REFERENCES

1. Cecil HL. A hollow kidney stone. *JAMA*. 1932;98(21):1803–1804.doi:10.1001/jama.1932.27320470001010.
2. Woodring T, Massengill A, Elkattah R. Vaginal geode associated with midurethral sling erosion. *Int Urogynecol J.* 2020 Apr;31(4): 847-848. doi: 10.1007/s00192-019-04099-1. Epub 2019 Aug 29. PMID: 31468098.
3. Wyner LM. Bladder "geodes:" an unusual manifestation of cystolithiasis. *J Urol*. 2014 Jun;191(6):1874-5. doi: 10.1016/j.juro.2014.03.079. Epub 2014 Mar 18. PMID: 24656676.
4. "Geode." The Gale Encyclopedia of Science. Retrieved June 22, 2022 from Encyclopedia.com: https://www.encyclopedia.com/science/encyclopedias-almanacs-transcripts-and-maps/geode-0

ANNUAL OF ASSEN ZLATAROV UNIVERSITY, BURGAS
BULGARIA, 2022, v. LI(1)

REPRODUCTIVE VIEW OF THE CITY OF BURGAS IN THE CONTEXT OF THE PSYCHO-SOCIAL FACTORS OF THE DEMOGRAPHIC CRISIS[1]

Petia Tzvetkova
E-mail: tzvetkovap@mail.bg

ABSTARCT

This study presents a survey of the psycho-social characteristics of childless families/partnering couples in the context of the social factor of the demographic map in the city of Burgas and as a part of reproductive problem in this region.

Attention is given on demographic indicators and regional administrative policy.

Keywords: *psychological, social factors, reproduction, demographic problems, Burgas*

INTRODUCTION

Our country is still in a period of economic and social transformation. Against this background, the demographic picture of Bulgaria at the beginning of the 21st century is unfavorable. The low birth rate and high death rate determine the negative natural growth in our country [1].

Population reproduction is a dynamic complex, conditioned by medical, biological, demographic and social conditions.

The in-depth analysis of the health status of the nation reveals serious reasons regarding the possibility of realizing the reproduction of the population. One of them, perhaps the most important, is related to the fertility possibilities of the partnering couple [2].

Realization to the maximum extent of the dreams of the Bulgarian family can be supported by creating an appropriate health and socio-economic environment [3]. The regional policy of each settlement would also be of particular importance.

Our interest in the conducted study was also provoked by surveying the influence of the psycho-social characteristics of childless families/partnering couples in the context of the social factor of the demographic map in the city of Burgas.

MATERIAL AND METHODS

The study covers a survey aimed at four target groups (a total of 209 persons) from the population of reproductive age, as well as members of the municipal administration in the city:

First group - "administration"
Second group - "medical professionals"
Third group - "patients with fertility problems"
Fourth group - "men and women of reproductive age without fertility problems"

RESULTS

According to NSI data, the population in the city of Burgas to 31.12.2020 was 409,750, of which 197,692 and 212,058 respectively were men and women. In active reproductive age (20-34 years) was 64,074, of which 32,132 men and 31,939 women. There is no information how many of them are with reproductive problems.

From the indicated data (Fig. 1), the positive coefficients of birth (8.5) and fertility (1.59‰) are visible, comparing them with other statistical regions or the whole country. Apparently, children are being born in the city, albeit not enough. Quite logically, the negative natural increase (-6.6‰) also follows, but again it is the best indicator compared to the one for our country.

[1] The article was presented at the Challenges for Medical Science and Practice in the 21st Century Congress of Medicine, Burgas, 1-3 September 2022

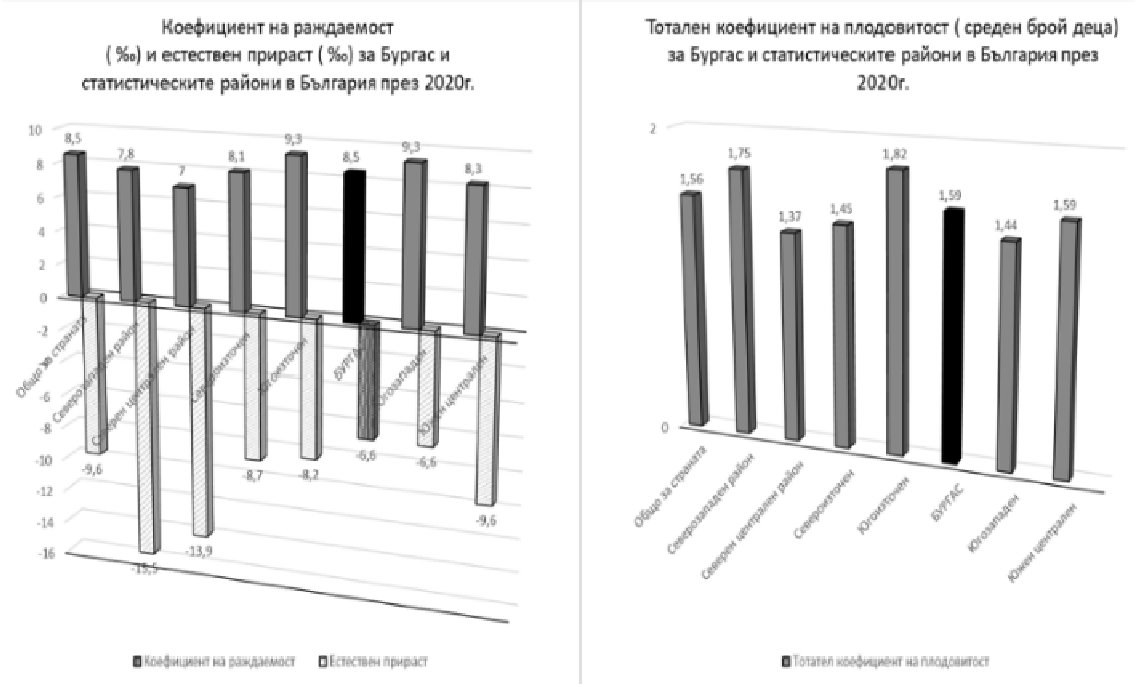

Fig. 1 Demographic indicators in the city of Burgas, compared with the country (NSI, 2020)

Let us look for an answer, why so many children are born, but the demographic problem is on the agenda for the population and the city administration.

From the survey conducted by NSI in 2012 at the national level, and from our survey, it is striking that only 14.6% for the country and 16.8% in the city realize that in order to have a positive increase, the modern family or partnering couples must /wish to have three or more children (Fig. 2).

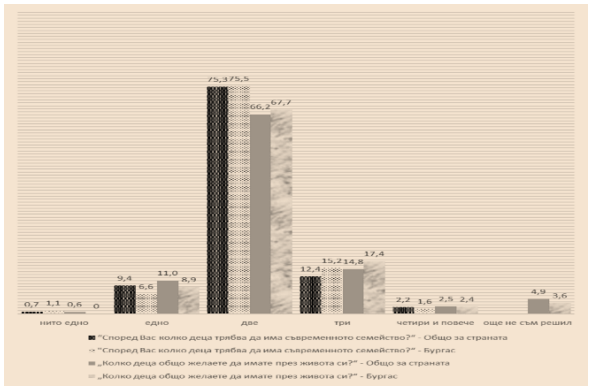

Fig. 2 How many children should the modern family have and how many children do you want to have in total in your lifetime? (NSI, 2012)

They are unanimous in their answers when they point out the factors influencing the choice of how many children to have.

The respondents shared that the most important reason for not having children were financial (17.8%) and economic difficulties (10.3%), advanced age (12.2%), lack of a partner (16.4%). The share of those devoted to careers and social commitments is not small (6.5%). According to 62.2%, it depends to what extent the decision whether to have a child/another child depends on the possibility of providing care, and in 44.5% is it predetermined by the proposed measures to support fertility?

The 22.6% realize that the medico-biological factor is an invariable part of the demographic crisis and that infertility is actually a disease (64.5%).

Among the surveyed 39 municipal councilors in the city out of a total of 51, twenty-seven of them believe that there is a demographic problem in the city and the medico-biological factor is an invariable part of it. Between 5 and 11 of them don't even know if there is one. The majority (32) do not know how many families in the city do not have children due to medical indications.

The summarized answers, respectively in 22.9% and 14.3% to both questions "I am not aware" and "does not affect" are in all probability due to the fact that medical professionals working in the field of reproductive medicine and biology are indebted to society us. Obviously, it needs further clarification. We find a similar finding in the recommendations that are ad-

dressed to the municipality and medical units of the city's territory, as we will note below.

Only that part of the population who have faced reproductive problems are well aware. In 53.3% they correctly seek medical help. But... in 46.7% - not at all. In all probability, this happens due to financial reasons (20.11%), lack of information (16.9%) and not good orientation for the right choice of specialist or simply the lack of such (4.4%) in the territory. Perhaps among them are also those who are disenchanted by "wandering", from office to office (3.4%) and think that treatment would not help them.

Demographic indicators and regional policy

Young parents-to-be are interested in the conditions in the settlement that are offered to them - opportunities for employment, commercial, communal-household and transport services, opportunities to receive and improve their education, cultural life and free time, security and personal safety.

They attach particular importance to the alternatives provided to them for raising and educating their children, guaranteed access to kindergartens and preschool forms of education.

Of course, the level of medical care is not unimportant.

The Municipal Administration in the city of Burgas successfully meets all these requirements:

= Unemployment in the city is 2.4%, against the background of 4.7% for the whole country, it is also lower than the whole Burgas region (3.8%);
= The average salary for Burgas Region for the third quarter of 2021. is BGN 1,188 and ranks the district in 17th place among other districts. The average gross salary in the third quarter of 2021 increased by 11.5% in the public sector and by 4.7% in the private sector, i.e. a good financial infrastructure is in place;
= Crime, especially domestic crime, has been reduced to a minimum - in 2020, 482 crimes were registered, taking into account a decrease compared to the previous year, 2019, when there were 668 crimes;
= Fully renovated transport infrastructure;
= On the territory of the city there are two universities and numerous colleges, providing excellent opportunities for obtaining highly qualified education and professional realization;
= 35 kindergardens, 55 primary, secondary and specialized schools with old history, new ideas and many opportunities to get a good education were opened;
= It is not an unknown fact that the city of Burgas is a spiritual and cultural center with incredible opportunities for citizens, guests and tourists to spend their free time.

- ✓ Assistance to young families with children.
- ✓ A program for financing the birth of a first child has been drawn up and implemented.
- ✓ Financial support for families with newborns.
- ✓ Provision of funds for a one-time financial incentive for parents to promote fertility.
- ✓ 52,000 BGN per year (2021) is allocated to the budget of the Municipality of Burgas to support people with reproductive problems - "IN VITRO PROCEDURES FUND ".

It can be seen that the activity of the regional leadership is directed in the right direction. There is definitely a problem related to improving the reproductive health of the population and especially of the couples in need of treatment.

In 44.5%, the decision whether to have a child/another child depends on fertility support measures.

When conducting the present study, we noticed the unanimous opinion of both the administration and the surveyed infertile couples in the direction of:

- Improving the quality of health services;
- Development of preventive medicine;
- Initiatives by medical institutions to attract leading specialists in the field of reproductive problems for counseling and treatment.
- Ensuring additional generally accessible awareness of the population about the problems with reproduction.
- The funds under the mentioned regulation are extremely unavailable, i.e. need for a "revision" of the measure.
- Formation of communities, Internet groups and forums for couples with reproductive problems, in which a competent specialist can participate and discuss.

The recommendations made would, in all probability, be an additional correct step in promoting fertility in two directions - the first is in the direction of increasing the natural increase, the second - providing a competent opportunity for early diagnosis and adequate treatment in existing reduced or absent fertility.

DISCUSSION

Living longer is a sign of a healthy and successful population, but when coupled with low birth rates, it raises questions that need to be addressed now [4].

The rate of population decline is telling. Of all the EU member states, the population of Bulgaria is decreasing the fastest [5].

The family with two children is the reproductive ideal in the minds of today's Bulgarian peoples. But the data from conducted during the census in 2001. sample fertility studies show a substantial discrepancy between the ideal of family size and the realization of reproductive desires. According to the research, most Bulgarian families (70%) wish to have two children, but due to economic difficulties, 60% of them have not been able to realize their ideal. In this sense, there are certain reserves for increasing the birth rate.

In the short term, they consist in creating conditions for reducing the number of delayed births, and in the medium and long term - in realizing to the maximum extent the ideal of the Bulgarian family - a family with two children by creating a suitable socio-economic environment for their upbringing and education. That is why the state's efforts should be aimed at creating suitable conditions for the birth, upbringing, upbringing, material security and social realization of as many children as the parental couple would like to have [3].

It is logical to argue that with the growth of the economy and income, more opportunities to raise a child are provided. However, most research on the subject proves that when economic conditions improve, the birth rate increases especially among the poorest strata of the population (Easterlin's theory) [6-8].

Perhaps the view is confirmed. Richard Easterlin was the first modern economist to study subjective happiness. In his 1974 book "how much can economic growth improve people's happiness", he proposed the so-called Easterlin paradox: an increase in income does not necessarily lead to an increase in happiness.

REFERENCES

1. NSI, Territorial Statistical Bureau-Southeast, Department of Statistical Studies, Burgas. Main characteristics of the population in the Burgas region in 2020; 2021.
2. Tzvetkova P. Medico-biological aspects of male infertility and their diagnostic significance. Scientific Foundation of Andrology «Prof. Dr. Dimitar Tsvetkov», S., 2013, 258.
3. MC. Updated national strategy for demographic development of the population in the Republic of Bulgaria, 2012-2030. No. 4.2 of Ministry Council dated 01.02.2012.
4. Focus – europarlament, Press service, 2008.
5. Kukov N. Comparative analysis of the main demographic factors in the Republic of Bulgaria and the world. https://ejournal.vfu.bg, 2020, 1-8.
6. Easterlin R.A. Does economic growth improve the human lot? Some empirical evidence. R. Davis, M. Reder (Eds.), Nations and Households in Economic Growth: Essays in Honor of Moses Abramovitz, Academic Press, New York, 1974, 89-125.
7. Easterlin RA. Income and happiness: Towards a unified theory. The economic journal, 2001 - academic.oup.com.
8. Easterlin R.A. Feeding the illusion of growth and happiness: a reply to Hagerty and Veenhoven. Social Indicators Research, 74, 2005, 429-443.
9. NSI. Census of the population and the housing stock in 2011. Book 1, Sample studies "Fertility and reproductive behavior of the population in the Republic of Bulgaria, Sofia, 2012, volume 4, 85.

ANNUAL OF ASSEN ZLATAROV UNIVERSITY, BURGAS
BULGARIA, 2022, v. LI(1)

SPERMATOLOGICAL INDICATORS ON TORSIO TESTIS[1]

Petia Tzvetkova
E-mail: tzvetkovap@mail.bg

ABSTARCT

This paper investigates the fertilizing ability of patients with Torsio testis and the occurrence of spermatopoietic disorders on gonadal functions.

We investigated 34 patients (average 24.81 ± 1.90 years old) with Torsio testis and 29 (average 25.63 ± 2.15 years old) healthy men as a control group. The following methods were used: andrological anamnesis and status; spermatological analysis of the ejaculate and sperm morphology according WHO [2010] using Automatic Sperm Class Analyser (Microptic, Spain); cytological analysis of sperm using Yashkovski staining technique; statistical significance was verified with Student's t-test and SPSS computer program.

In Torsio testis' patients the volume of the ejaculate is in the lower range, a change in the pH is minimal and normal viscosity. Normozoospermia patients showed increase in the percentage of static and non-progressive mobile sperm and consequently - decrease in the progressively mobile cells percentage. Oligozoospermia patients showed even worse indicatiors. We noticed the decrease of middle and fast moving sperm percentage.

There are a sperm morphological changes: an increased abnormalities percentage in the sperm head, in the individual tail parts, observed cytoplasm retention around the cervix or/and part of the median share of the sperm rarely.

Cytological and light microscopic examination of seminal fluid showed a varied sperm picture with multiple disabilities that convert them to functionally inactive because of suppression or disturbance in the normal course of the spermatopoietic process in patients with Torsio testis.

Keywords: *sperm, Torsio testis, fertility*

INTRODUCTION

It is well known that early treatment of patients with Torsio testis is the way to preserve the gonads. The degree of stored testicle is 56% [1,2]. However, it is a fact that even these "saved" gonads have spermatopoietic disorders in their functions [3], even if the localization of the process is unilateral. [4] It is astonishing that infertility can follow the unilateral forms of the disease, although there is a presence of "healthy" contralateral gonads [3].

Different answers are available why there is a pathological spermiogramme in these patients, even more so that there is a healthy contralateral testicle [4] It is not clear whether the cause is primary as a result of congenital inferiority of the gonads or is secondary to the result of seminal vesicular torsion. [3,5]. But one thing is clear - the unilateral function of the testicle is not equivalent to fertility.

The aim of the paper is to investigated influence of vesicle disease Torsio testis on patinet's spem fertilizing ability.

PATIENTS AND METHODS

We were investigated 34 patients (average 24.81 ± 1.90 years old) with Torsio testis and 29 (average 25.63 ± 2.15 years old) healthy men as a control group.

The following methods were used:

- andrological anamnesis and status;
- spermatological analysis of the ejaculate and sperm morphology according WHO [6] [2010] using Automatic Sperm Class Analyzer (Microptic, Spain);
- cytological analysis of sperm using Yashkovski staining technique;

[1] The article was presented at the Challenges for Medical Science and Practice in the 21st Century Congress of Medicine, Burgas, 1-3 September 2022

The results are given as mean ± SD.

In conducting this research, we have followed all the recommendations of the Ethics Committee Approval.

RESULTS

One of the major evaluations of seminal plasma begins with its physico- chemical properties determination: volume, pH and viscosity. Such a study is informative with regard to the initial information on the exocrine function of the testes and the condition of the adherent sex glands. They all determine the total ejaculated volume.

In Torsio testis' patients the volume of the ejaculate is in the lower range (1.90 ± 0.15 ml). Decreased amount of plasma, produced in acute scrotum can be explained by delayed surgical treatment resulting on a fertility capacity impairment of the "single testicle" pathology.

There is a morphological change: increased abnormalities percentage mainly in the sperm head in Torsio testis patients (Fig.1, Table 2).

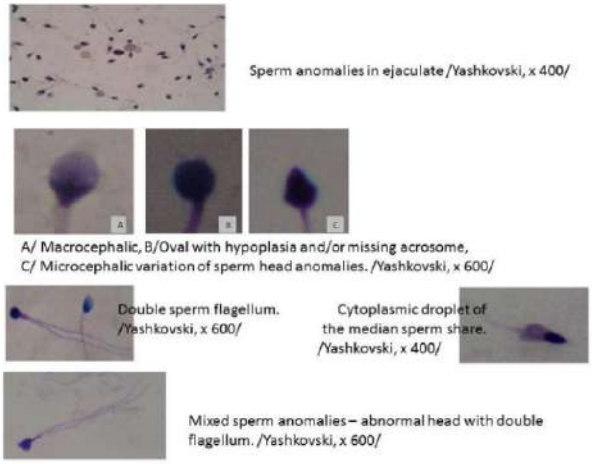

Fig. **1** Sperm anomalies in ejaculate on Torsio testis' patients

Table 1. Sperm concentration (millions/ml) and motility analysis on patients with Torsio testis

Progression	**Percentage** (%)	**Concentration**
NORMOSPERMIA n=13		
Static	12.9 ± 0.99%	8.2±0.65
Non-progressive motile	44.4 ± 1.13 %	28.4±0.59
Progressive motile	42.7± 2.22%	27.3± 1.13
TOTAL	**100.0%**	**64.0±3.33**
OLIGOSPERMIA n=17		
Static	98.3± 6.66%	11.5±2.12
Non-progressive motile	1.2± 0.78%	0.1±0.07
Progressive motile	0.4± 1.14%	0.0
TOTAL	**100.0%**	**11.7±3.43**
CONTROL GROUP n=29		
Static	0.2± 0.01%	0.2±0.09
Non-progressive motile	7.3± 0.76%	6.1±0.93
Progressive motile	92.4± 0.99%	77.0±0.46
TOTAL	**100.0%**	**83.3±1.12**

Table 2. Sperm morphology and velocity (μm/s) on Torsio testis' patients

CONTROL GROUP n=29	Total	Static	Slow	Medium	Rapid
Head Area	14.7±0.8	12.5±2.22	9.0±1.17	15.2±1.35	14.7±4.12
Round Cells	9.1±0.43	mill/mL	(< 5 mill/mL)		
Circular tracks	2541±231	89.7±0.39 %			
NORMOSPERMIA n=45					
Head Area	6.4±2.22	9.7±0.98	8.0±0.14	6.0±0.98	4.8±1.12
Round Cells	0.4±0.61	mill/mL	(< 5 mill/mL)		
Circular tracks	919±112	51.5± 1.2%			
OLYGOSPERMIA n=76					
Head Area	17.0±1.11	17.0±1.13	10.2±2.44	0.0	4.2±1.23
Round Cells	2.1±0.65	mill/mL	(< 5 mill/mL)		
Circular tracks	3±1.55	1.2± 1.2%			

A change in the ejaculate pH obtained from patients with Torsio testis is minimal relative (7.55-7.60) to the control group. The studies showed normal ejaculate viscosity except for two patients.

The study of motility showed that even in Normozoospermia patients suffering from Torsio testis, there is an increased percentage of static and non-progressive mobile sperm and consequently decreased percentage of mobile cells, compared to healthy controls. In Oligozoospermia patients the indicators are even worse (Table 1). We notice the decrease of middle and fast moving sperm percentage in Torsio testis patients.

Torsio testis patients were the least exposed to morphological changes (Table 3) in the individual tail parts (0 – 2.00%), for example - double flagellum 1.00%. We observed cytoplasm retention around the cervix or/and part of the median share of the sperm rarely - 1.00%. Light microscopic examination of Torsio testis patients' seminal fluid showed a varied sperm picture with multiple disabilities that convert them to functionally inactive.

Table 3 Anomalies in sperm morphological forms in Torsio testis' patients

Anomalies in sperm morphological forms in Torsio testis' patients:	**Total %**
Sperm head	**42**
- macrocephalic	11
- microcephalic	15
- oval	3
- elongated	15
- double	
Sperm flagellum	**2**
Cytoplasmic droplet	**1**
Combined anomalies	**3**

DISCUSSION

The disease occurs in 1/4000 men aged under 25 and in 1/160 men over 25 years old for year [7,8]. Studies indicate that twisting of 720 degrees induces ischaemia, sufficient to destroy the tubuli seminiferi epithelium. [2,9] Experimental testicular ischemia/reperfusion (e.g. Torsion/Detorsio) in rats and/or mice induced germ cell reduction and apoptosis, seminal epithelial vacuolization and decreased sperm production [5,10].

We can safely add the importance of hypoxia, hyperthermia and deteriorated antioxidant protection to factors for impaired spermatogenesis.

Besides the total number, perhaps the most important unit in the fertility capacity of the male genital cells is their mobility and, above all, the percentage of fast moving sperm in the ejaculate. Studies on male sperm motility have led some authors to consider this quality as a marker for good prognostication of male fertility in in vivo and especially in in vitro fertilization. [1,11].

Progressive and highly progressive movement is characteristic of normal healthy sperm and any variation in environmental conditions lead to relevant disorders affecting the specified parameters and motility in general, and therefore an altered fertility. Physico-chemical factors have the most influence on the motility of the germ cells: viscosity [12], osmotic pressure, temperature and ejaculate oxygen concentration [13]. Such a finding we did, comparing the data for viscosity and pH, which show that the combination of hyperviscosity, although reported in isolated cases, with increased acidity of the medium greatly increases the proportion of weakly movable gametes (between 80-95%), reaching 100% static, regardless of concentration (Normo/Oligozoo-spermia) or male genital pathology.

Sperm motility is the first visible indication of changes in distortion physico-chemical conditions of semen, regardless of the etiological cause. In the case of Torsio testis, the percentage of fast moving sperms decreases while weakly moving and immobile cells increase.

The abnormal ejaculate cells ratio to the total sperm count is one of the main factors in male fertility determination. Typically, the reduced amount of spermatozoa in the seminal fluid and/or the increased presence of morphologically immature abnormal spermatozoa (at the expense of normal) are the result of suppression or disturbance in the normal course of the spermatopoietic process.

The morphological picture in the vascular pathology study showed a 48% presence of metamorphic cells. Summarizing the data from the performed studies, we found that in the results related to the concentration of the gametes with normal and / or disturbed morphology showed a tendency to increase of injured cells percentage in a large part of the Normo- and Oligozoospermia ejaculates of Torsio testis patients. There are also cases where abnormal cells are in a small amount, only if for Normospermia ejaculates this is expected, it is of interest to Oligozoospermia patients and is important for more specific adequate therapy application. [4]

The degree of degenerative changes in morpho-functional qualities of male genital cells is closely related to the etiological factor of the disease process and the severity of spermatogenesis damage [12].

Oligosospermic ejaculates but with a high percentage of vital, morphologically normal, genital cells with good motility may be well prognostic for fertility, as some of the observed cases with Torsio testis [4].

CONCLUSION

In most cases, the high-grade torsion testicle not restored in time, caused permanent spermatogenesis disturbances, resulting in infertility and, in some cases, sterility.

REFERENCES

1. Fehér ÁM, Bajory Z.; A review of main controversial aspects of acute testicular torsion. J. Acute Disease 2016, 5 (5):5-8.
2. Naouar S, S Braiek, R El Kamel; Testicular torsion in undescended testis: A persistent challenge. Asian Journal of Urology, 2017 (4): 111-115.
3. Arap MA, FC Vicentini, M Cocuzza, J Hallak, K Athayde, AM Lucon, S Arap, M Srougi.; Late hormonal levels, semen parameters, and presence of antisperm antibodies in patients treated for testicular torsion, J Androl 2007 (28), 5: 528–532.
4. Da Justa D, C Granberg, C Villanueva, L Baker; Contemporary Review of Testicular Torsion: New Concepts, Emerging Technologies and Potential Therapeutics. J Pediatr Urol, 2013 (9): 1-12.
5. Karaguzel E, M Kadihasanoglu, O Kutlu; Mechanisms of testicular torsion and potential protective agents. Nature Reviews Urology 2014 (11), 1: 391–399.
6. World Health Organization (2010). Special program on research, development and research training in human reproduction Annual Tech. Report., Geneva, WHO.
7. Cubillos I, Palmer J., Friedman SC, Freyle J, Lowe FC, Palmer LS; Familial testicular torsion, J. Urology, 2011, (185),10: 2469–2472.
8. Friedman AA, Ahmed H, Gitlin JS, Palmer L; Standardized education and parental awareness are lacking for testicular torsion.Journal of Pediatric Urology 2016, (12), 1:66.e1-166.e82.
9. Lysiak JJ, Zheng S, Woodson R, Turner TT; Caspase-9-dependent pathway to murine germ cell apoptosis: mediation by oxidative stress, BAX, and caspase 2. Cell and Tissue Research, 2007 (328), 4: 411–419.
10. Turner TT, Lysiak JL; Oxidative stress: a common factor in testicular dysfunction. J. Andrology, 2008, (29), 4: 488–498.
11. Elzanaty S, Richthoff J, Malm J, Giwercman A ; The impact of epididymal and accessory sex gland function on sperm motility. Human Reproduction, 2002, (17), 2: 2904-11.
12. Tzvetkova P. (2013) Medical and biological aspects of male infertility and their diagnostic significance Bulgarian Science Foundation of Andrology "Prof. Dr. Dimitar Tsvetkov », S, 258.
13. Moghimian M, M. Soltani, H. Abtahi, J. Adabi, N. Jajarmy; Protective effect of tunica albuginea incision with tunica vaginalis flap coverage on tissue damage and oxidative stress following testicular torsion: Role of duration of ischemia, Journal of Pediatric Urology, 2016, (12), 390.e1-390.e6

ANNUAL OF ASSEN ZLATAROV UNIVERSITY, BURGAS
BULGARIA, 2022, v. LI(1)

ASSOCIATION BETWEEN ADMA, OXIDATIVE STRESS AND ENDOTHELIAL DYSFUNCTION IN METABOLIC SYNDROME[1]

Ganka Bekyarova, Yoana Kisselova-Kaneva*, Nicolai Bekyarov**, Stefka Stoeva*
*Faculty of Pharmacy, University „Prof. Parackev Stoyanov", Varna
**Medical Faculty, University „Prof. Parackev Stoyanov", Varna
E mail: ganka.bekyarova@abv.bg

ABSTRACT

Endothelial dysfunction, characterized by decreased bioavailability of nitric oxide (NO) is one of the major factors in the pathogenesis of metabolic syndrome (MetS). Increased plasma level of asymmetric dimethyl arginine (ADMA), an endogenous inhibitor of nitric oxide synthase (eNOS) is marker of endothelial dysfunction and cardiometabolic risk. Enzyme heme-oxygenase-1 (HO-1), catalyzing degradation of heme to carbon monoxide and bilirubin, has antioxidant and cytoprotective effects in various stress. Data about the role of HO-1 in the pathogenesis of ED in MetS are scarce. The aim of the study was to examine the association of plasma levels of ADMA, HO-1 and malondialdehyde (MDA) as marker of lipid peroxidation and oxidative stress in people with MetS. Material and Methods: According to NCEP-ATP III criteria for the MetS the participants of the study were divided in two group: metabolic) (n =30) and control (nonmetabolic) (n=14) groups. Plasma HO-1, ADMA were investigated in the biochemistry laboratory using the ELISA methods. Plasma lipid peroxidation in was assayed by MDA levels detected by thiobarbituric acid reactivity (TBAR). Results: Plasma levels of ADMA increased (by 21%, p<0.01) and HO-1 (by 31%, p<0,05) and MDA (by 63%, p<0,01) in people with MS when compared to those of the control one. A positive association between ADMA and MDA and ADMA and HO-1 in the plasma were noted in people with Mets. In conclusion, the results of the present study indicate that the study of plasma biomarkers such as ADMA, HO-1 and MDA is important for the evaluation of ED in clinical practice.

***Key words**: ADMA, oxidative stress, HO-1, endothelial dysfunction, metabolic syndrome*

INTRODUCTION

Metabolic syndrome (MetS) is becoming a serious public health problem. The main risk factors of MetS are associated with an increased risk of cardiovascular disease, the occurrence of stroke, type 2 diabetes mellitus and an increased risk of mortality. MetS stimulates the onset of early atherosclerosis, its development and accelerates the incidence of cardiovascular complications associated with atherosclerosis and diabetes mellitus. Endothelial dysfunction (ED), characterized by decreased bioavailability of nitric oxide (NO) is one of the major factors in the pathogenesis of MetS [1]. Increased plasma level of asymmetric dimethyl arginine (ADMA), an endogenous inhibitor of nitric oxide synthase (eNOS) is marker of endothelial dysfunction and cardiometabolic risk [2]. A possible mechanism for reducing eNOS activity is the inhibitory effect of free radicals and cytokines on the expression of this enzyme in the vascular endothelium.

As an inducible stress protein, HO-1 is widely accepted to be a highly sensitive and reliable marker of oxidative stress [3]. HO-1 is antioxidant enzyme that exerts beneficial effects through the protection against oxidative damage [4]**.** Heme-oxygenase-1 (HO-1), catalyzes the degradation of heme to carbon monoxide (CO) and bilirubin which have also antioxidant and cytoprotective effects [5]. Data about the role of HO-1 in the pathogenesis of ED in MetS are scarce.

The aim of the study was to examine the association of plasma levels of ADMA, HO-1 and malondialdehyde (MDA) as marker of lipid peroxidation and oxidative stress in people with MetS.

[1] The article was presented at the Challenges for Medical Science and Practice in the 21st Century Congress of Medicine, Burgas, 1-3 September 2022

METHODS

Subjects, groups

According to NCEP-ATP III criteria [6] for the metabolic syndrome (the presence of three or more of the following: waist circumference ≥102 cm (men), ≥88cm (women); blood pressure ≥130/85mm Hg or treatment for hypertension; triglycerides ≥1.7 mmol/l (≥150mg/dl); HDL-cholesterol <1.03 mmol/l (<40 mg/dl) (men), <1.29 mmol/l (<50 mg/dl) (women) the participants of the study were divided in two group: metabolic, n=30 and control (nonmetabolic) (n=14) groups. Information of personal history of diabetes mellitus, hypertension, obesity and dyslipidemia as component of MetS, genetic predisposition of risk factors: age, unhealthy life styling (diet rich of carbohydrate, lipids, poor of vegetables, fruits and antioxidants, physical activity) were assessed through a structured interview. The control group clinically healthy individuals who volunteered to participate in the study. The study was approved by the local Ethical Committee at the Medical University of Varna (Protocol № 86/26.09.2019). Written informed consent was obtained from all participants in the study. Data regarding personal information were coded and kept confidential. Forty fourth people (36 females, 8 males) aged from 20 to 61 years were included in the study.

Table 1. Baseline characteristics of the study groups

	Control Group N=14	**MetS Group N=30**
Age (years)	38,7+1,62	53,8+1,91
Genetic predisposition (Yes/No)	No	20 (67%)
Diabetes (Yes/No	No	16 (54 %)
Arterial hypertension Yes/No)	No	19 (63 %)
Obesity (Yes/No	No	18 (60 %)
Physical inactivity	No	21 (70 %)
Unhealthy life styling	No	24 (80 %)

Blood collection

Fasting blood was collected from the jugular vein in vacutainers (EDTA). Plasma was separated by centrifugation at 800 rpm for 10 min, aliquoted and storage at -20^{o}C. Subsequent analyses were performed immediately after thawing of the samples.

Measurement of plasma ADMA and HO-1 concentrations

ADMA plasma concentrations were determined using ELISA assay kit (DLD Diagnostica GMBH, Germany) after it was validated locally. Data are presented in mmol/L.

HO-1 plasma concentrations were determined using ELISA assay kit (EKS-800, Stressgen Bioreagents; now Assay Designs, Ann Arbor, MI, USA). Data are presented in ng /mL.

Measurement of MDA Levels

As indicator of lipid peroxidation, plasma MDA levels were detected as described by Porter et al with some modifications as follows: with the aim of protein precipitation to 250 μL of 30% trichloroacetic acid were added to 100 μL plasma sample. After centrifugation at 3000 rpm/room temperature/10 min 150 μL supernatant were mixed with 150 μL 0.67% thiobarbituric acid, adjusted to pH 7.0 with 0.1 N Na OH. After 20 min of incubation in water bath at 96^{o}C samples were immediately cooled in ice water. 200 μL from each sample were transfered in 96 ELISA plates and absorption at λ=532 nm was measured on Synergy 2 multiplate reader (BioTek, USA). Absorption was adjusted using a mixture of deionized water and thiobarbituric acid (1:1) as blank. The concentration of MDA in samples was calculated using calibration curve. Results are expressed as mean±SEM nmol. MDA concentration in each plasma sample was measured in triplicate.

Statistical analysis

Data were presented as mean ± SEM, or percentage (%), as appropriate. Data analysis was performed on GraphPad Prism v. 8.3. and SPSS v. 23. Standard statistical methods such as descriptive statistics, unpaired Student's t-test for normally distributed parameters, and one-way ANOVA with Bonferroni correction were used.

RESULTS

Plasma levels of ADMA increased (by 21%, $p<0.01$) (Fig. 1), MDA (by 63%, $p<0,01$) (Fig. 2) and HO-1 (by 31%, $p<0,05$) (Fig. 3) and in people with MS when compared to those of the control one. A positive association between ADMA and MDA ($r=0,545$, $p<0,05$) in the plasma were noted in people with Mets.

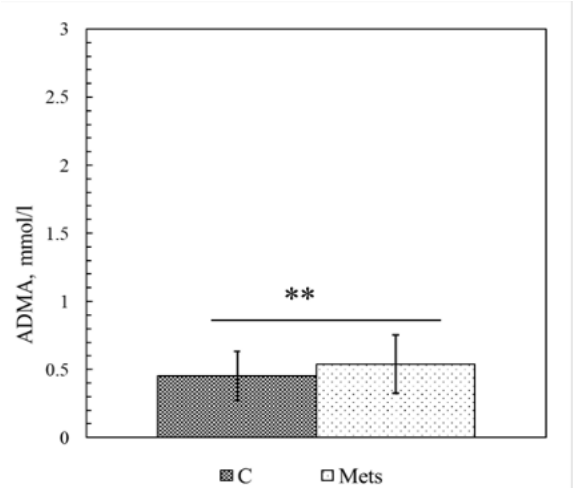

Fig. 1 Plasma Levels of ADMA mmol/L in the people with MetS. Results are given as mean ±SEM; **p <0, 0001 controls (C) vs MS case

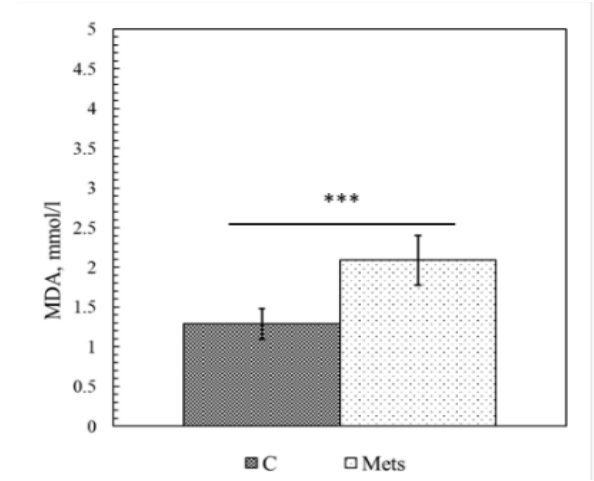

Fig. 2 Plasma Levels of MDA (mmol/L) in the people with MetS. Results are given as mean ±SEM; ***p <0, 0002 controls (C) vs MetS case

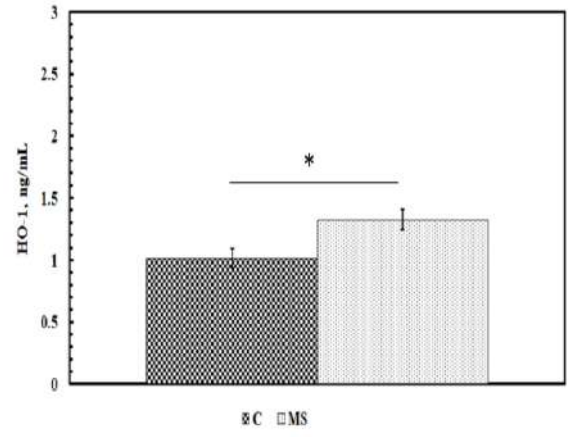

Fig. 3 Plasma Levels of HO-1 (ng/mL) in the people with MS. Results are given as mean ±SEM; *p <0, 01 controls (C) vs MS case

DISCUSSION

In present study we investigated the association of plasma levels of ADMA an endogenous inhibitor of nitric oxide synthase is marker of endothelial dysfunction, HO-1 and MDA as marker of lipid peroxidation and oxidative stress in people with MetS.

In the current study we found a significant positive association between serum MDA, marker of oxidative stress and ADMA as a marker endothelial dysfunction. It is known that ADMA is metabolized by dimethylarginine dimethylaminohydrolases 1 (DDAH1) to dimethylamine and citrulline. On the other hand, ADMA is produced by degradation of methylated proteins by the action of enzymes called protein arginine methyltransferases type I (PRMT-I) [7]. The expression of PRMT in endothelial cell is upregulated by the presence of native or oxidized LDL cholesterol both of them increased in these MetS patients [8].

It is suggested that oxidative stress may stimulate ADMA production and/or inhibit ADMA degradation that lead to decrease inhibition of eNOS and reduction of NO availability [8]. A possible mechanism for reducing eNOS activity is the inhibitory effect of free radicals and cytokines on the expression of this enzyme in the vascular endothelium.

The superoxide anion radicals in turn reacts with the NO radical, thus reducing the bioavailability of NO in favor of the formation of ONOO which leads to eNOS uncoupling via oxidation of BH4 [9]. The uncoupled eNOS shifts the nitroso-redox balance favoring production of O_2 − rather than NO, resulting in further increased formation of endothelial ROS and the activation of redox-sensitive genes that contribute to endothelial dysfunction. It is possible to speculate that increased ADMA concentration and oxidative stress in causing a reduction of NO availability may be responsible for ED [8].

The reduced bioavailability of NO due to reduced eNOS activity and/or NO degradation leads to impaired endothelium-dependent vasodilatation, tendency to thrombus formation and remodeling of the vascular wall. Oxidative stress can also worsen endothelial damage by eliciting an inflammatory response and increasing expression of proinflammatory cytokines and to contribute to progression of CVD - components of MetS [9].

ADMA may also inhibit antioxidant activity of superoxide dismutase (SOD), glutathione pe-

roxidiase and catalase and increases oxidative stress and endothelial dysfunction [10]. This was accompanied by increased circulating levels of the lipid peroxidation and oxidative stress marker- MDA. Oxidative stress was present in our study according to the increased levels of MDA in MetS.

Enzyme HO-1 is the body's first line of defense against oxidant attack. Although HO-1 is expressed at low levels in endothelial cells under basal conditions, it is highly inducible in response to various pathophysiological stresses/ stimuli [4]. It has been reported that HO-1 induction inhibited ROS production in aorta isolated from in animals with fructose-induced MetS [11]. We found increase plasma HO-1 levels in people with MetS. We hypothesize that HO-1 is more compensatory in nature, and the elevated levels support the view that it has the capacity of a marker of oxidative stress in the vascular wall. Data about plasma levels of HO-1 human with metabolic syndrome are very scarce. The elevated plasma HO-1 levels have been reported in diabetes [12]. In clinical case heme oxygenase-1 deficiency oxidative stress causes enhanced endothelial cell injury [13].

HO-1 has been shown to be important for atenuating the overall production of reactive oxygen species (ROS) through its ability to degrade heme and to produce carbon monoxide (CO), biliverdin/bilirubin, and the release of free iron [14].

HO-1 may restore reduced eNOS activity and compensate for the loss of NO bioavailability not only by inhibiting NADPH oxidase activity generation of superoxide radicals, but also by increasing SOD and catalase and antioxidant capacity of EC in Mets [11, 15].

Also, increased HO-1 and heme degradation products can improve vascular function, possibly exerting anti-inflammatory, anti-proliferative and anti-apoptotic effects [16]. According to a number of authors, the study of HO-1 provides an assessment of the body's adaptation mechanisms and possibilities for therapeutic influence.

CONCLUSION

In the current pilot study, we found that plasma HO-1 and ADMA (endogenous eNOS inhibitor) levels are increased in people with Mets. We suggest that induction of HO-1 is an adaptive response against oxidative stress-mediated decreased eNOS activity, loss of no availability and ED in people with MetS. The study of the relationship between ADMA, HO-1 and oxidative stress would contribute to elucidate the complex pathophysiological mechanisms of endothelial dysfunction in MetS and this would allow the use of these markers in screening the risk of early atherosclerosis in metabolic syndrome.

REFERENCES

1. Palomo I. et al., 2011, Elevated concentration of asymmetric dimethylarginine (ADMA) in individuals with metabolic syndrome, *Nitric Oxide* 24(4):224-228.
2. Jamwal S. and S. Sharma, 2018, Vascular endothelium dysfunction: a conservative target in metabolic disorders. *Inflammation Research* 67(5):391-405.
3. Peterson S.J. et al., 2009, Targeting heme oxygenase: therapeutic implications for diseases of the cardiovascular system, *Cardiology Review,* 17(3):99-111.
4. Kim, Y.M. et al., 2011, Heme oxygenase in the regulation of vascular biology: from molecular mechanisms to therapeutic opportunities, *Antioxidant Redox Signaling* 14:137-146.
5. Facchinetti, M.M., 2020, Heme-Oxygenase-1, *Antioxidant Redox Signaling* 32(17):1239-1242.
6. Expert Panel on Detection, Evaluation, and Treatment of High Blood Cholesterol in Adults. Executive summary of The Third Report of The National Cholesterol Education Program (NCEP) expert panel on detection, evaluation, and treatment of high blood cholesterol in adults (adult treatment Panel III). *JAMA* 2001; 285:2486–2497
7. Vallance P. and J. Leiper, 2004, Cardiovascular biology of the asymmetric dimethylarginine: dimethylarginine dimethylaminohydrolase pathway, *Arteriosclerosis Thrombosis Vascular Biology* 24(6):1023-1030.
8. Pope A.J., K. Karuppiah and A.J.Cardounel, 2009, Role of the PRMT-DDAH-ADMA axis in the regulation of endothelial nitric oxide production, *Pharmacological Researsh,* 60:461-465.
9. Sydow K. and T. Munzel, 2003, ADMA and oxidative stress, *Atherosclerosis* Suppl 4:41–51.
10. Cooke J.P., 2005, ADMA: its role in vascular disease, *Vascular Medicine*. 10, Suppl 1: S11-17.
11. El-Bassossy H.M., N. Hassan and M.N.Zakaria, 2014, Heme oxygenase-1 alleviates vascular complications associated with

metabolic syndrome: Effect on endothelial dependent relaxation and NO production, *Chemico- Biological Interaction* 223:109-115.
12. Bao W. et al., 2010, Plasma heme oxygenase-1 concentration is elevated in individuals with type 2 diabetes mellitus, *PLoS One* 5(8): e12371.
13. Leiva E.,et al, 2013, High levels of iron status and oxidative stress in patients with metabolic syndrome, *Biological Trace Element Research* 151(1):1-8.
14. Abraham N.G.and A. Kappas, 2005, Heme oxygenase and the cardiovascular-renal system, *Free Radical & Biology Medicine* 39(1):1-25.
15. Pae H.O. et al., 2010, Role of heme oxygenase in preserving vascular bioactive NO*, Nitric Oxide* 23:251-257.
16. Abraham N.G. and A. Kappas, 2008, Pharmacological and clinical aspects of heme oxygenase, *Pharmacological Review* 60:79-127.

ANNUAL OF ASSEN ZLATAROV UNIVERSITY, BURGAS
BULGARIA, 2022, v. LI(1)

METASTATIC BRAIN TUMOURS[1]

S. Chavdarov, St. Shishkov*, Sv. Todorov, E. Laleva, K. Minkova, M. Mihaylova
*Department of Neurosurgery, University Hospital, Burgas
E-mail: dr.kilic@abv.bg

ABSTRACT

Clinically, secondary malignancies of the cerebrum represent more than 50% of all brain tumours. It has been shown that cerebral metastases occur in 15-30% of all diagnosed cancer patients. Most are from lung (44%), breast (10%), kidney (7%), melanoma (3%), and undetected primary neoplasms (10%). Paediatric ones are very rare and are most commonly from neuroblastoma, rhabdomyosarcoma and Wilms tumours. The route of metastasis is hematogenous. Clinical symptoms include epilepsy, headache, graded changes in neurological status to coma and death.

By performing imaging studies with CT, MRI, and PET scans, we aim to clarify the tumour process and localization and plan the surgical approach. The treatment is complex, including surgical intervention, symptomatic medication, radiotherapy and chemotherapy. With surgical management, we try to prolong the patient's quality and length of life.

In a large percentage of cases, metastatic tumours are life-threatening and their correct diagnosis and subsequent timely therapeutic management are of utmost importance. Combined medical, surgical and radiotherapeutic approaches give encouraging results in prolonging the patient's life.

Key words: *brain, therapeutic approach, brain metastases*

INTRODUCTION

Intracerebral metastases are one of the most common clinical malignancies, accounting for more than half of brain tumours [1, 4]. Clinicopathologically, they represent abnormal uncontrolled development of cells from the nervous system, meninges, and all cellular structures in the brain. The aetiology is diverse and complex.

In 15-30% of patients with cancer, metastases to the central nervous system occur, with primary foci in the lung (44%), breast (10%), kidney and gastrointestinal tract (6-7%), and malignant melanoma (3%) [7, 9].

Clinical symptoms include headache, limb weakness or paralysis, nausea and vomiting, convulsive seizures and fits, ataxia, disorientation, visual and speech disturbances [1, 2].

The aim of our study is to review the clinical symptomatology, aetiology, and treatment of non-brain metastases and to present two case reports of patients with brain metastases.

MATERIALS AND METHODS

Diagnosis of metastatic tumours in the brain includes, first of all, the patient's symptomatology and the presence of another malignant process in the body, diagnosed or not.

This is followed by CT with or without contrast enhancement, MRI with or without contrast enhancement, the aim of contrast studies being to illustrate the blood vessels in the brain that are in close proximity to the tumour or are feeding the tumour, for more precise surgical treatment [6, 7]. Also, it is of key importance to take a biopsy for histological verification and typification. Lumbar puncture is of limited use, but can be included in studies [1, 3, 5].

RESULTS

After conducting imaging studies, blood tests and taking a detailed status and history of the patient's condition, clinical manifestation of symptoms and the presence of Ca process, when

[1] The article was presented at the Challenges for Medical Science and Practice in the 21st Century Congress of Medicine, Burgas, 1-3 September 2022

a metastatic formation is present in the brain, cerebellum or spinal cord, its removal is most often done surgically.

The therapeutic management depends on the size, number and location of the tumour, whether it compresses important brain structures, where the primary focus is, the general condition of the patient and side effects [7, 8, 9].

Surgically, the aim is to remove as much of the formation as possible and take material for biopsy and verification [10].

Through new surgical methods and technologies, such as neuronavigation, intraoperative monitoring, and microsurgical technique under optical magnification, the risk of complications is significantly reduced.

Besides surgical treatment, the treatment includes courses of chemo- or radiotherapy, Gamma knife, Cyberknife, True beam, and drug therapy corticosteroids, diuretics, and antiepileptic drugs [5, 6].

CLINICAL CASE 1

A man of age corresponding to his actual age was admitted to the neurosurgery department. The patient complained of dizziness, severe headache and ataxia. After performing MRI of the brain, a metastatic mass in the cerebellum was detected, leading to the presentation of this symptomatology (Fig. 1).

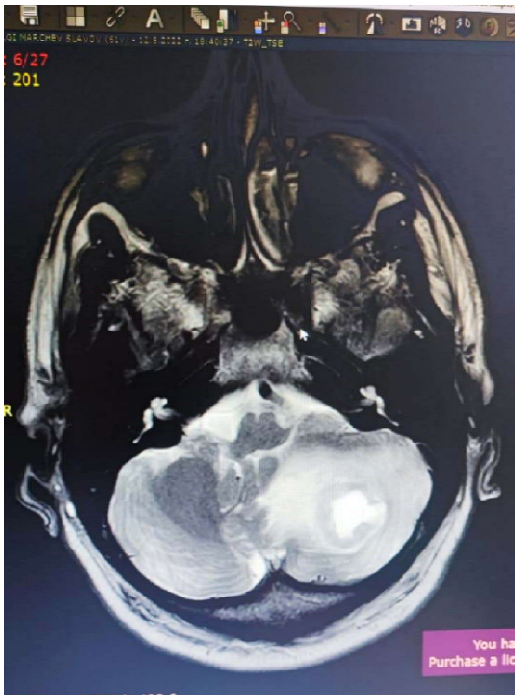

Fig. 1 MRI, Patient 1, before surgery

The patient was operated on by a team of neurosurgeons, and through neuronavigation, microsurgical technique under optical magnification, intraoperative monitoring and meticulous haemostasis, the tumour formation was removed. Postoperatively, a control CT of the brain was performed without the presence of haemorrhage (Fig. 2). The patient was verticalized, with regression in somatic and neurological status and discharged 6 days after the surgical intervention.

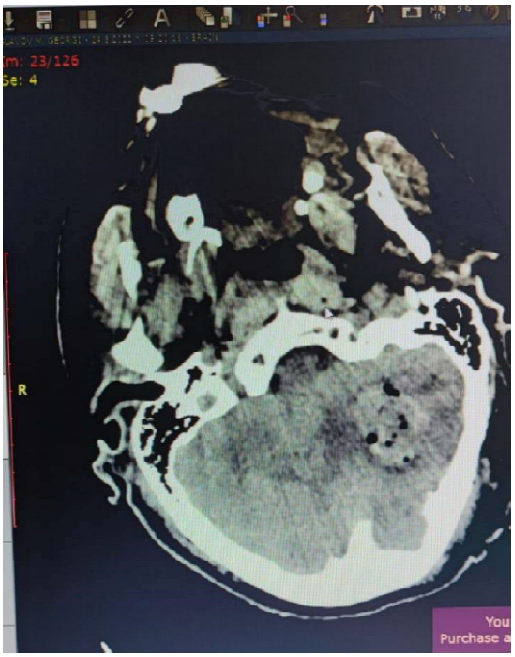

Fig. 2 CT, Patient 1, after surgery

CLINICAL CASE 2

A man of apparent age consistent with his actual age was admitted to the neurosurgery department with the development of spontaneous generalized seizure. The patient had no other complaints, with a co-morbidity of long-standing hypertension, which he had treated as prescribed.

On admission to the department, he underwent an imaging-diagnostic study, MRI, which revealed a metatastic formation in the right frontal lobe that led to the onset of these seizures (Figs. 3, 4). The patient was operated on by a team of neurosurgeons and through neuronavigation, microsurgical technique under optical magnification, intraoperative monitoring and meticulous haemostasis, the tumour formation was removed.

Postoperatively, a control CT scan of the brain was performed without the presence of haemorrhage and the patient was discharged 5 days after surgery with regression in symptomatology and improvement in neurological status (Fig. 5).

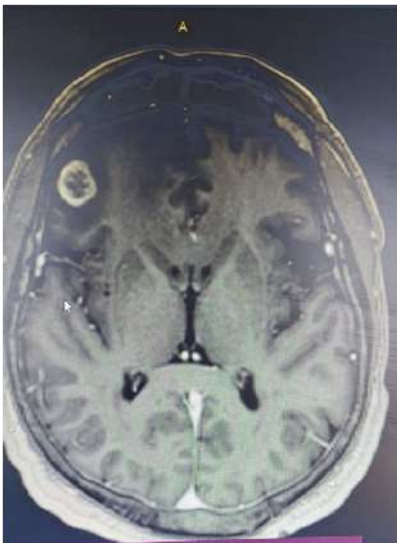

Fig. 3 MRI, Patient 2, before surgery

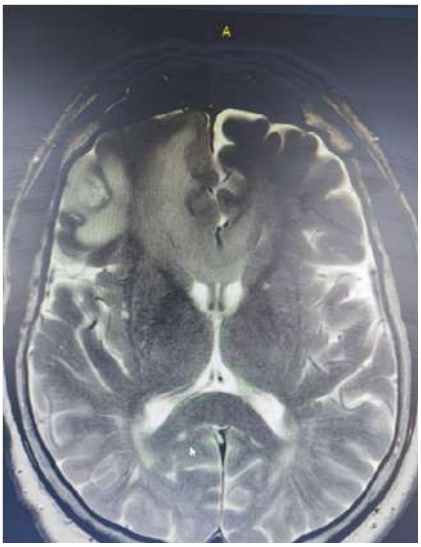

Fig. 4 MRI, Patient 2, before surgery

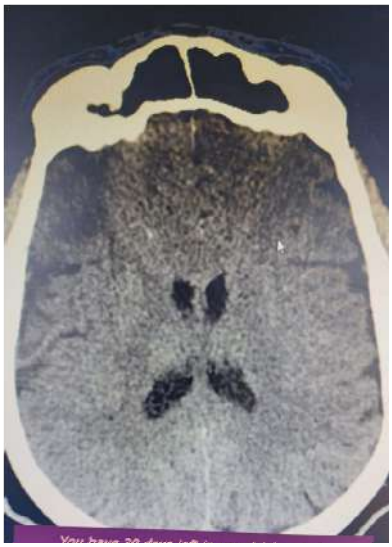

Fig. 5 CT, Patient 2, after surgery

CONCLUSION

Intracranial metastases are life-threatening entities, so it is important to diagnose them on time, choose the therapeutic management and conduct drug therapy to prolong the patient's life and improve his or her neurological condition [6,1 0].

REFERENCES

1. Greenberg, Mark S., Handbook of Neurosurgery, 9th edition.
2. Metastatic brain tumors, American Association of Neurological Surgeons.
3. Chetan Bettegowda, M.D., Ph.D., Metastatic brain tumors, John Hopkins Medicine.
4. Johnson JD, Young B. Demographics of brain metastasis. Neurosurg Clin N Am. 1996; 7:337–344.
5. Vieth RG, Odom GL. Intracranial Metastases and their Neurosurgical Treatment. J Neurosurg. 1965; 23:375–383.
6. Agazzi S, Pampallona S, Pica A, Vernet O, Regli L, Porchet F, Villemure JG, Leyvraz S. The origin of brain metastases in patients with an undiagnosed primary tumor. Acta Neurochir (Wien). 2004; 146:153–157.
7. Davis PC, Hudgins PA, Peterman SB, Homan JC. Diagnosis of Cerebral Metastases: Double-Dose Delayed CT versus Contrast-Enhanced MR Imaging. AJNR. 1991; 12:293–300.
8. Sills AK. Current treatment approaches to surgery for brain metastases. Neurosurgery. 2005; 57:S24– 32; discussion S1-4.
9. DeAngelis LM. Management of Brain Metastases. Cancer Invest. 1994; 12:156–165
10. Kindt GW. The Pattern of Location of Cerebral Metastatic Tumors. J Neurosurg. 1964; 21:54–57.

ANNUAL OF ASSEN ZLATAROV UNIVERSITY, BURGAS
BULGARIA, 2022, v. LI(1)

VERTEBROPLASTY[1]

Sv. Todorov, St. Shishkov*, S. Chavdarov, K. Minkova, M. Mihaylova, E. Laleva
*Department of Neurosurgery, University Hospital Burgas
E-mail: svetoslavtodorovbg@gmail.com

ABSTRACT

Spinal fracture is a condition that threatens the normal functioning of the spinal cord. It is most common in osteoporosis, traumatic back injury, vertebral metastases, other spinal tumors, and hemangiomas.

Vertebroplasty is performed in cases where traditional methods of treatment do not work, in case of long-lasting and worsening pain and immobilization.

This is a gentle, minimally invasive intervention that provides stability, strengthens the vertebrae and relieves pain. Under X-ray guidance, bone cement is injected into the body of the fractured vertebra.

Indications for performing the method can be: uncomplicated compression fracture in any part of the spine as a result of traumatic effects, progressive hemangioma, creating a threat to the anatomical safety of the vertebrae, local oncological process in the spinal canal, adversely affecting the quality of the bony structures of the spinal elements.

The contribution of the proposed method is to reduce the use of analgesic drugs, to achieve lasting pain relief, to prevent the patient from being bedridden and immobilized, which poses a serious risk to his health, especially if in old age.

Keywords: *spinal vertebra, bone cement, vertebroplasty*

INTRODUCTION

Spinal fracture is a condition that actually threatens the normal functioning of the spinal cord. There is a risk that part of the fractured vertebra may enter the spinal canal and cause compression of the spinal cord itself or the nerve roots. This can lead to neurological deficits - paresis or paralysis of the relevant part of the body and limbs, depending on the level of damage.

The most serious injuries occur in fractures in the cervical spine, consisting of 7 vertebrae, followed by the thoracic spine, consisting of 12 vertebrae, and the lumbar spine, consisting of 5 vertebrae, sacrum and coccyx.

Vertebroplasty is a method invented and put into practice in 1984. Its main purpose was the removal of hemangiomas of individual vertebrae.

Over time, the spectrum of application of the procedure has expanded and is currently used for compression fractures of the structural elements of the spine, which most often occur against the background of advanced osteoporosis.

Vertebroplasty is a surgical intervention in which bone cement is injected into the body of a fractured vertebra, which limerises and hardens in about ten minutes, thus hardening and strengthening its structure. The manipulation is performed under X-ray control.

General anesthesia is preferred to maximize comfort for the patient and the neurosurgeon. In addition to healing the vertebra, vertebroplasty also achieves permanent pain relief, the main goal being to prevent the patient from lying down and becoming immobile, which poses a serious risk to his health, especially if he is elderly.

Indications for committing the manipulation are:

- uncomplicated compression fracture in any part of the spine, resulting from traumatic effects;
- progressive haemangioma posing a threat to the anatomical safety of the vertebrae;

[1] The article was presented at the Challenges for Medical Science and Practice in the 21st Century Congress of Medicine, Burgas, 1-3 September 2022

- a local oncological process in the spinal canal, affecting the quality of the spinal structures;
- the absence of positive pro- changes after conservative treatment for vertebral body splitting, characterized by partial loss of mobility, preservation of pain and formation of spinal curvature;

Contraindications for performing the procedure are:

- acute inflammatory process localized in the bone tissue of the spine;
- severe compression of the spinal cord and nerve endings,
- extensive damage to the spine from metastases;
- poor blood coagulation;
- allergic reaction to one or more components of the bone more limer material;

Vertebroplasty is used for fractures of the spine after trauma, due to osteoporosis, or for tumors in the spine, especially metatarsal. The diagnosis of "vertebral fracture" is most often made after spondylo-lography, but in order to assess the necessity and possibility of vertebroplasty, CT or MRI is also performed at the appropriate level.

MATERIAL AND METHODS

A 64-year-old woman presented with a history of back and low back trauma, more severe when slipping and falling on a hard surface.

The neurological examination carried out to assess the functions of the nervous system and the presence of their disorders in the form of neurological symptoms and syndromes revealed vertebra syndrome, no paresis. From the spondylography performed there is evidence of a fracture of the Th12 vertebra (Fig. 1).

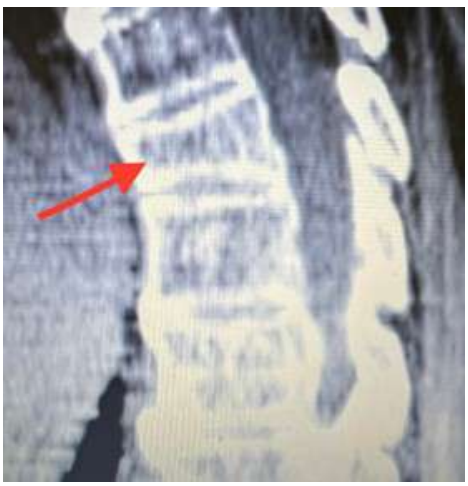

Fig. 1 Thoracic spine fracture - preoperative

RESULTS

The patient was operated one day after the trauma. Vertebroplasty was performed under general anesthesia and X-ray control - C shoulder. The patient was in the supine position during the procedure. Through a small incision in the area of the injured vertebra, bone cement was injected into it using a metal needle. The metal needle at the level of the thoracic and lumbar region is inserted transspedicularly. The most important characteristic of the bone cement is its curing speed - about 6 to 11 minutes. During this period it is injected and the fracture is filled.

After performing this manipulation, it is necessary for the patient to be on bed rest for 1-2 hours.

She was dehospitalized on the third day with regression in vertebral and pain syndromes without paresis (Figs. 2 and 3).

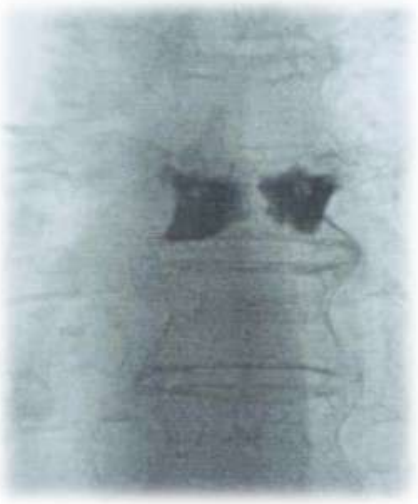

Fig. 2 Condition after vertebroplasty

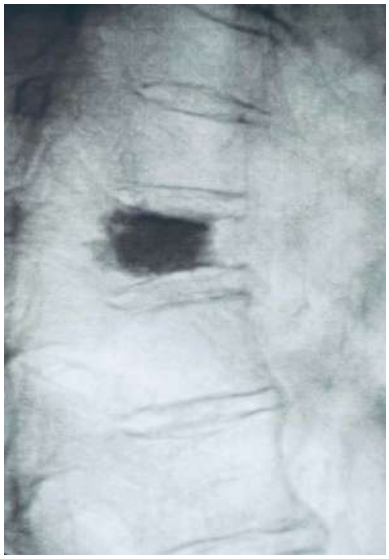

Fig. 3 Condition after vertebroplasty

CONCLUSIONS

The short hospital stay of the patient is an advantage to note in this intervention because within two or three days he is discharged.

The operation is covered by the National Health Insurance Fund and there is no co-payment on the part of the patient, which is essential for quite a few patients.

REFERENCES

1. A. Quinones-Hinojosa, Schmidek and Sweet: Operative Neurosurgical Techniques, 2-Volume Set Indications, Methods and Results 7th Edition - April 22, 2021.
2. Mark S. Greenberg, Handbook of Neurosurgery, 9th edition, 2020.
3. A. Karkesilyan, S. Baev, "Surgery - Clinical Surgery Volume 5:Neurosurgery", 2000, Znanie.
4. Matthew J. Provenzano, Kieran P. J. Murphy, and Lee H. Riley, Bone Cements: Review of Their Physiochemical and Biochemical Properties in Percutaneous Vertebroplasty, AJNR Am J Neuroradiol. 2004 Aug; 25(7): 1286–1290.
5. Katharina E. Schmid, Bronek M. Boszczyk, Michael Bierschneider, Andreas Zarfl, Björn Robert & Hans Jaksche, Spondylitis following vertebroplasty: a case report, European Spine Journal volume 14, pages 895–899 (2005).
6. J. D. Laredo & B. Hamze, Complications of percutaneous vertebroplasty and their prevention, Skeletal Radiology volume 33, pages493–505 (2004).
7. Mckiernan, Fergus, Faciszewski, Jensen, Ron, Quality of Life Following Vertebroplasty, The Journal of Bone & Joint Surgery: December 2004 - Volume 86 - Issue 12 - p 2600-2606.

Assen Zlatarov University
ANNUAL, Vol. LI, BOOK 1, 2022
TECHNICAL AND NATURAL SCIENCES

Design and layout
Libra Scorp Publisher
www.meridian27.com

Printed in M&BM Ltd.
www.mbm-bg.com

Edition of
Assen Zlatarov University
www.btu.bg

ISSN 2603-3968

BURGAS, 2022


ISSN 2603-3968
9 772603 396002